9-26-2023

A Field, Petrological, and Geochronological Investigation of the Chief Joseph Dike Swarm

Mary Joyce Mass
Portland State University

A Field, Petrological, and Geochronological Investigation of the Chief Joseph Dike Swarm

by

Mary Joyce Mass

A thesis submitted in partial fulfillment of the
requirements for the degree of

Master of Science
in
Geology

Thesis Committee:
Martin J. Streck, Chair
John Bershaw
John A. Wolff
Emily Cahoon

Portland State University
2023

Abstract

The Columbia River Basalt Group is the youngest continental flood basalt province in the world and covers an aerial extent of 210,000 km^2 covering Oregon, southern Washington, and eastern Idaho. Eruptions occurred between approximately 17 million and 6 million years ago, with 92% of eruptions occurring within the first million-year interval. Aside from mapping and some bulk compositional data, few studies have focused on the Chief Joseph dike swarm in NE Oregon, the main eruptive center of the Columbia River Basalt Group. Prior to this study there were no published age dates for the Chief Joseph dike swarm.

This project includes geochemical and petrographic data of 147 dikes across the main portion of Chief Joseph from the Oregon/Washington state border in the north to the southern extent of the swarm. This project also reports $^{40}\mathrm{Ar}/^{39}\mathrm{Ar}$ dates of 22 dikes from the northern and southern part of the study area. Developing a geochronological framework for magma activity at depth is significant in our understanding of storage and transport as well as for age relationship of intrusive CRBG magmas with ages and stratigraphy of subaerial lava flows vs. This project focuses on using geochemistry, petrography, and age dates to correlate select dikes of the Chief Joseph dike swarm with the units of the Grand Ronde Basalt, the Imnaha Basalt and other main phase formations, and on using these data to establish an age progression. Our new ages for subterraneous magmas of main phase units of the CRBG extend the age range of these formations and establishes ages for a newly identified Eckler-PGB type magma which is represented across the swarm. The new age of 17.22 ± 0.22 Ma for an Eckler-PGB like dike in the southern portion of the swarm establishes that the Chief Joseph dike swarm was active beginning at the same time as the Monument dike swarm began its activity further to the west. This suggests that the first eruptions of the CJDS began with magmas derived from a

metasomatized shallow mantle with a strong subduction zone signature, which is reflected in the Eckler-PGB basalt followed by magmas that had a more plume like signature.

We conclude that there are age progressive trends in the geochemical signature of magmas becoming more evolved and younger along strike to the north. This study also supports the magma storage model put forth by Wolff et al. (2008) and Webb et al. (2019) where the main magma storage location is located in the Vale region of central eastern Oregon. This is supported by the geochemical diversity found in the southern portion which lies in the Vale region, there is a wider and older age range of dikes established in this area, and lastly the lack of silicic volcanism in the central or northern portion of the CJDS suggest little to no storage time of magmas sourcing the dikes there. This suggests that magma traveled from the southern portion of the CJDS in the Vale region to other eruptive locations throughout the swarm.

Acknowledgments

I would like to thank the chair of my thesis committee and advisor, Martin J. Streck for all your advice, edits, and support through the last four years. Thanks also to the support and feedback of my committee John Wolff, Emily Cahoon, and John Bershaw. And most importantly, I would like to thank my husband William Mass for your endless support of me, love, friendship, and edits of my work throughout the years, you are my dearest friend, and I could not have accomplished this without you. Thank you to everyone at WSU for their support, friendship, and instruction for sample prep at the XRF-ICPMS lab including John Wolff, Ashley and Arron Steiner, and Rachelle Hart. Grabbing drinks with all of you at Paradise brewing was so memorable. Thank you to Rachelle Hart for letting me use your unpublished Roza data as a comparison when classifying my PGB-Eckler Mtn. geochemical data, it added so much insight into my results. Thanks to the group at OSU Argon lab including Dan Miggins, Daniel Heaton, and Anthony Koppers for all your help processing and analyzing my samples for argon dating. Thank you to Emily Cahoon and all the graduate students in the department who met up for beers while I was in Corvallis OR, it made the trip so much more fun.

To all my field and lab assistants over the many summers of work, Andrew Dunning thanks for playing wild west soundtracks and smashing rocks with me in Hells Canyon OR as well as taking amazing pictures of the comet NEOWISE during field work—that trip was unforgettable. Thank you so much to my husband William Mass and to Matt Shelden for joining my sampling by raft along the Grande Ronde River my first summer, it was fun but not always easy and I appreciate you. Thank you to Liza Jane for all your help with fieldwork, your company made the trip so fun. To my other field assistants Heather Ziff and Samuel Tobey who did a multiday camping rafting trip to sample dikes along the Grande Ronde River, it was so fun even though we had to abort the trip due to wildfires. Thanks to Darlene Verduzco and Heather Ziff

who each spent a week in the lab at OSU helping to prepare my samples for argon dating, your support and comradery made that trip so fun and memorable.

Thank you to Tim Ferguson at the Idaho Power Company who let us sample dikes in the Brownlee reservoir. Thank you so much to Brock and Nick Owen from the Bureau of Land management who let us in through a locked gate to the peak of Big Lookout Mountain and allowed us sample there by Jeep. Thank you to Heather Ziff and Rachel Sweeton who joined me during this week in the field, who endured the sound of a drill, intense heat, and blood sweat and tears.

To all my friends and family that have supported me throughout the years, including my dear sister Amelia Frost who has been an endless source of emotional support throughout my life and especially during my thesis. Thank you to my amazing friends Vanessa Swenton and Darlene Verduzco who are stuck with me for life, you have both been so supportive, amazing, offer unconditional love, and reach out when I need it the most, I so appreciate you both. Thank you to Luke Fredenburg (Von Wafflehousen) for your kindred sense of humor, I wish you didn't live so far away. Thank you so much to my Dungeons and Dragons group who made these past few years so much better. Thank you also to Chanel Thieme for your unconditional friendship. Thanks to the rest of my cohort Larissa Sleeper and Cameron, I am so proud of you both. Thanks to Lena Fox, Cassandra Black, Angela Stetson, Daniel Sheik, and Javeria Aziz for all your comradery on and off campus, you all are the best.

Table of Contents

List of Figures

Introduction

Large igneous provinces (LIPs) include voluminous flood basalts that are often attributed to the impingement of a mantle hotspot plume beneath the lithosphere (Wolff et al., 2008). The Columbia River Basalt Group (CRBG) is the youngest continental flood basalt province in the world and spans an area of approximately 210,000 km^2 covering Oregon, southern Washington, and eastern Idaho (Reidel et al., 2013). The eruptive interval of the CRBG occurred from 17.2 Ma to 6 Ma with the oldest members, the Picture Gorge and Steens Basalt, and the youngest flows the Saddle Mountains Basalt (Kasbohm and Schoene, 2018; Moore et al., 2019; Cahoon et al., 2020). Most of the magma (~95%, approximately 195,500 km^2) erupted during the first million years of the main phase of the CRBG which includes the Steens, Imnaha, Grande Ronde, and Picture Gorge Basalt (Reidel et al., 2013; Kasbohm and Schoene, 2018). These flood basalts erupted from dike swarms, the largest of which is the Chief Joseph dike swarm located in SE Washington and NE Oregon.

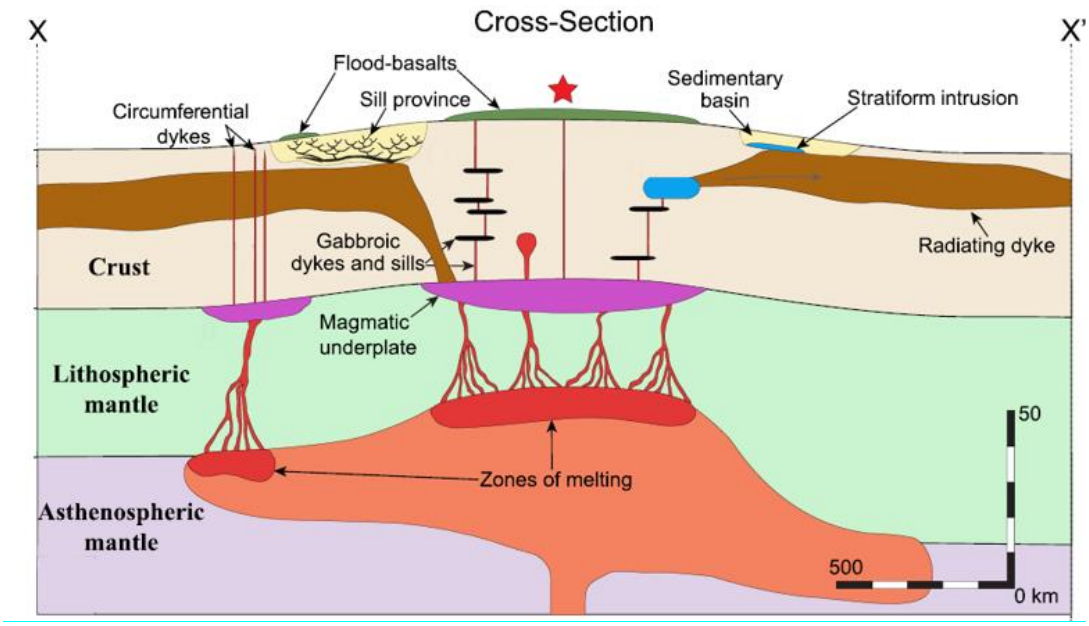

Figure 1. Framework for the plumbing system of continental large igneous provinces (LIPs) associated with mantle plumes (Ernst et al., 2019).

Recently proposed models for the subsurface framework of LIPs suggest that as a mantle plume spreads out and pools beneath the lithosphere, it can result in uplift and the formation of dikes near the surface (Ernst et al., 2019). Magma chambers can form above the plume at the base or within the crust to create spatially offset eruptive centers. Afterward, magma can be transported laterally from these magmatic reservoirs for distances of >2000 km from the plume center (Ernst et al., 2019, Figure 1). Isotopic and geochemical data as well as surficial geological deposits suggest there was a centralized magma storage location for the CRBG (Hales et al., 2005; Wolff et al., 2008; Schmandt and Humphreys, 2011; Streck et al., 2015; Webb et al., 2019). The Chief Joseph dike swarm produced the most voluminous unit of the CRBG, the Grande Ronde Basalts. The association of silicic volcanism within the southern portion yet lack thereof in the central to northern portion of this dike swarm bears on where erupted magma had minimal to no storage time (Webb et al., 2019; Ernst et al., 2019; Streck et al., 2023).

This project is a part of a more extensive collaborative study funded by the National Science Foundation which will address the broader question of determining the location of sources that fed the Chief Joseph dike swarm. In addition to the petrologic, geochemical analysis, and age dating investigated in this project, rock magnetic techniques will be applied in future research by other researchers. This combination of research techniques will determine how the dikes correlate to other erupted basalt members of the CRBG (Streck et al., 2019). Proposed locations for magma feeding the Chief Joseph and the other dike swarms include the Wallowa Mountains, the Vale Region, and McDermitt Caldera on the border Oregon/Nevada border (Camp, 1995; Hales et al., 2005; Wolff et al., 2008; Webb et al., 2019, Figure 2).

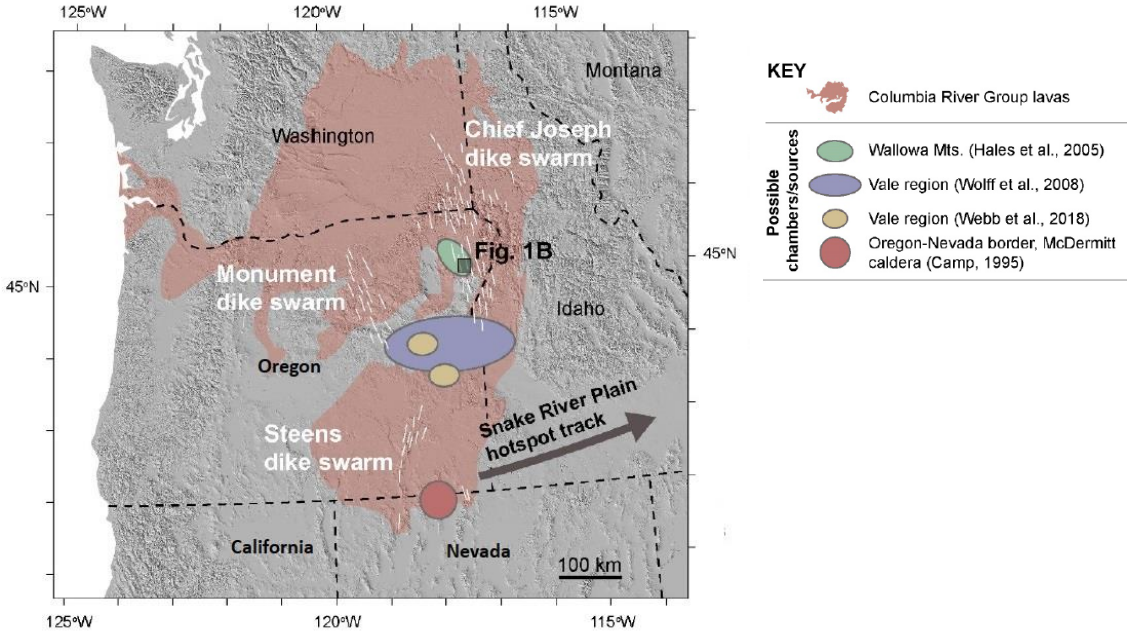

Figure 2. Regional Map highlighting the extent of the Columbia Basalts (red) as well as the proposed storage areas that are hypothesized to have fed the Joseph Dike Swarm. (Image modified from Streck et al. NSF grant proposal, submitted, 2019).

To date there have been relatively few investigations focusing on these dike swarms aside from mapping them and the occasional bulk chemical analysis, which remain largely unpublished. Additionally, no age dates are known to exist for the dikes of the Chief Joseph dike swarm, although there are age dates for dikes in both the Steens and Monument dike swarms (Camp, 1995; Barry et al., 2013; Cahoon et al., 2020). This project divides the Chief Joseph dike swarm into three sections: the northern portion in SE Washington, the central portion which includes the Wallowa Mountains, and the southern portion which straddles the central Eastern Oregon and Idaho border, as seen in Figure 3 in boxes 1, 2, and 3 respectively.

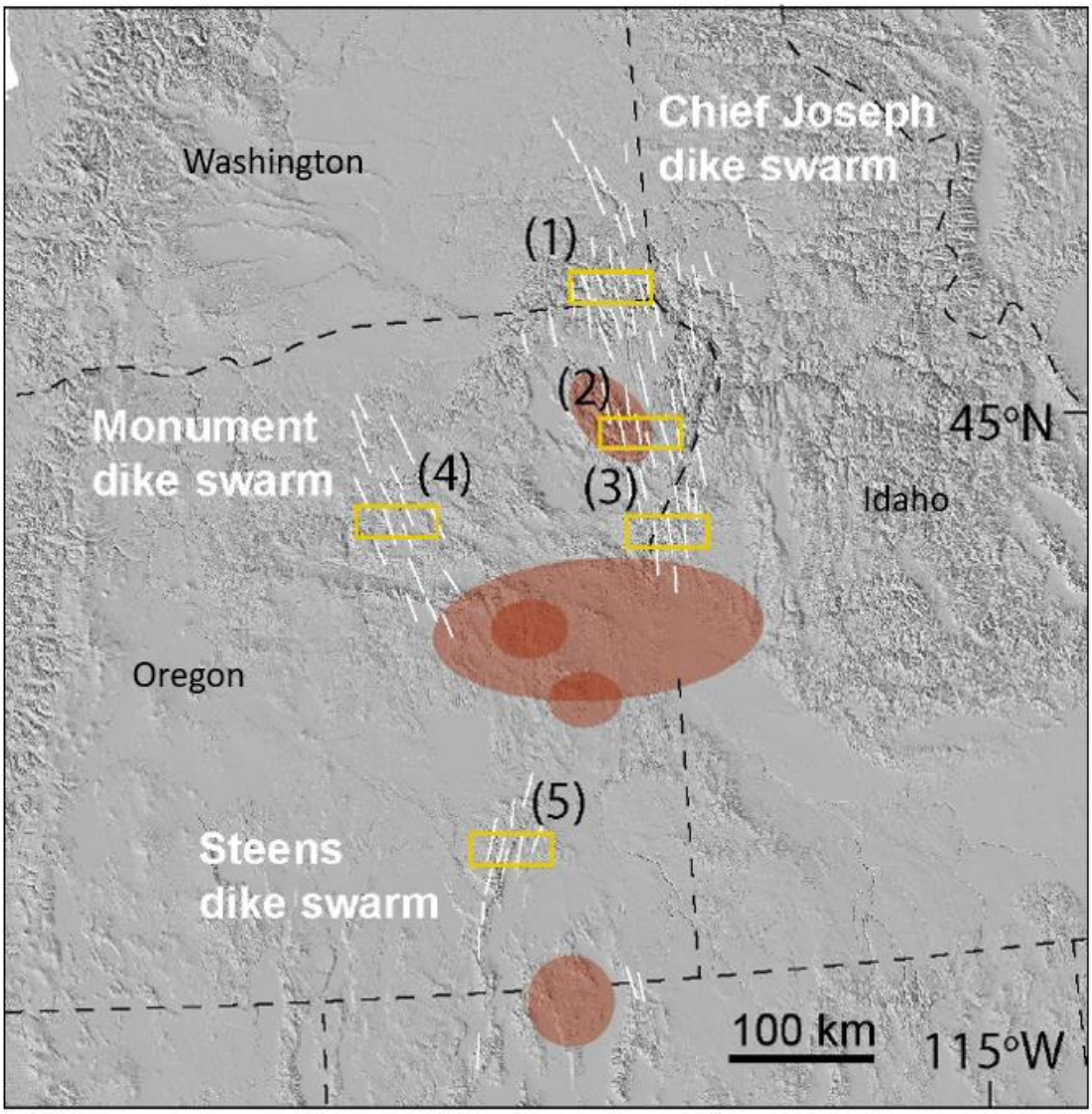

Figure 3. Study locations are relative to proposed magma storage areas for the broader National Science Foundation funded project. (Image is taken from Streck et al, NSF grant proposal, submitted 2019).

Dating dikes in the Chief Joseph dike swarm (CJDS) is significant in understanding the timing of eruptions and gives us insight into the magma storage location (Streck et al., 2019). Age dates across the swarm will point to the source area for the Grande Ronde Basalt—the most voluminous CRBG unit—and the first unit known to erupt from the swarm, the Imnaha Basalt. For this study, 147 samples were collected across the swarm for petrographic, XRF and ICPMS analysis, and 22 of these samples were selected for $^{40}\mathrm{Ar}/^{39}\mathrm{Ar}$ age dating. The geochemical data from sampled dikes were correlated with flows of the Grande Ronde, Imnaha Basalt, and

other formations with assistance from Ashley Steiner at Washington State University. Results from this study will also assist in settling the long-standing debate as to the staging area for magmas leading to the Columbia River Basalt province and will provide insight into the eruptive behavior of continental hotspot induced flood basalts when the plume head interacts with the base of the lithosphere.

Background

Regional Geology

The prevailing model for the generation of the Columbia River Basalts (CRB) is that they were sourced from the mantle plume which is now located under Yellowstone in Wyoming (Camp and Hanan, 2008; Camp, 2013, Figure 4). It has been proposed that this plume was located just off Cape Blanco, Oregon, around 50 Ma (Wells et al., 2014), and that this plume is thought to have sourced another LIP—Siletzia—which rapidly erupted within a short window of time from 56 Ma to 49 Ma and accreted immediately to the western margin of North America. Following these eruptions, the hotspot was overridden by North American plate around 42 Ma. There was a paucity of eruptions related to the plume between 34 Ma to 17 Ma due to travel under the Cascade Arc (Wells et al., 2014). Around 17 Ma, the plume is estimated to have been located in eastern Oregon where the eruptive activity producing the lavas of the CRBG began.

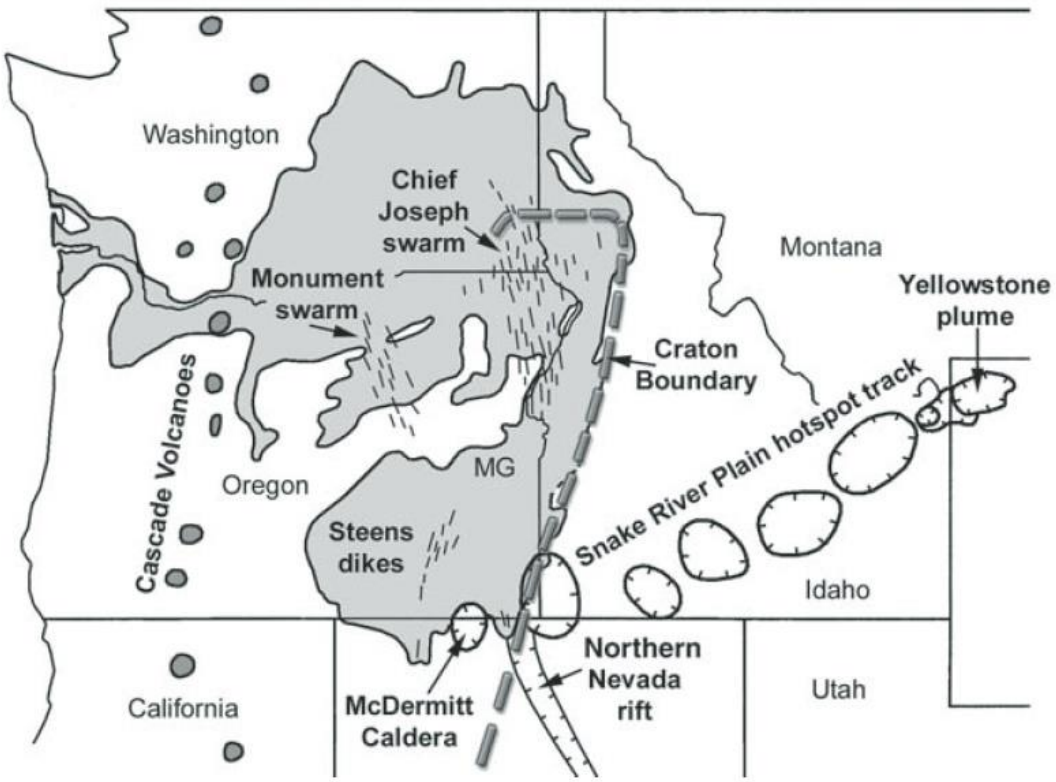

Figure 4. Map of the Columbia River flood basalt province, showing dike locations and areal distributions of the CRBG (dark grey). Image modified from (Camp et al., 2013).

Most of the lavas of the Columbia River Flood Basalt erupted from NNW-SSE trending dikes located in NE Oregon, SE Washington, and Eastern Idaho that together comprise the Chief Joseph Dike Swarm (Figure 4). Other dike swarms are the NW trending Monument Dike Swarm that give rise to the lavas of the Picture Gorge Basalt and nearly S-N trending Steens Dike Swarm, which produced lavas of the Steens Basalt. Eruptions from the CJDS began around 16.6 Ma erupting 95% of their total lava within the first million years (Kasbohm and Schoene, 2018). The remaining 5% erupted over the following 10 million years (Reidel et al., 2013). However, the first of these eruptions from any dike swarm originated from the Monument dike swarm in central eastern Oregon at 17.23 ± 0.04 Ma (Cahoon et al., 2020). These were followed by the eruptions to produce the Steens Basalt at 17 Ma (Moore et al., 2019). Imnaha flows were the first flows that

erupted from the Chief Joseph dike swarm in NE Oregon around 16.7 Ma to 16.4 Ma (Figure 4) (Wolff and Ramos, 2013; Kasbohm and Schoene, 2018). The Imnaha flows were followed by the most voluminous eruptions from the Chief Joseph dike swarm—the Grande Ronde Basalt (GRB) – which account for 87% of the total eruptive material of the CRBG and the GRB has an aerial extent of 149,000 km^2 (Reidel et al., 1989). In the meantime, the dikes that make up the NW-SE trending Monument dike swarm around Picture Gorge and the John Day valley produced lavas of the Picture Gorge Basalt from 17.23 to ~16 Ma (Cahoon et al., 2020).

The distance between the main eruptive center for the Columbia River Basalts—the Chief Joseph dike swarm—and the Yellowstone Hotspot track located at the Oregon-Nevada border at the McDermitt Caldera is around 400 km (Hales et al., 2005; Reidel et al., 2013) (Figure 4). This observation has been used as evidence against the plume model source for the CRBs. However $^{40}\mathrm{Ar}/^{39}\mathrm{Ar}$ geochronology and field relationships in the Malheur Gorge show that the Imnaha conformably overlies the Steens Basalt (Hooper et al., 2002). Further evidence for a plume source for the CRBs are elevated $^{3}\mathrm{He}/^{4}\mathrm{He}$ ratios derived from olivine phenocrysts in the Snake River basalts suggesting a deep mantle source (Camp, 2013). The leading hypothesis by most researchers is that a plume was responsible for the CRBG and Snake River Plain hotspot track magmatism, yet few models have been put forth describing plume-lithosphere interaction.

A recent model explains observed behaviors of LIPs in which the plume head can spread out underneath the lithosphere resulting in uplift and dike formation on the surface (Ernst et al., 2019). Magma chambers can then form above the plume at the base of the crust creating spatially offset eruptive centers. Magma is transported laterally distances of >2000 km from the plume center (Ernst et al., 2019). The spatial separation between the Chief Joseph dike swarm and the Yellowstone hotspot track could be due to the transport of magma in dikes from a central magma

storage location. Proposed storage areas for the Chief Joseph dike swarm are the Wallowa Mountains (Hales et al., 2005), Vale region (Wolff et al., 2008, Webb et al., 2019),) Oregon-Nevada border, McDermitt Caldera (Figure 4)(Camp, 1995).

The first of these proposed magma reservoirs for the Columbia River Basalts is located beneath the Wallowa Mountains in NW Oregon (Hales et al., 2005, Figure 5). This area underwent a small amount of pre-eruptive subsidence and then post-eruptive uplift of several hundred meters. Over time, the uplift reached up to around 2 km (Hales et al., 2005). Teleseismic tomographic images indicate that a high velocity zone is located under the Wallowa Mountains (Hales et al., 2005; Schmandt and Humphreys, 2011), Figure 5). This high-velocity zone is thought to represent focused delamination of the lower eclogitic crust, causing the Wallowa Mountains to rise buoyantly.

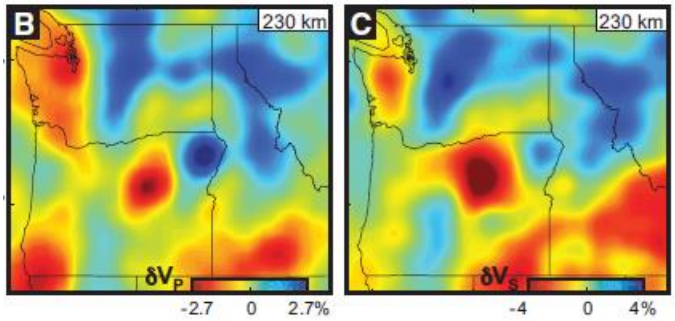

Figure 5. A Teleseismic tomography image at 230 km depth indicating a high velocity zone (blue) located under the Wallowa Mountains. B: P-wave velocity variations, C: S-wave velocity variations. Image taken from (Schmandt and Humphreys, 2011).

A second proposed magma reservoir for the CRBG is the area in the vicinity of the town Vale, located in central-eastern Oregon along the border between the North American craton and the accreted terrains of Oregon and Idaho (Figure 2, Wolff et al., 2008; Webb et al., 2019). The Grande Ronde Basalt contains Sr isotopic signatures of $^{87}Sr/^{86}Sr > 0.704$, suggesting an interaction with the North American craton indicated by the $^{87}Sr/^{86}Sr = 0.706$ isopleth (Wolff et

al., 2008). Rhyolites in the western Snake River Plain also have Pb isotope signatures comparable to those in samples of the Grande Ronde Basalt. This evidence suggests that the system of magma chambers which supplied all the CRBG lies across the central- eastern Oregon and Idaho border and is constrained on the east and west to the area defined in Figure 2. Wolff and others propose that there were laterally extensive magma chambers that sourced the Grande Ronde and the Imnaha magmas which were then transported by dikes to eruptive centers. Geochemical signatures of the Picture Gorge Basalt and the Steens Basalt indicate that they did not share the same reservoir, but because the CRBGs are theorized to travel laterally through dikes, their magma chambers lie in the same "convergence zone" (Wolff et al., 2008).

Two specific locations in the Vale area have been proposed by Webb et al. (2019) as magma storage sites for the Grande Ronde Basalts (Figure 3). Bimodal volcanism is associated with continental flood basalts and evidence for localized magma reservoirs can be found with these associated units (Webb et al., 2019). In central-eastern Oregon, there are two voluminous rhyolitic centers erupted coevally with two local units of the Grande Ronde Basalt— the Hunter Creek Basalt and Birch Creek lavas—and can be found intercalated in the field. The rhyolite centers are the Littlefield rhyolite and the Dinner Creek Tuff, both of which erupted at 16.1 Ma (Streck et al., 2015; Webb et al., 2019). Both the Grande Ronde Basalt as well as the Imnaha Basalt are thought to have traveled via dikes from shallow magma storage areas to the CJDS, where the lack of silicic volcanism north of southern portion of the dike swarm suggests that the erupted magma had minimal to no storage time (Webb et al., 2019; Streck et al., 2023).

Another model places the magma reservoir for the CRBG in the area below the McDermitt Caldera on the Nevada-Oregon rift zone (Camp, 1995). In this model the plume head is blocked by the subducting Farallon slab as the North American plate overrides it preventing a hotspot track from forming west of McDermitt caldera. The plume head then spreads laterally northward;

the surface reflection of this process is a similar northward migration of the CRBG dikes. The voluminous eruptions from the Chief Joseph dike swarm are attributed to a weak spot along the North American craton and the accreted terrain, which underwent at least one extensional event in the Tertiary. Evidence for this model is uplift from the plume along the Oregon-Nevada border, indicated by a low-density anomaly in the mantle. Geochemical data also point to the Imnaha representing the northward-propagating plume head. In contrast, the Grande Ronde Basalt suggests magma mixing of a subcontinental lithospheric mantle source above a plume head (Camp, 1995).

This study seeks to acquire the evidence needed to pinpoint the magma storage location for the CJDS. Age dates obtained from this study combined with future rock magnetic data are critical in identifying the magma flow direction within the CRGB. The flow direction and geochronological trends established in this thesis shed light on the location of the magma reservoir and in a broader context, the behavior of LIP's.

Stratigraphic Field Relations

An early stratigraphy of the CRBG was established using drill cores from the Basalt Waste Isolation Project in the Pasco Basin, located in southern Washington (United States. Department of Energy, 1982). The lava flows from the CRBs pooled here as they flowed west (Landon and Long, 1989). The various Grande Ronde Basalt flows can be challenging to differentiate in the field due to their homogeneity, so other methods have been established to identify and correlate flow units. One way to correlate groups in the Grande Ronde units is by using changes in the magnetic polarity. These magneto-stratigraphic units were first established by Swanson and Bentley (1979), who described the four polarity shifts during the eruption of

the GRB from oldest to youngest as R1, N1, R2, and N2 respectively (Swanson and Bentley, 1979). Swanson and Bentley (1979) state that most flows of the Imnaha Basalt have a normal polarity, yet Barry et al. (2013) state that the Imnaha flows are currently placed in a period of rapid reversals. However, no reversals are currently recognized in the field (Swanson and Bentley, 1979; Barry et al., 2013).

Geochemical characteristics of the GRB, the Imnaha, Wanapum, Picture Gorge Basalt (PGB), as well as other formations and members of the CRBG, are used in this study to correlate sampled dikes with associated flow units. Previous work has shown that the GRB are generally fine-grained tholeiitic basalts that contain approximately 52 to 57 wt% SiO_2. Diagnostic elements that can be used to correlate flows are TiO_2, P_2O_5, CaO, Cr, MgO, Zr, and Ba (Landon and Long, 1989; Reidel et al., 2013). Previous studies indicate the flows of the Imnaha Basalt range in SiO_2 from 49.2 and 51.8 wt%, are porphyritic, often containing abundant plagioclase phenocrysts which can measure greater than 2 cm in length (Kleck, 1976). Subunits of the Imnaha include the American Bar and Rock Creek unit. Flows of the lowest American Bar subunits have affinities that resemble flows of the Picture Gorge Basalt (Swanson and Bentley, 1979). However, unlike the other CRBG formations, the Picture Gorge Basalt erupted from the Monument dike swarm in central Oregon (Figure 3). The PGB ranges in SiO_2 from 49 to 53 wt % and—like the Imnaha—typically contain large phenocrysts of plagioclase (Wolff and Ramos, 2013; Fredenberg, 2022). The flows of the Wanapum Basalt are chemically diverse. This study identified dikes that may be correlated with the Roza and Eckler Mountain members. One of the youngest flows of the Wanapum, the Roza member is characteristically plagioclase-phyric, and has a SiO_2 content of approximately 51.1 wt% (Swanson and Bentley, 1979; Martin, 1991). Rectangular zoned plagioclase evenly distributed throughout the flow that makes the Roza member easily identifiable in the field. The Eckler Mountain member includes the basalt of

Dodge, one of the oldest units in the Wanapum formation. This unit is relatively primitive and contains high MgO of ~ 6.2 wt % with a SiO_2 range of 50 to 51 wt% (Hooper et al., 1995).

Study Area

The north portion of the CJDS includes 3500 km^2 of semiarid deep canyon country, where samples were predominantly collected in an area at the confluence of the Grande Ronde and Snake Rivers, as well as Joseph Creek along the eastern edge of Washington and Oregon along the Idaho border. Although this area is almost entirely covered by Columbia River Basalt, the country rock is exposed along the Snake River on the OR-ID border in deeply incised canyons. There, dikes intrude the Wild Sheep Creek Formation which consists of volcanic sandstone overlain by argillite, volcaniclastic rocks, limestone and metabasalt (Vallier, 1974).

The geographic central part of this study is within the Wallowa Mountain and surroundings, composed of rocks ranging from the Paleozoic to the mid-Miocene. The Paleozoic rocks are in the highest reaches of the mountains, some overlain by Columbia River Basalt flows. This area has been uplifted and exposes granite plutons intruded by dikes of the CJDS (Ross, 1938).

The study area in the southern portion of the dike swarm consists of 2,453 km^2 of high desert terrain with gently rolling hills of CRBG flows as well as exposed Jurassic plutons and accreted terrane rocks. Also included in this area is the Hells Canyon River valley which has steep terrain that exposes beautifully stacked lava flows and dikes from the Imnaha and Grand Ronde Basalt units. The country rock consists primarily of the Jurassic Weatherby Formation, which includes the Burnt River schist, serpentinite, amphibolite, and metamorphosed volcanic

rocks. The Country rock that dominates the mountains in this area is granodiorite plutons that are lower Cretaceous and upper Jurassic (Brooks, 2006).

Methods

Field Work

This study explores temporal and geochemical trends within basaltic dikes of the CJDS, organized by the geographic location of dike samples (i.e. North, Central, and South). Field work consisted of selecting dikes from previously mapped data as targets for sampling and analysis. Target dike locations within each area were chosen based on dike density, proximity to roads, and accessibility. Previously mapped dikes are localized on mountain peaks and in river valleys where erosion, lack of infrastructure, and accessibility facilitated field mapping.

The north portion of the dike swarm had very sparsely digitized, published, and accessible dike data. To further investigate optimum target dike locations, I digitized dikes that were mapped by Peter Hooper from a collection of 7.5-minute and 15-minute quadrangles in Idaho, Oregon, and Washington that are housed at Washington State University, Pullman (WSU). I also digitized a dike data set from the Washington Department of Natural Resources (WDNR) of Asotin County, WA that had great coverage of dikes along the Grand Ronde River along the eastern Washington and Oregon border. Locations for field work within this area were chosen based on the density of mapped dikes in canyons and their proximity to roads. The Grand Ronde River section was a choice sampling area due to the density of mapped dikes and was predominantly sampled by raft as there was minimal to no road access to these dikes (Figure *6*).

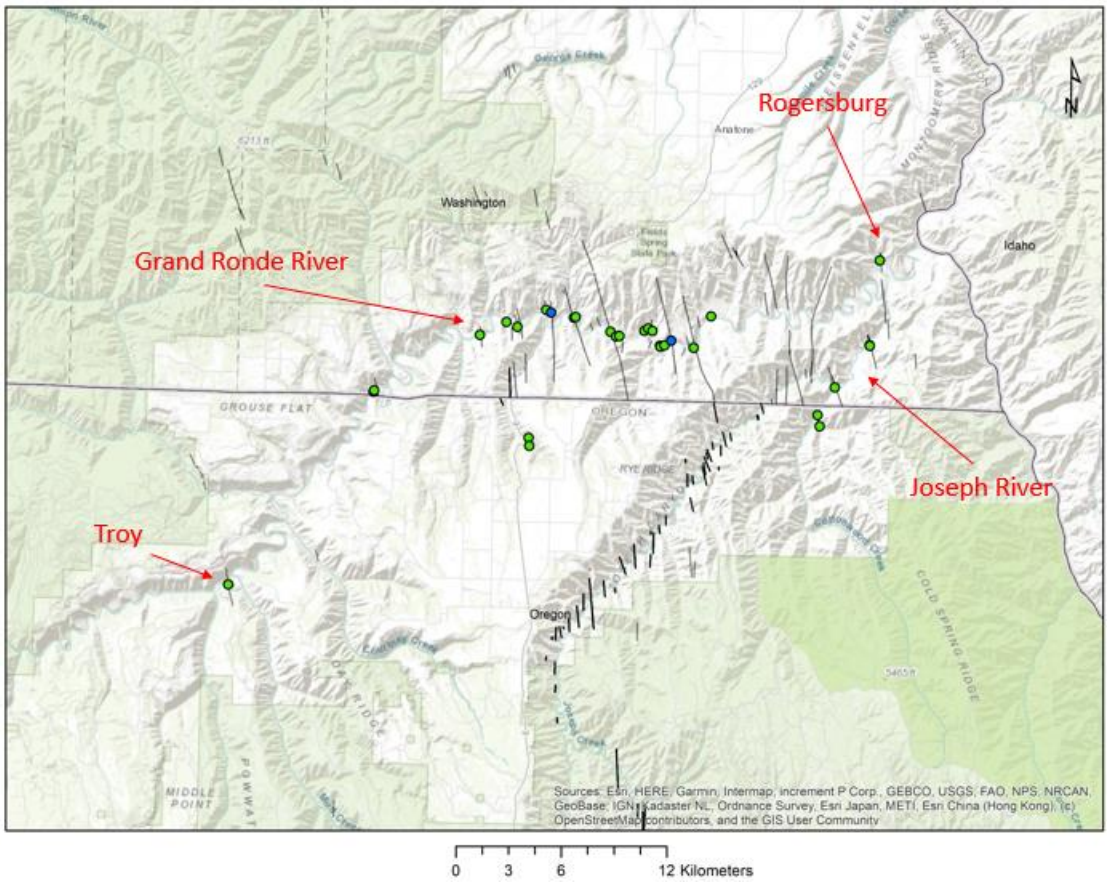

Figure 6. Study area in the northern portion of the CJDS, this figure includes sample locations, samples (seen in green), and the Taubeneck dataset (Morris et al., 2020).

In the northern portion of the CJDS, dikes exclusively intrude younger CRBG flows. These dikes were characterized by vertical relief from the topography, baked/glassy margins, and in some cases horizontal columnar jointing. Approximately 5 kg of material was sampled per dike for geochemistry and possibly subsequent age dating. Samples were taken from the middle of the dike and—when possible—were chipped in the field, getting rid of the weathering rinds. Glassy margins were sampled when present for possible future analysis.

In the central portion of the CJDS targeted areas include I-82, Little Sheep Ck. Hwy., and the Brownlee reservoir. The legacy dataset of William Taubeneck was also used to narrow down target sample locations (Morris et al., 2020). The Cornucopia area just north of Red Mountain in the SE area of the Wallowa Mountains was a significant sample area (Figure 7).

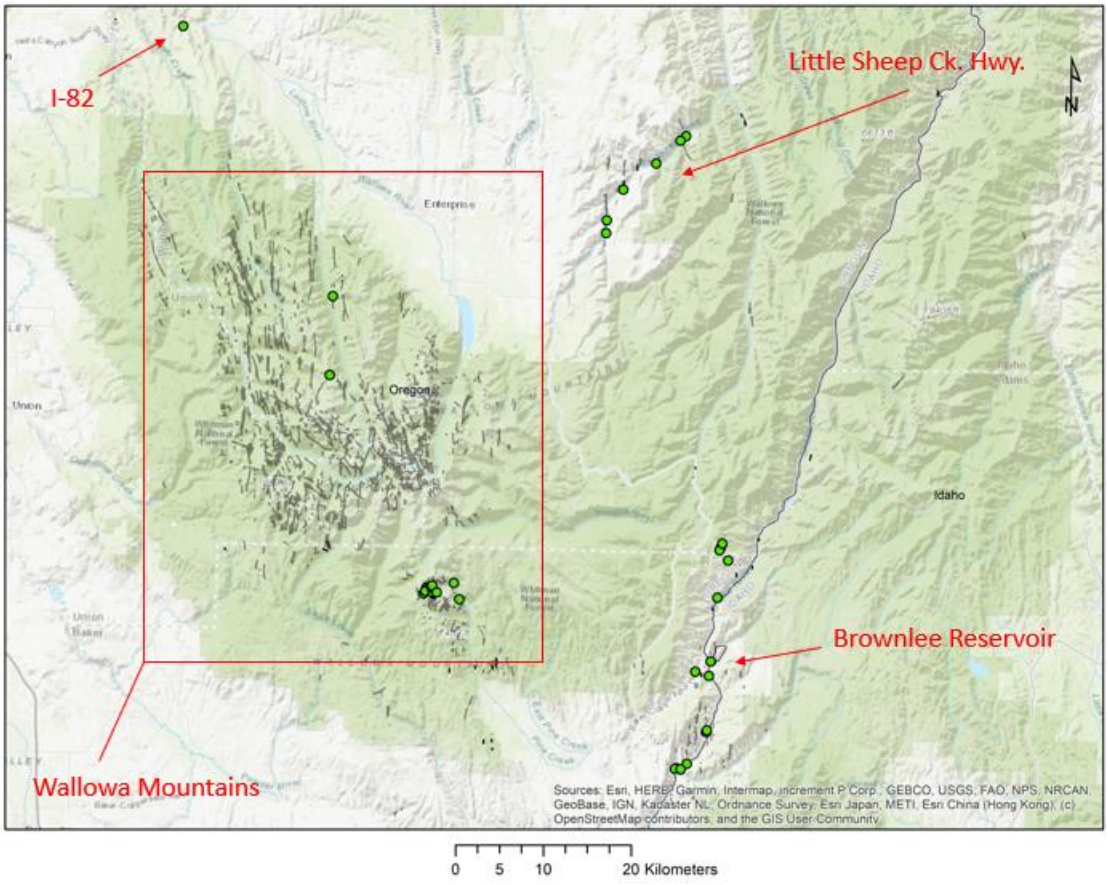

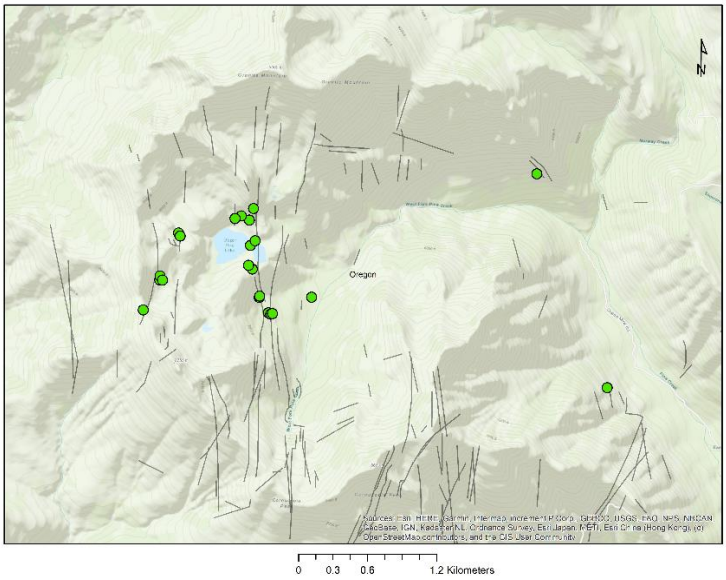

Figure 7. Study area in the central portion of the CJDS and includes the Wallowa Mountains and the surrounding areas (A), the Cornucopia sampling area is shown in (B). Dike data (shown in grey) is from the legacy dataset of William H. Taubeneck (Morris et al., 2020). Green data points are samples from this study.

Sampling in this area required backpacking to sample dikes. This area was dominated by glacially reworked granite plutons intruded by CRBG dikes exhibiting predominantly NNW strike, with a few exceptions. Thirty-four kg of samples were taken for petrographic, geochemistry, and age dating, and were brought down by a pack horse.

In the south portion of the dike swarm, the dataset of William H. Taubeneck was used to narrow down target locations for a focused field campaign (Morris et al., 2020). Three main locations were chosen based on dike density, Big Lookout Mountain, San Pedro Mountain, and a section of Hells Canyon ranging from Ontario, OR to Richland, OR plus select secondary locations (Figure 8). Optimum dikes were selected for field investigation out of each of these areas using Google Earth imagery to identify outcrops. Dikes that are well exposed in this region have the appearance of a linear brown coloration or have visible topographic relief on aerial imagery.

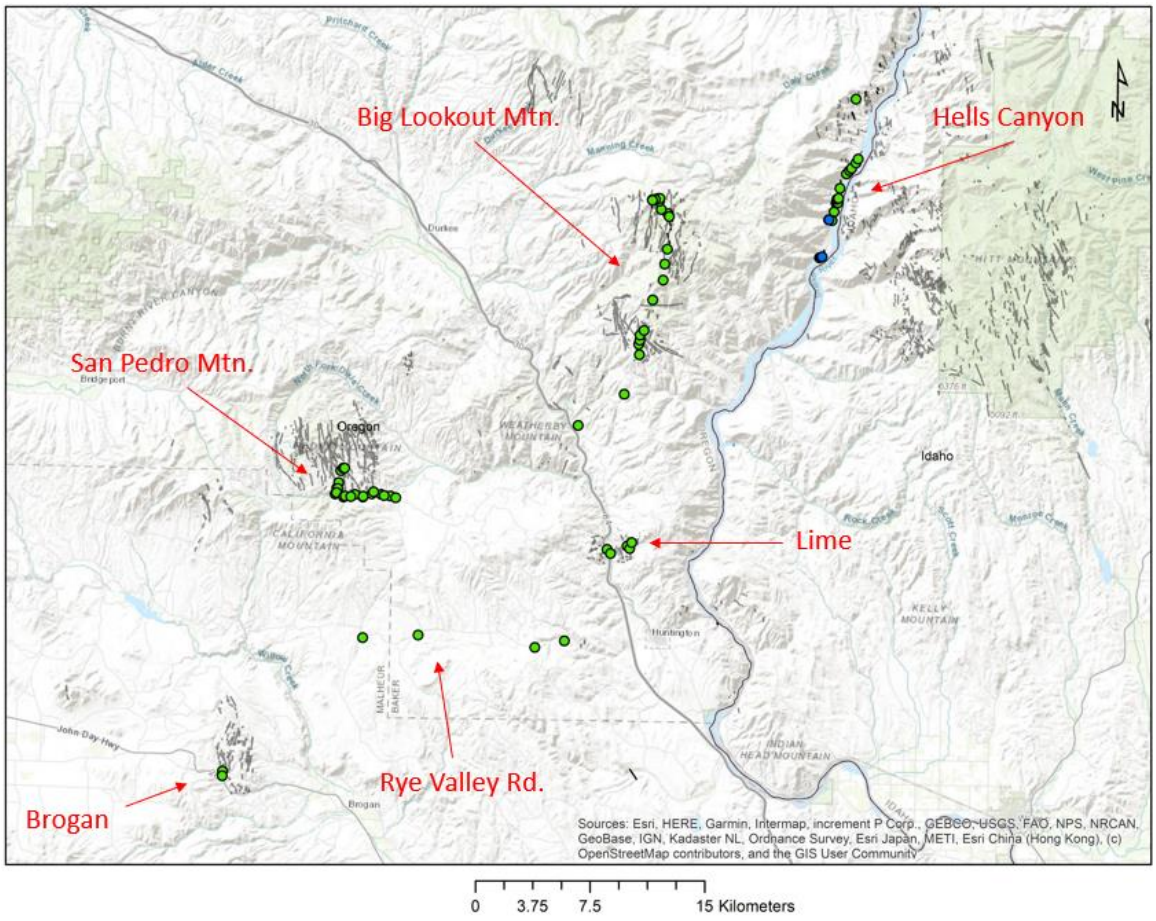

Figure 8. Study area in the southern portion of the CJDS, this figure includes sample locations, samples (seen in green), and the Taubeneck dataset (Morris et al., 2020).

Dikes in the southern portion were easily identified, as they were the only mafic units present in the study area and exclusively intrude limestone and Jurassic age granodiorite. The sampled dikes were almost all entirely exposed due to roadcuts. However, when exposed across smooth topography, there was a lack of vegetation marking their location.

Geochemical Analysis

Major and trace element data was acquired using the X-ray Florescence (XRF) and Inductively Coupled Plasma – Mass Spectrometry (ICPMS) at the Peter Hooper GeoAnalytical Lab at Washington State University (WSU). Samples were selected for geochemistry based on a low degree of weathering. As dikes in the south were weathered more relative to central and northern dikes, determining the effect that weathering has on the geochemistry was important to establish data integrity. A weathering rind and relatively un-weathered sample of MM-CRB-

09 were selected for geochemical analysis to establish any variations in geochemistry (Appendix A: Sample Whole Rock (XRF & ICP-MS) and Location Data).

Data were acquired for 147 dike samples, sixty-nine of which are in the southern portion, forty-six of which are in the central portion, and the remaining thirty-two are located in the northern portion of the CJDS. Samples were first prepared by being crushed into un-weathered ~ 1-inch chips and then crushed to < ½ cm pieces using the rock crusher at Portland State University. At WSU, sample preparation followed the analytical procedures of the GeoAnalytical lab at WSU and are outlined in Appendix B: XRF & ICPMS procedures (WSU). Chips for each sample were ground to powder using a low Ta-Nb tungsten carbide swing mill and then mixed using 2:1 pure dilithium tetraborate ($Li_2B_4O_7$). This mixture was then fused in charcoal crucibles at 1000°C in a muffle furnace for 5 minutes and then allowed to cool. The bead is then reground in a swing mill and a portion of the powder is set aside. The rest is fused again in the furnace for another 5 minutes at 1000°C resulting in a glass bead. Approximately 5 mg of powder set aside was analyzed using the ICP-MS at WSU, and the glass beads were analyzed using the XRF at WSU.

Statistical Methods

Ashley Steiner's supervised machine learning program leverages linear support vector machines and a learning database of 3,700 CRBG XRF samples to examine individual geochemical features and classify unknown unknown lavas into formations, members, and flows (Steiner and Wolff, 2020).

Thin Sections

Thin sections of 110 sampled dikes in the northern and southern portions of the CJDS were made for petrographic analysis. Thin sections were prepared at Spectrum Petrographics located in Vancouver Washington. To produce the thin sections, samples were cut into a billet

measuring approximately 1 x 2 inches, then attached to 1.5 mm glass using an optically non-interfering adhesive. Next, the sample was cut to approximately 1/6 of an inch thick, then ground down to 40 microns using a polariscope to measure thickness. Finally, the thin sections were polished for microprobe analysis using 0.5 mm diamond grit. Full slide photographs of each thin section were taken at Spectrum Petrographics using a custom 3D printed lightbox and a Sony Alpha A7R II using a macro lens.

$^{40}Ar/^{39}Ar$ Geochronology

$^{40}Ar/^{39}Ar$ analysis was acquired at the Noble Gas Mass Spectrometry Lab at Oregon State University (OSU). Samples were initially selected for $^{40}Ar/^{39}Ar$ analysis based on their degree of magmatic evolution within my geochemical data set for the CJDS. These samples included the least and most evolved samples as well as samples within the continuum between those end members. A final group of eight representative samples was selected from this group based on the lack of interstitial alteration in the groundmass as well as a lack of alteration within plagioclase. A second batch of samples for dating was selected based on: 1) dikes belonging to the geochemical type for this area that is reminiscent of the Picture Gorge Basalt that erupted from the Monument dike swarm in central Oregon; 2) dikes identified as having compositions of Wapshilla Ridge basalt of the GRB; and 3) dike samples with compositions spanning the whole range of the CJDS, which could be used to look for age progressive trends.

Sample preparation followed the analytical procedures of the Argon lab at OSU and are outlined in Appendix D: Age Dating Procedures. Un-weathered rock chips of each sample were crushed in an ASC Scientific Jaw crusher model JC-300-Q at OSU. The crusher was taken apart and thoroughly cleaned to avoid contamination between samples. Once crushed into a powder, the samples were sieved using progressively finer mesh ranging from >500 to <180 μm. The fraction to be used from the sieved samples was chosen based on both the dominant crystal size

as well as crystal quality within the groundmass. Each sample was then run over a hand magnet using an amperage of 0.01 A – separating the crystals from the groundmass. The sample was then placed in a sequence of acids (1N HCl, 6N HCl, 1N HNO3, 3N HNO3) and placed in a mild ultra-sonic bath at 50°C using a Branson machine. After acid leeching, the samples are rinsed and dried in a 55°C VWR oven and then crystals with inclusions and ground mass particles were separated out using a Franz model LB-1. Once this process was complete, ideal grains were then hand picked out for irradiation.

Samples were irradiated in quartz vials using the TRIGA experimental reactor at OSU along with Fish Canyon Tuff sanidine to monitor neutron flux (FTC-NM(R98) (4E36-14) (28.201 ±0.023 Ma, (Kuiper et al., 2008). The $^{40}Ar/^{39}Ar$ analysis was performed using the ARGUS VII multi-collector using the incremental heating method until a significant amount of ^{39}Ar was released. Age calculations were performed using ArArExperiments software version 4.6.0.9 using the currently accepted K-decay constant of 5.530 ± 0.097 x 10^{-10} 1/yr (Steiger and Jäger, 1977; Koppers et al., 2003). For all other constants used in the age calculation refer to Table 2 in Koppers et al., (2003). Further details of the analytical procedures are described in Duncan and Keller (2004).

Results

Dike orientation, location, and lithology

Chief Joseph Dike Swarm—Northern Section

In the northern portion of the CJDS a total of 31 dikes were sampled. The northern portion lies north of 45.7 N latitude and is located north of the Wallowa Mountains. Dikes were sampled along the Grand Ronde River by raft, from Troy, Oregon to Rogersburg, Washington, and along Joseph Creek in Washington as seen in Figure 6 . Dikes sampled in the north had a characteristic

dominant strike of NNW (Morris et al., 2020). These dikes are tholeiitic basalt to basaltic andesites, are extremely dense, and range in color from black, grey, to bluish grey. Dikes exclusively intrude older CRBG lavas (Figure 10) and often have glassy margins and are generally fine-grained aphyric (Figure 19) to sparsely plag-phyric (Figure 20).

Northern dikes have horizontal columnar jointing (Figure 11) or massive texture, as well as vertical relief in valleys (Figure 10). They range from 1.4 m to 11 m in width with an average of 5 meters (Figure 9). Some show vertically oriented vesicle bands along margins suggesting devolatilization during ascent (Figure 12). Field photos show characteristic dikes found in the northern portion of the CJDS.

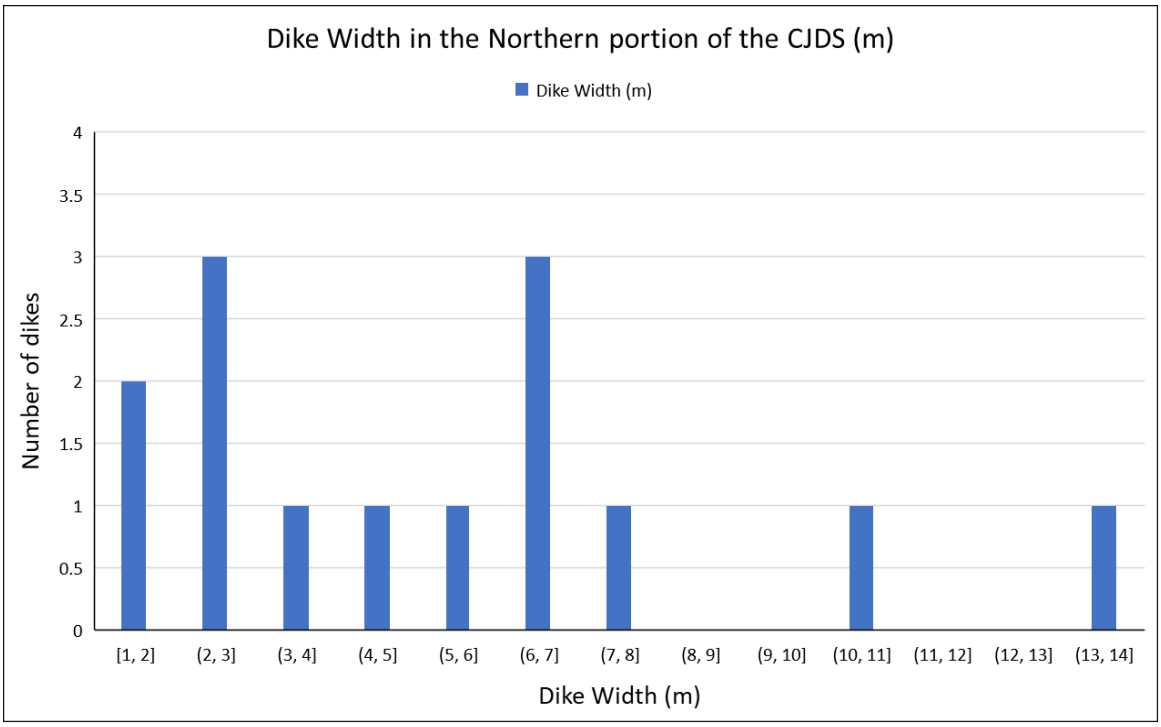

Figure 9. Dike width in the northern portion of the CJDS.

Figure 10. Photo of dike MM-CRB-62 taken along strike and sampled along the Grand Ronde River at 46.0371493, -117.2065328, showing vertical relief as well as the crosscutting relationships of northern dikes, intruding older CRBG flows.

Figure 11. Dike MM-CRB-58 showing horizontal columnar jointing.

Figure 12. Dike MM-CRB-69 showing vertically oriented vesicle bands along margins suggesting devolatilization during ascent.

Chief Joseph Dike Swarm—Central Section

The central portion of the CJDS includes the Wallowa Mountains in eastern Oregon and the surrounding low-lying areas. Samples were collected along the Snake River in Hells Canyon at the Brownlee Reservoir, along Little Sheep Ck. Hwy, and a stop along hwy. I-82 (Figure 7). In the Wallowa Mountains, sampling was mainly done in a glaciated valley just south of Red Mtn. and north of Cornucopia Peak (Figure 7).

Dikes in the Cornucopia area of the Wallowa Mountains exclusively cut through granite above approximately 1800 m in elevation. Below this elevation, dikes intrude CRBG flows instead. Although the CRBG flows are lower in elevation here they are younger than the granite in the area, they are on the downthrown block of normal faults. Dikes in the low-lying areas around the Wallowa Mountains intruded metamorphic country rocks of the Wallowa terrane or CRBG lavas. Like in the north, the dominant strike of dikes in this area is north or NNW as is typical of the CJDS elsewhere. However, there were dikes sampled, especially in the Wallowa Mountains, that had atypical strikes (Figure 7). In the central portion, the dike width ranged from 70 cm to 20.1 m wide with an average of 8.5 m (Figure 13). Twenty-six dikes were sampled in the Wallowa Mtn. area and twenty were sampled in the low-lying areas around the Wallowas. Dikes in the Wallowas that were sampled intrude granite, have dikelets (very thin dikes that can branch off of larger dikes or be solitary), and can have granite lenses present

within the dike (Figure 14, Figure 15). Dikes in the low-lying areas intrude older CRBG flows and metamorphic terrain in Hells Canyon in the lowlands.

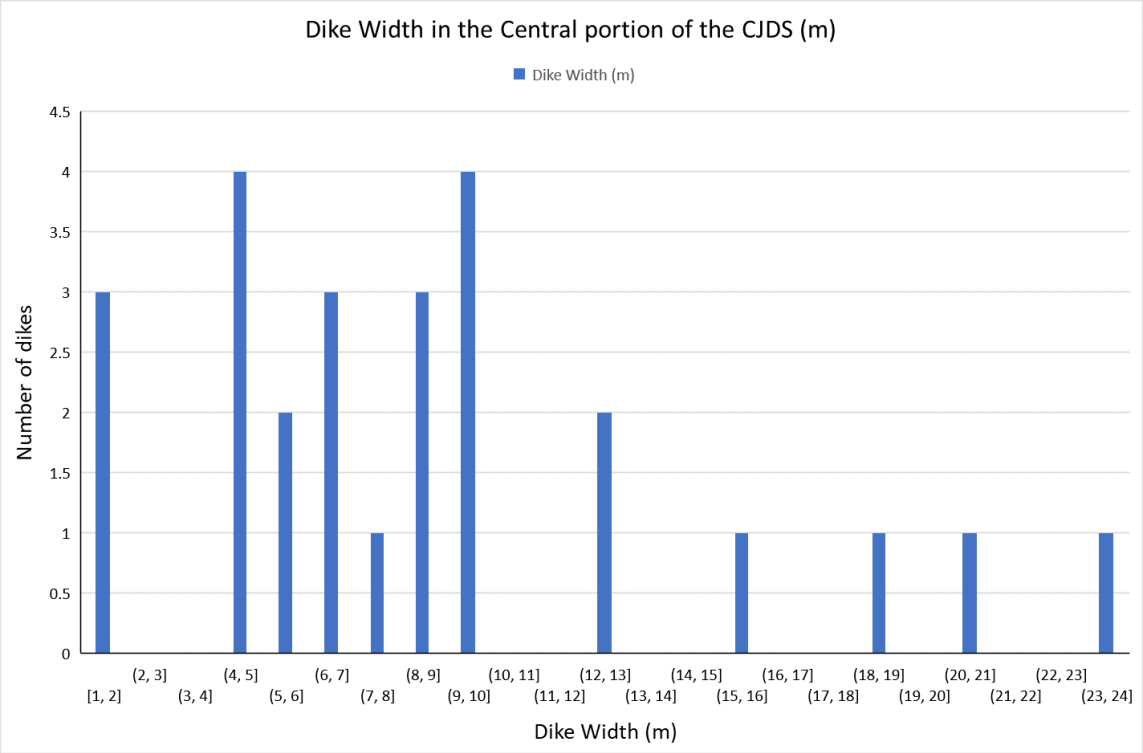

Figure 13. Dike width in the Wallowa Mtns and surrounding low lying areas.

Figure 14, A dikelet in granite plutons in the Wallowas.

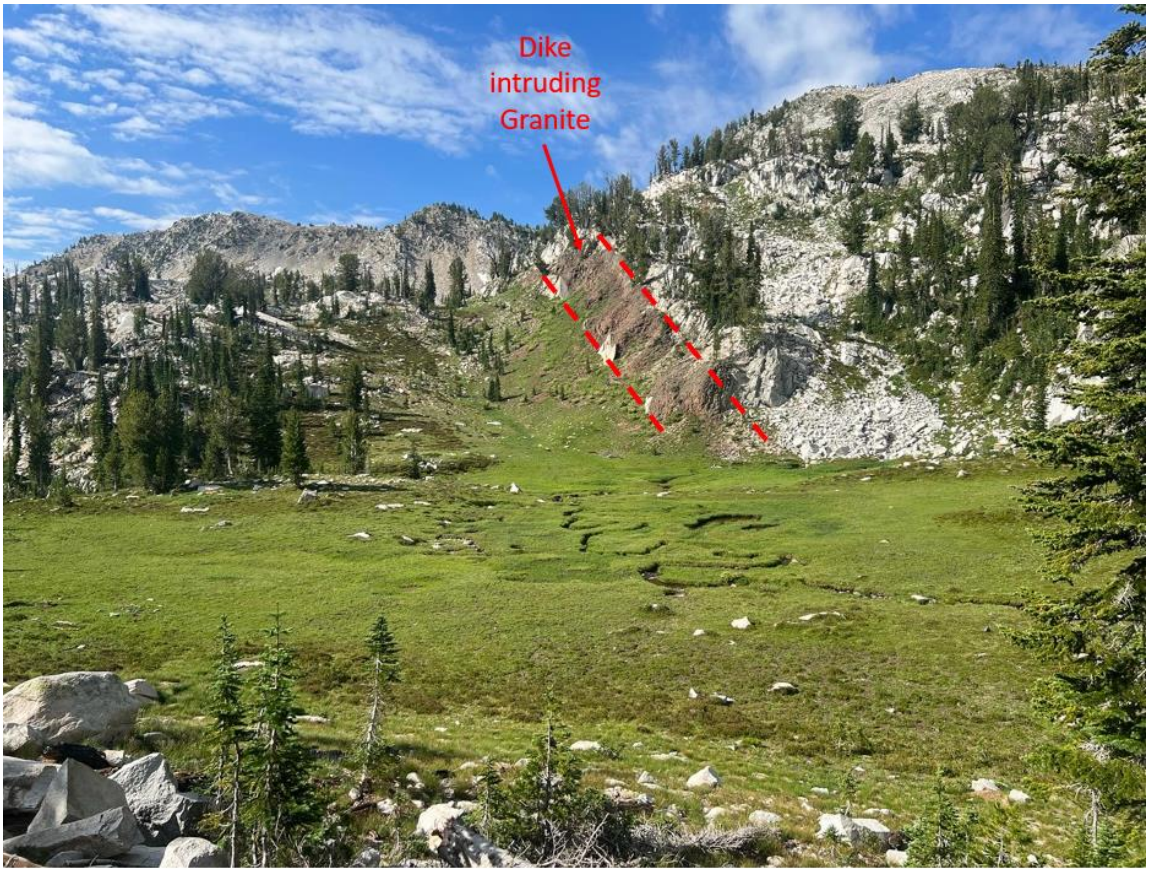

Figure 15. Dike in the Wallowas intrudes a granite pluton in a glaciated area.

Chief Joseph Dike Swarm—Southern Section

In the south, dikes were sampled in the following general locations: Big Lookout Mtn., San Pedro Mtn., and along the Snake River north of Huntington, OR as well as along Rye Valley Rd, Lime, near Brogan, and the Brownlee reservoir (Figure 8). The total number of dikes sampled in these areas is 69. The dominant strike is N to NNW in this region, typical of the CJDS. Dikes in the south range from 5 to 10 m and has an average width of 9 m (Figure 16).

Dikes in the south have little to no vertical relief and are typically massive in texture with the less well-preserved exhibiting conchoidal weathering patterns. Dikes in this southern section intrude metamorphic rocks that include schist and some limestone of accreted terranes or granodiorite plutons (Figure 17). Texturally these dikes range from being coarsely porphyritic

with plagioclase phenocrysts between 0.3 - 2 cm (Figure 19) to aphyric or sparsely phyric (Figure 20).

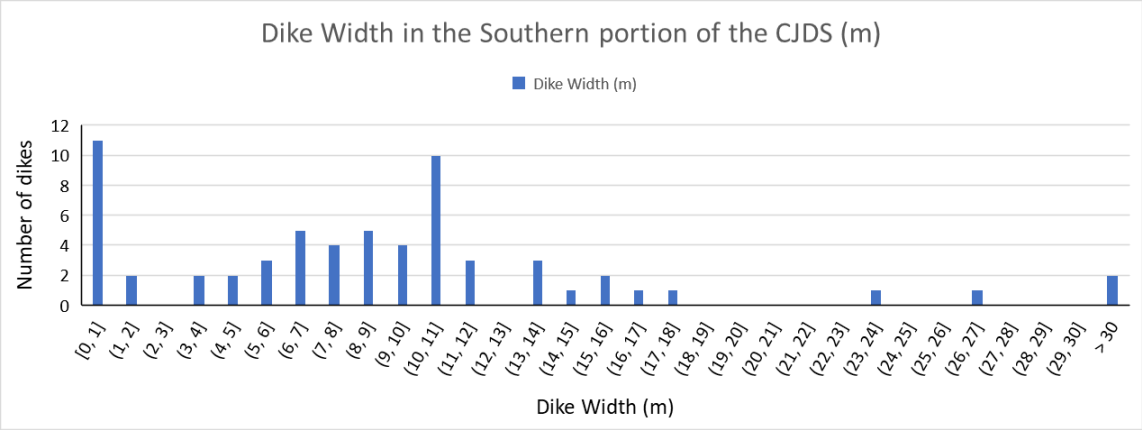

Figure 16. Dike width in the Southern portion.

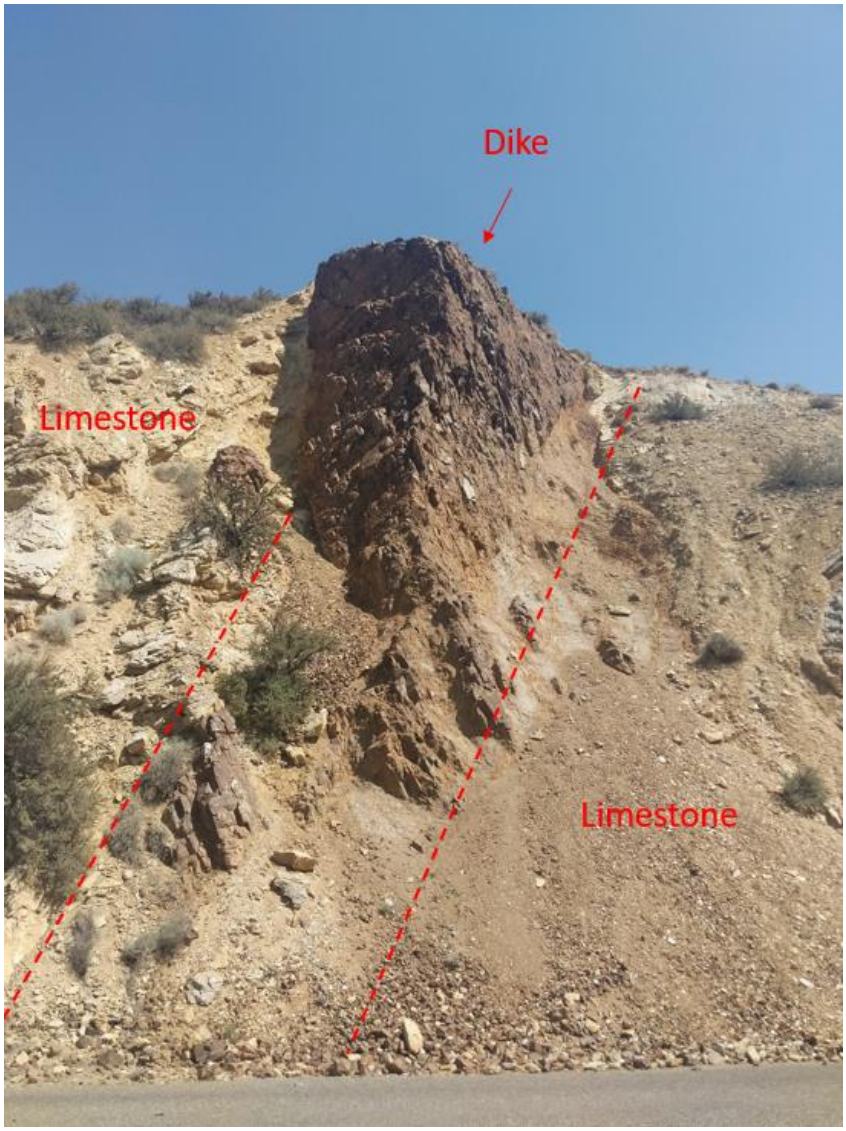

Figure 17. Dike MM-CRB-78 shown with limestone contact.

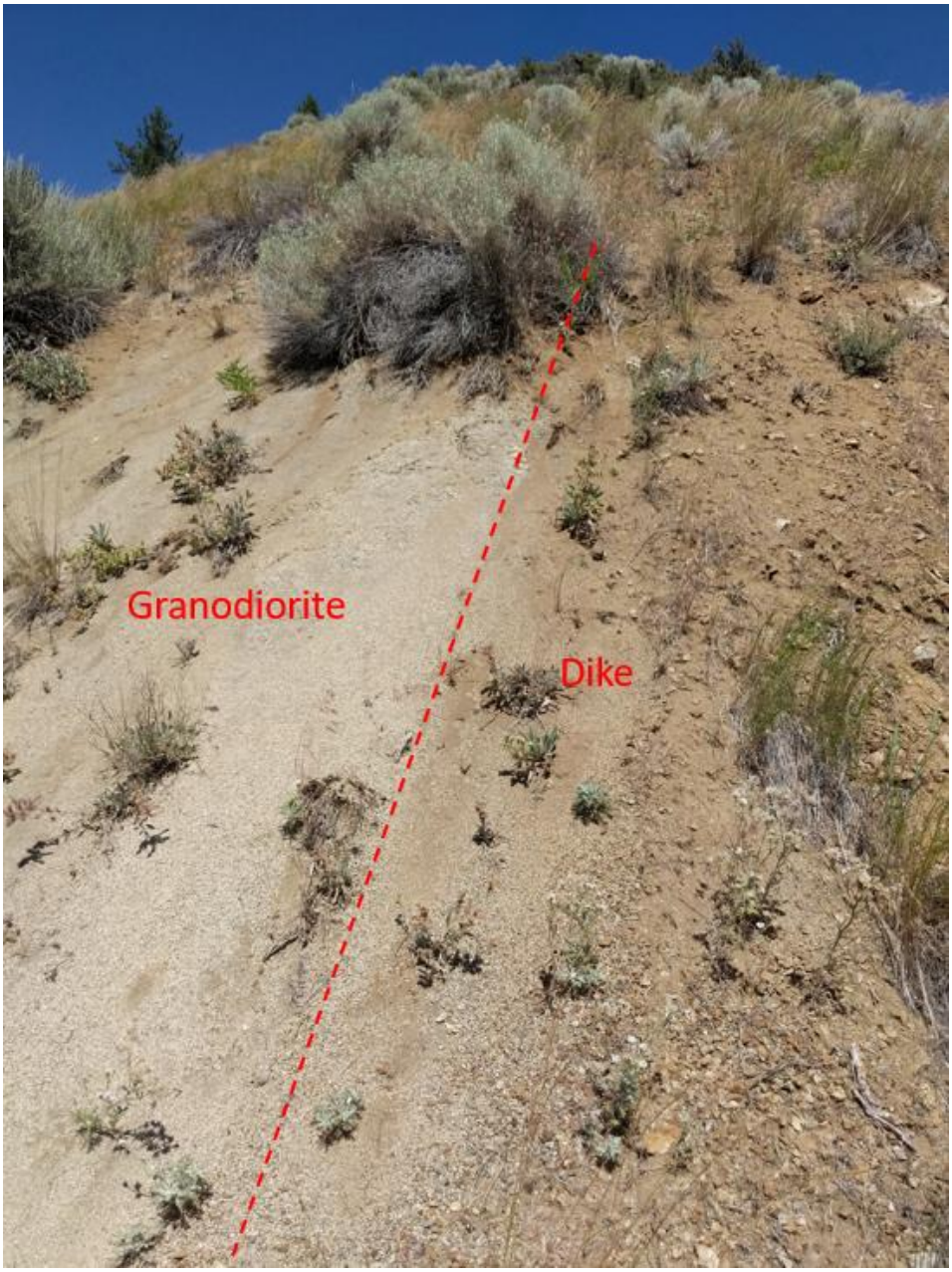

Figure 18. Dike MM-CRB-18b intruding a granodiorite pluton south of Pedro Mountain.

Figure 19. Sample MM-CRB-05 showing cm sized plagioclase phenocrysts.

Figure 20. Sample MM-CRB-08, an example of an aphyric sample in the south.

Composition of Chief Joseph dikes

The sampled dikes of the Chief Joseph dike swarm display a compositional diversity that captures the compositional range of subaerial CRBG lava flows from the early eruptions of the Imnaha Basalt to later units such as the lavas of the Wanapum (Figure 21). This broad range of compositions is represented across the dike swarm, but dikes of more localized areas can capture most of the compositional array of the combined data set (Figure 22 through Figure 29 arranged from southernmost locality of the CJDS going northward).

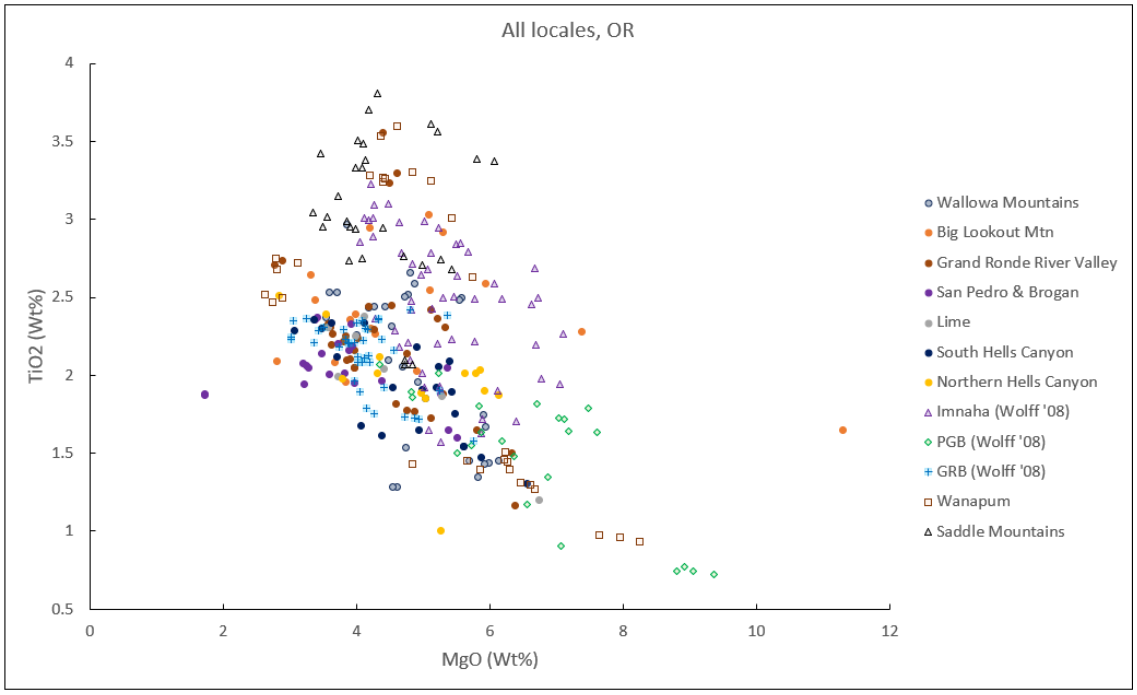

Figure 21. Samples from this study are plotted with TiO2 vs. MgO - two of the diagnostic elements of the CRBG.

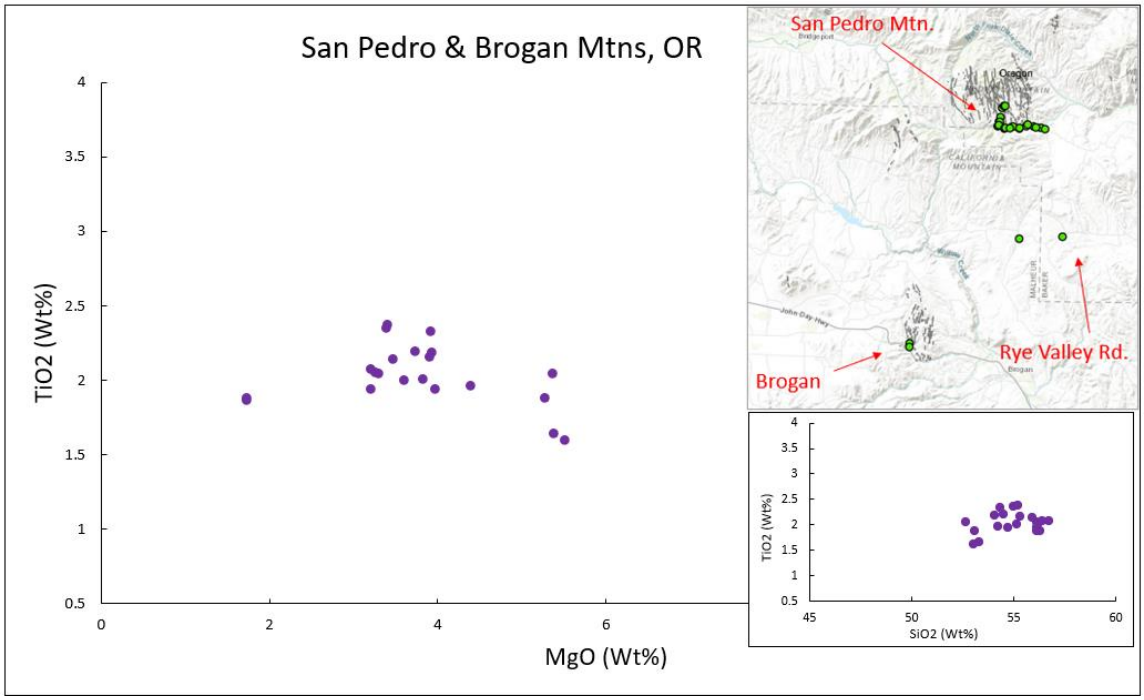

Figure 22. Samples from San Pedro Mtn. and the Brogan area which lies N and NW of Brogan, OR.

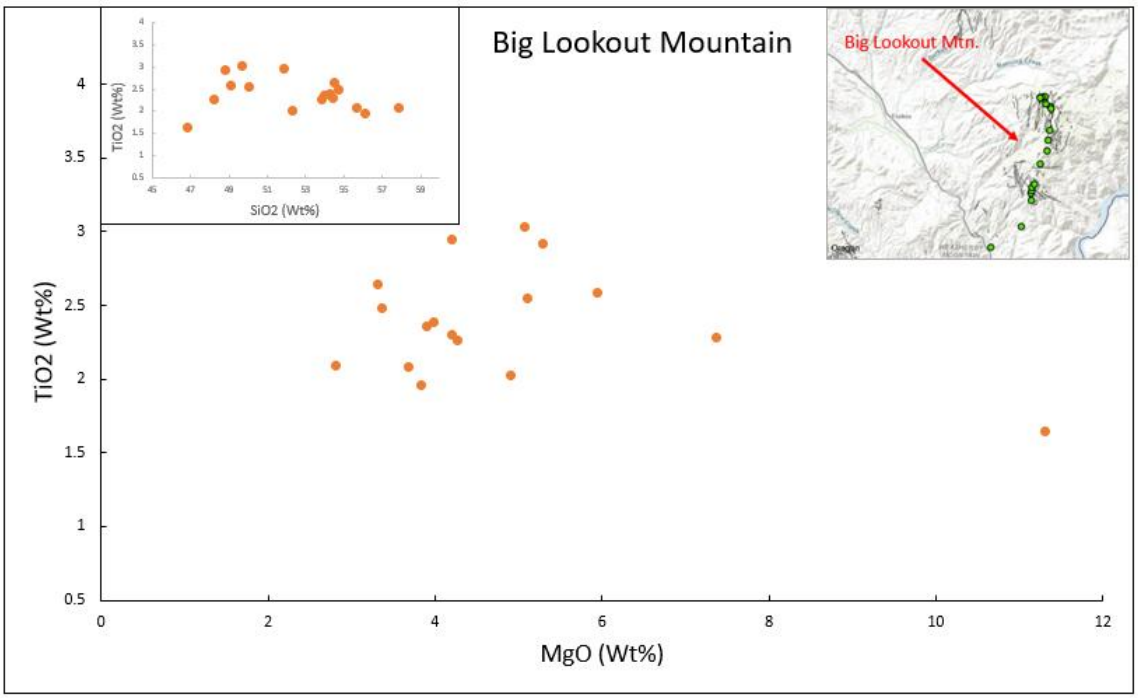

Figure 23. Samples from Big Lookout Mtn. which lies N and NW of Brogan, OR.

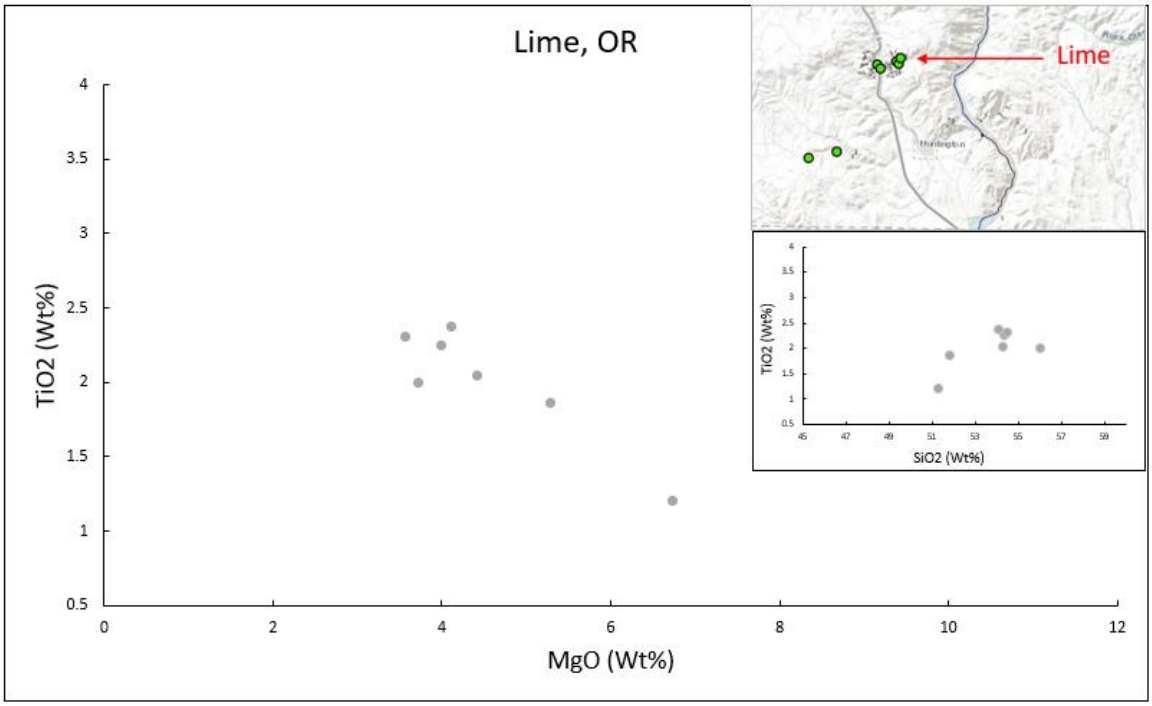

Figure 24. Samples from Lime Oregon which lies E of Brogan, OR.

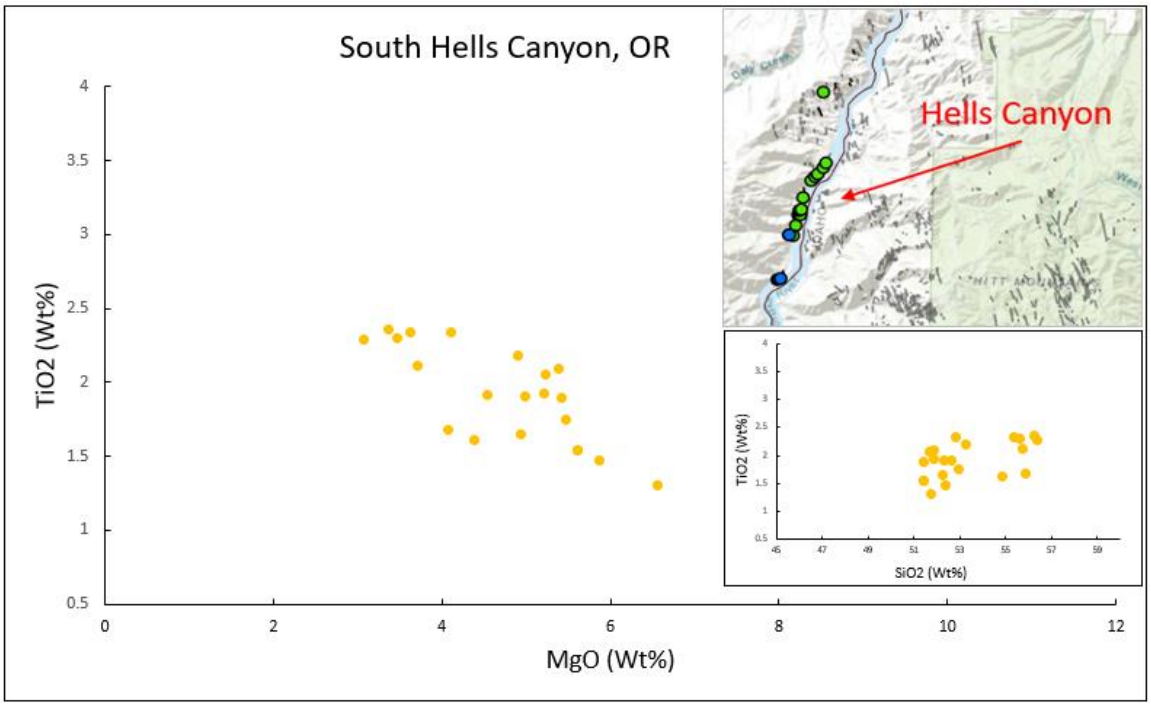

Figure 25. Samples from S. Hells Canyon which lies south of Richland Oregon and north of Ontario, OR.

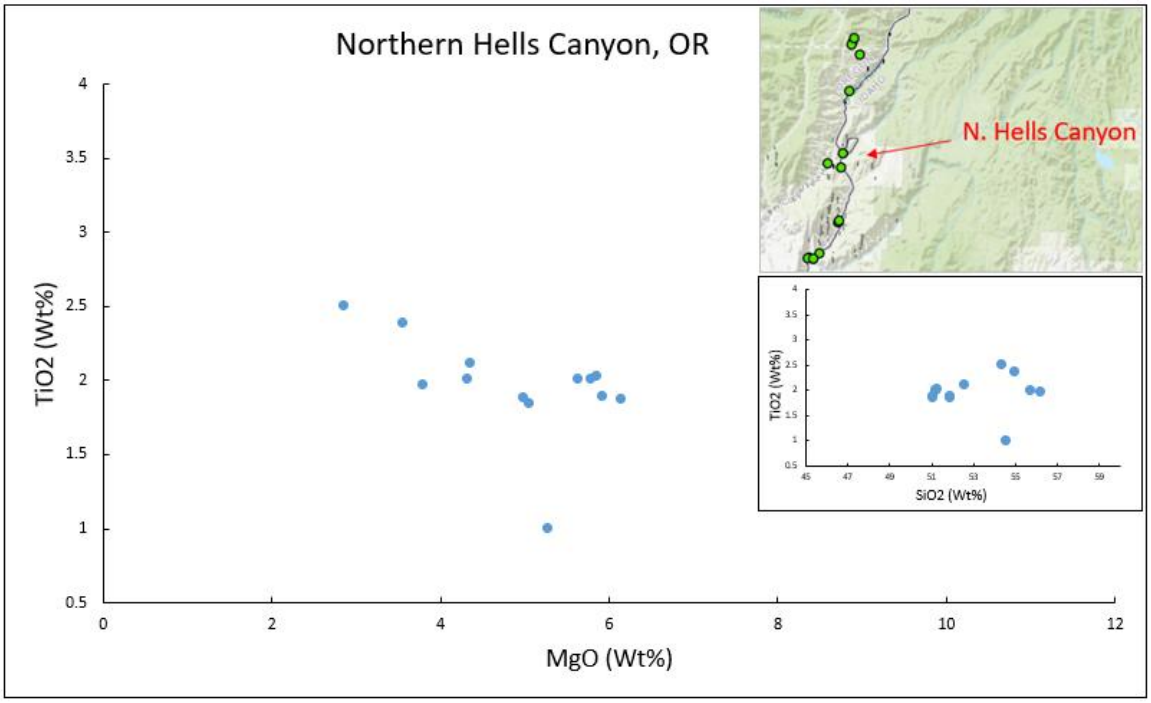

Figure 26. Samples from N. Hells Canyon which lies south of Richland Oregon and north of Ontario, OR.

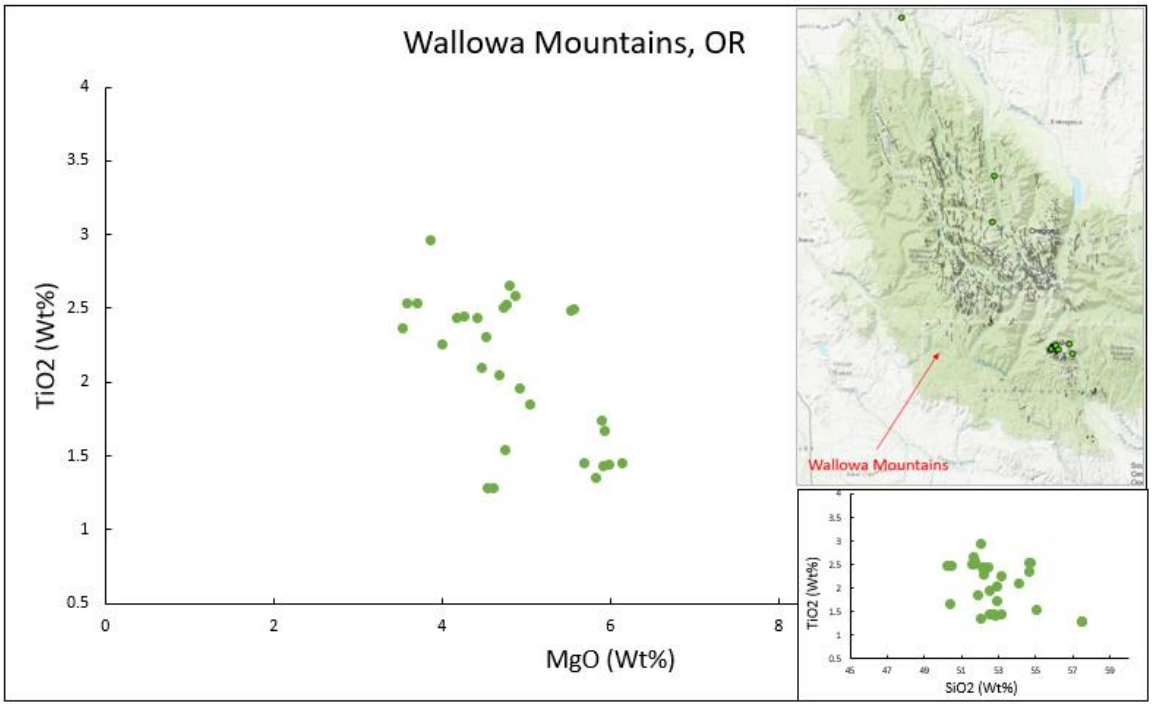

Figure 27. Samples from the Wallowa Mountains which lies North or Big lookout Mtn. and W of Hells Canyon Oregon.

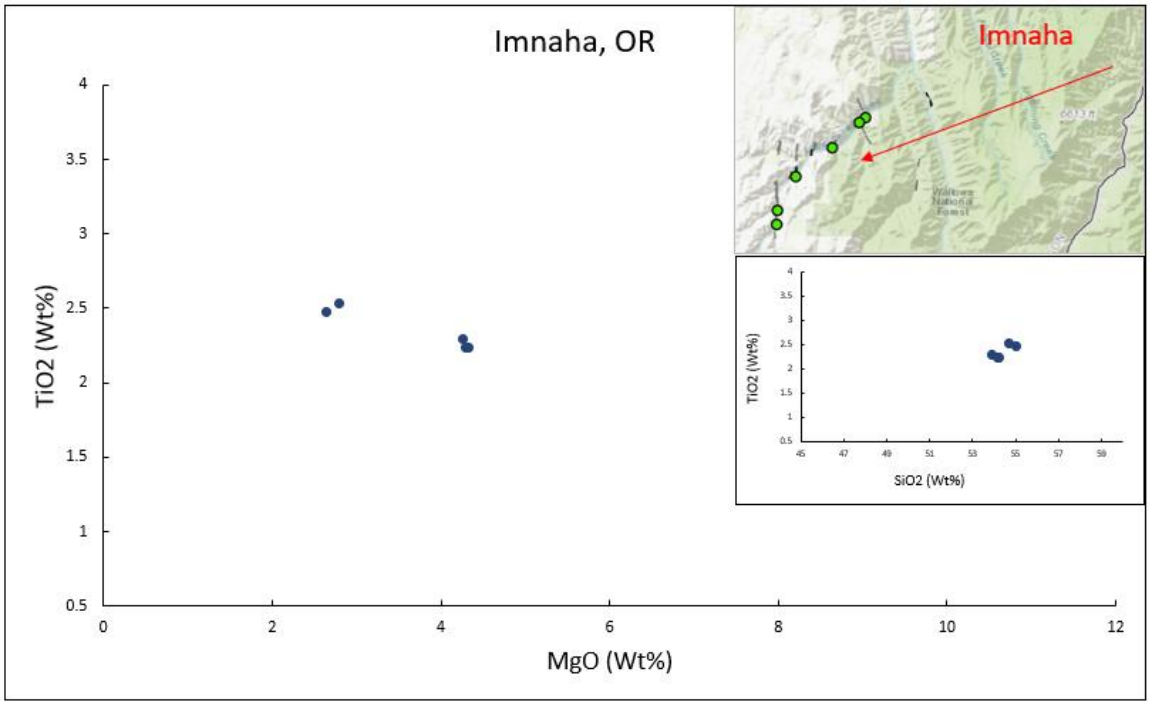

Figure 28. Samples from the Imnaha area which lies NE of the Wallowas and S of the town of Imnaha Oregon.

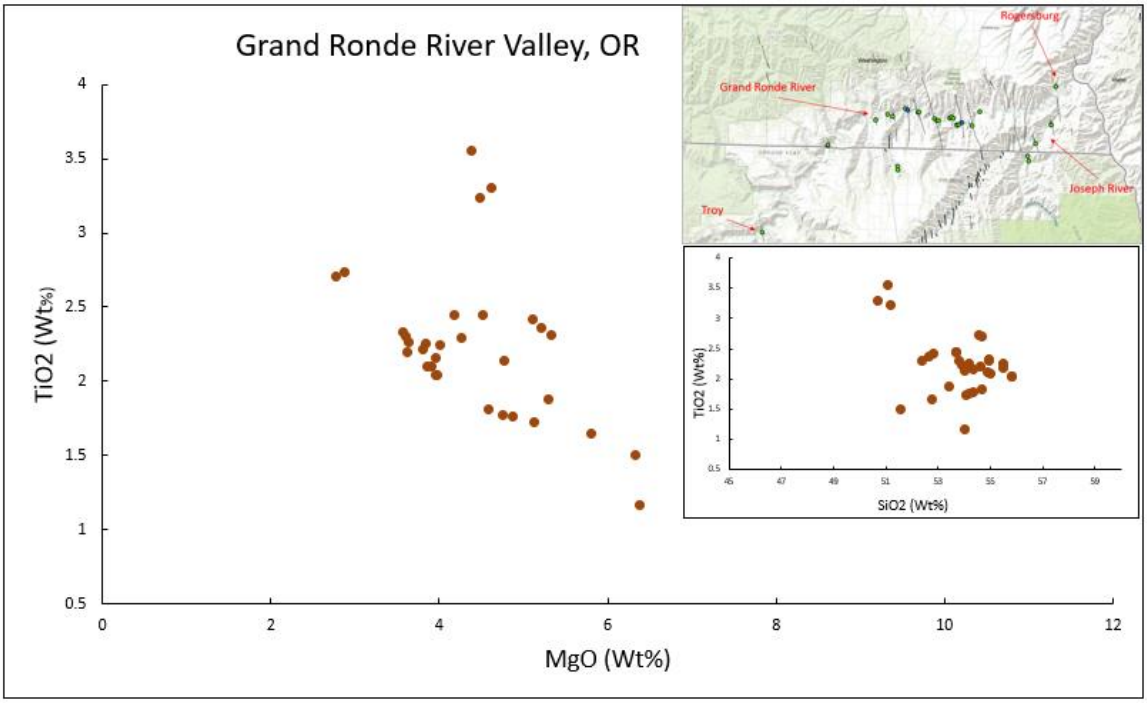

Figure 29. Samples from the Grande Ronde River valley which lies along the WA, ID, OR border.

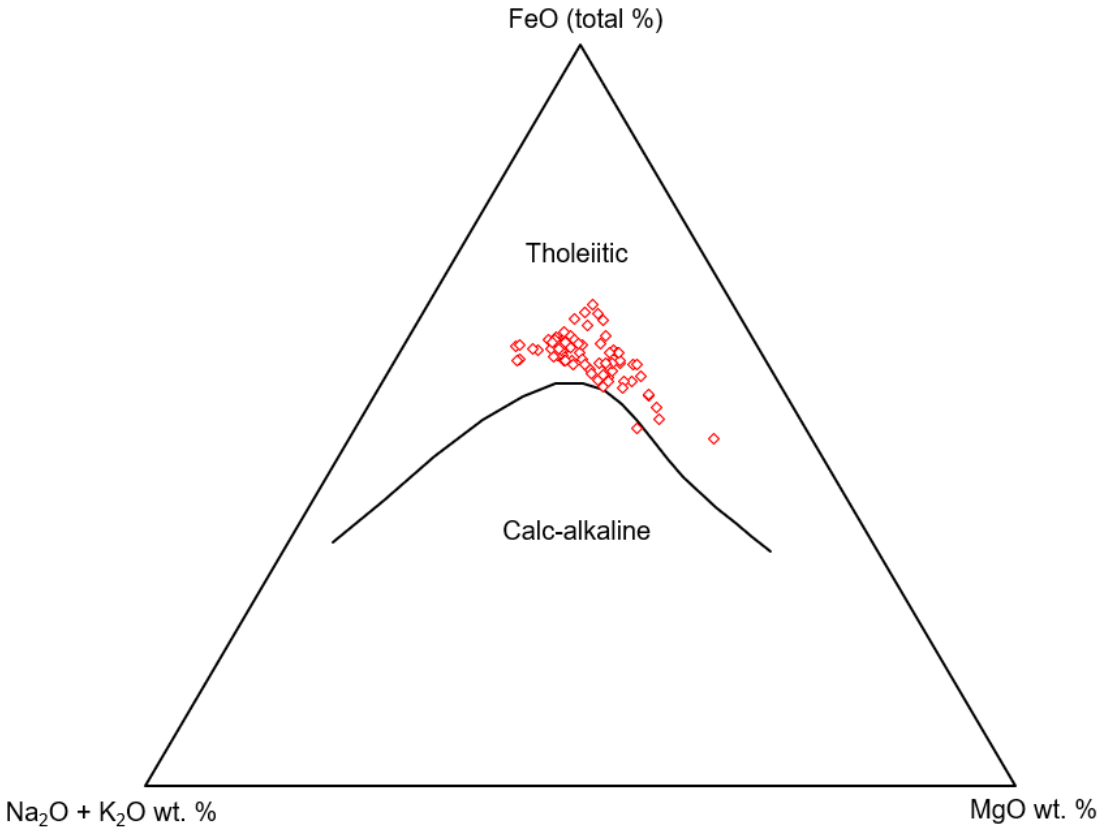

Figure 30. Samples from this study are identified as tholeiites except for sample MM-CRB-97 that straddles the tholeiitic/calc-alkaline boundary. Ternary diagram template from Irvine & Barager 1971 and developed into an excel file by Marshall et al (1996).

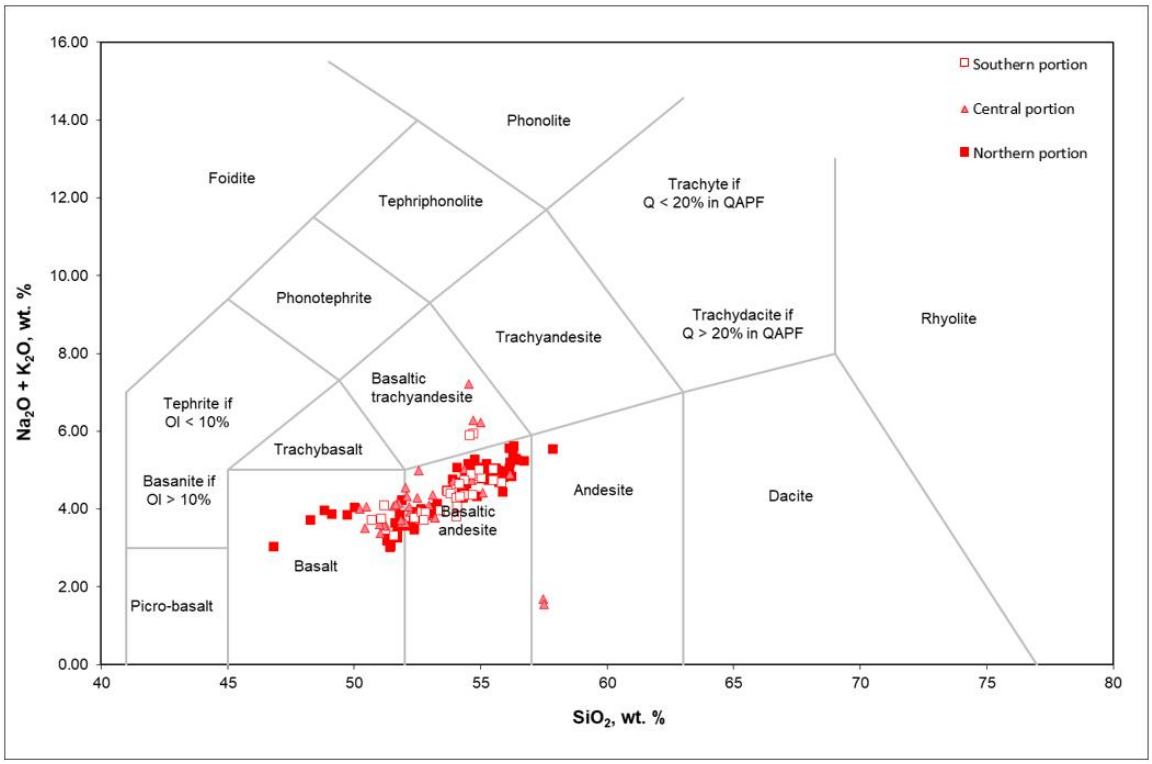

Figure 31. Total alkalis vs. SiO_2 plot showing the geochemical diversity across the strike of the CJDS. Solid red squares are samples in the south, white squares with a red border are samples in the north, while red triangles are samples taken in the central portion of the dike swarm. Total alkali diagram from (Maitre, 1989).

In a total alkali vs. SiO_2 plot, samples collected across the CJDS range from basalt to andesite. There are a handful of samples in the north and central portion of the swarm that are classified as basaltic trachyandesite. Two samples in the central portion and one sample in the south are classified as andesites. About half of the samples collected in the south and the central portions are classified as basalt while the other half are basaltic andesites. By contrast, the samples from the northern portion are predominantly classified as basaltic andesites.

The entire geochemical dataset was initially treated in its entirety to observe compositional ranges and to observe trends without specific consideration of what unit individual dikes may be correlated with. Plotting elemental data of all sampled dikes of the CJDS against SIO_2 reveal two magmatic evolutionary trends (Figure 32). I will refer to the two trends seen in Figure 32 as the low silica trend ranging from 46.82% to 51.19% SiO_2 and the high silica

trend ranging from 51.3% to 58.0%. Most major elements vary systematically along these two trends, with some progressively increasing (e.g. K_2O) and others decreasing (e.g. MgO,). The exception to this variance is MnO (Figure 35).

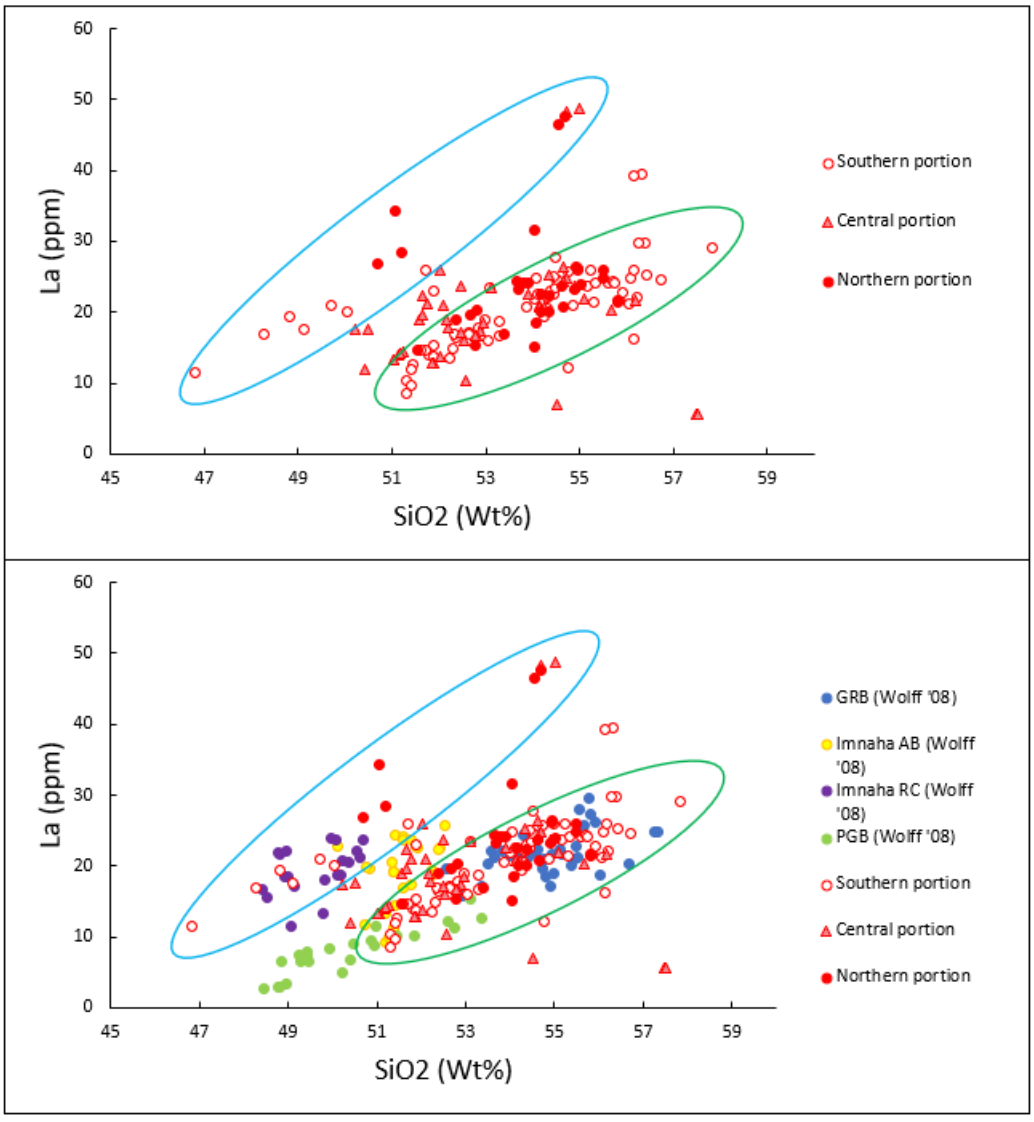

Figure 32. La vs. SiO_2 plot clearly displaying the low SiO_2 and high SiO_2 trend. The blue envelope indicates what we've identified as the low Silica trend from 47% to 52% SiO_2 while the trend seen in the green envelope from 51% to 57% SiO_2 indicates the high Silica trend. Imnaha, GRB, and PGB geochemistry is from (Wolff et al., 2008) and the data in red are from this study.

When compositions of samples from this study are compared to data of main-phase CRBG lava flow units including the Picture Gorge, Imnaha, and the Grande Ronde Basalt (main-phase geochemical data from Wolff et al., 2008), the following is apparent. There are dikes from all sections (northern, central, and southern sections) that define the low Si and high Si trend and the transitional samples. The low silica trend coincides with samples from the Rock Creek subunit of the Imnaha Basalt and the high silica trend with the PGB, lower American Bar subunit samples, and Grande Ronde Basalt. Middle to Upper American Bar Basalt samples fall in between—and—into both trends Figure 32).

Major elements vs. SiO_2

As samples are tholeiitic, they follow the expected magmatic evolutionary pattern seen in tholeiitic suites when plotted against SiO_2 such as in increase in FeO*, TiO_2, $P2O_5$, and K_2O while CaO and MgO decrease. This low and high silica trend can be seen in all major elements vs. SiO_2 except MnO (Figure 35).

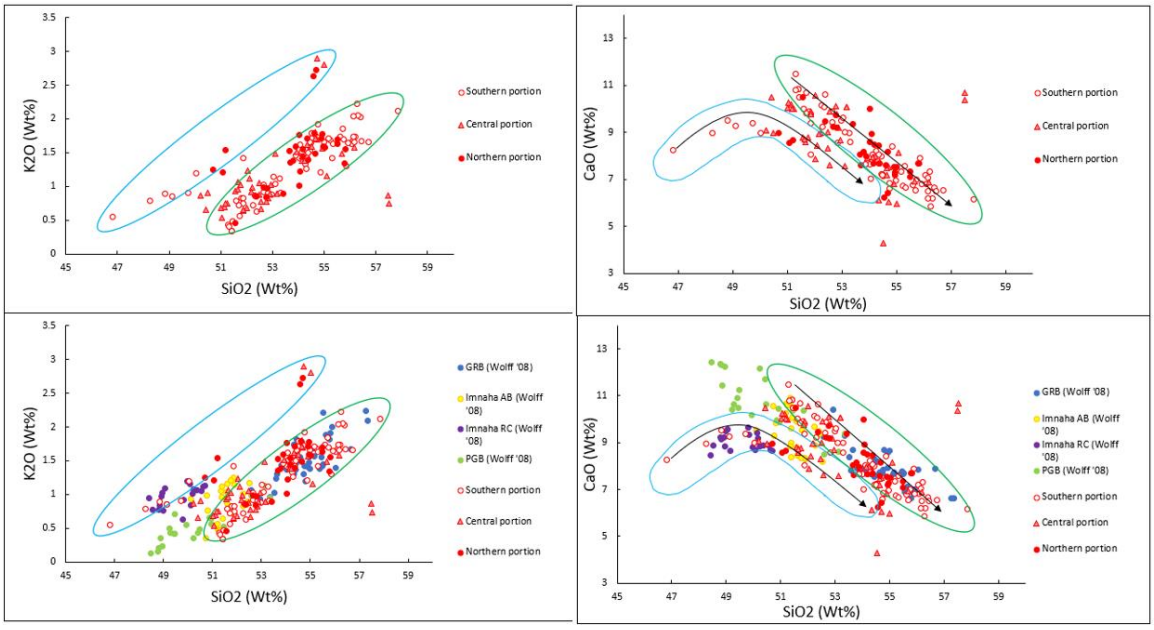

Figure 33. Low and high SiO_2 trends shown in a K2O vs. SiO_2 plot. The blue envelope indicates what has been identified as the low silica trend from 47% to 52% SiO_2 while the trend seen in the green envelope from 51% to 57% SiO_2

indicates the high silica trend. Imnaha, GRB, and PGB geochemistry is from (Wolff et al., 2008) and the data in red are from this study.

The trend in the low silica group seen in the CaO vs. SiO_2 plot indicates that pyroxene is the dominant phase fractionating from the melt until the SiO_2 content reaches ~49.2 wt%. However, pyroxene is not seen fractionating from the high silica group and the decrease in Ca and increase in SiO_2 is due to the fractionation of plagioclase.

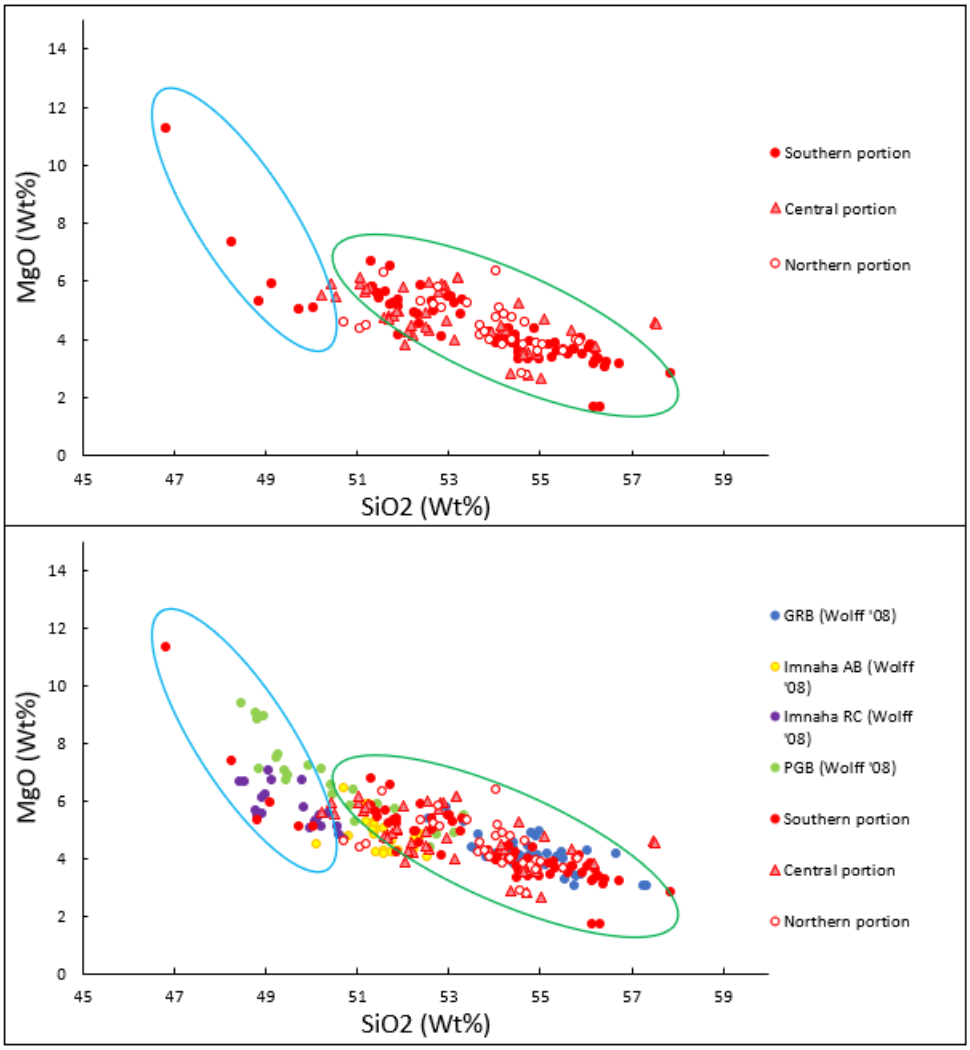

Figure 34. Low and high SiO2 trends shown in a MgO vs. SiO2 plot. The blue envelope indicates what we've identified as the low Silica trend from 47% to 52% SiO2 while the trend seen in the green envelope from 51% to 57% SiO2 indicates the high Silica trend. Imnaha, GRB, and PGB geochemistry is from Wolff et al. (2008) and the data in red are from this study.

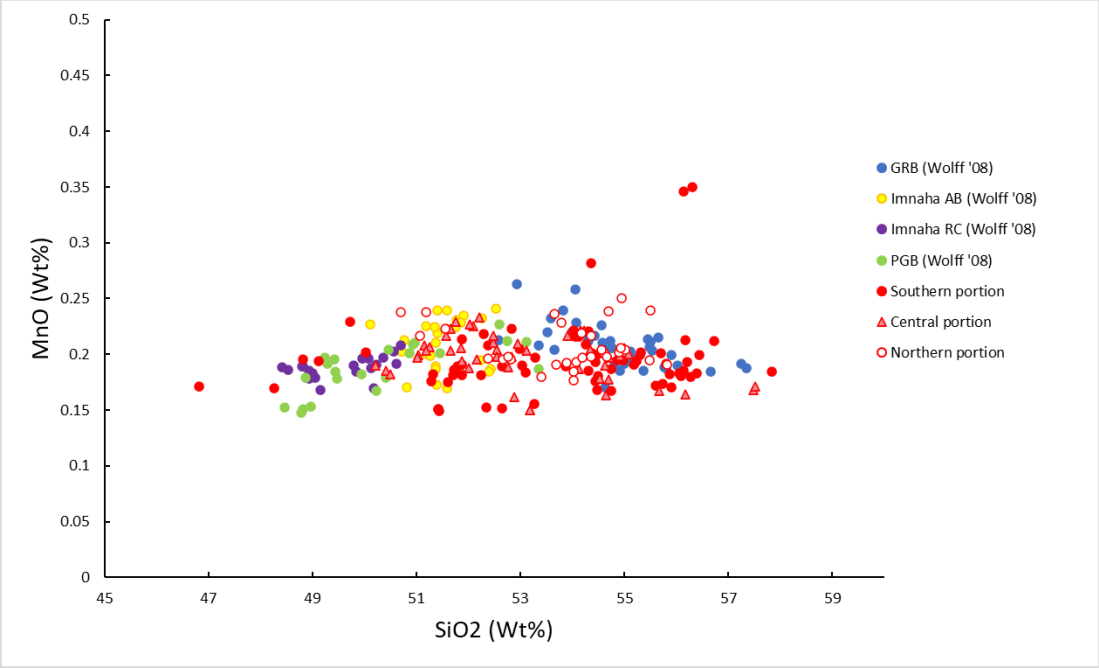

Figure 35. No apparent trend seen in a Mno vs. SiO_2 plot. Imnaha, GRB, and PGB geochemistry is from Wolff et al. (2008) and the data in red are from this study.

Trace elements vs. SiO_2 and MgO

The low and high SiO_2 trends can be seen in all trace elements vs SiO_2 except Cs, likely due to alteration. Select trace element plots are shown below.

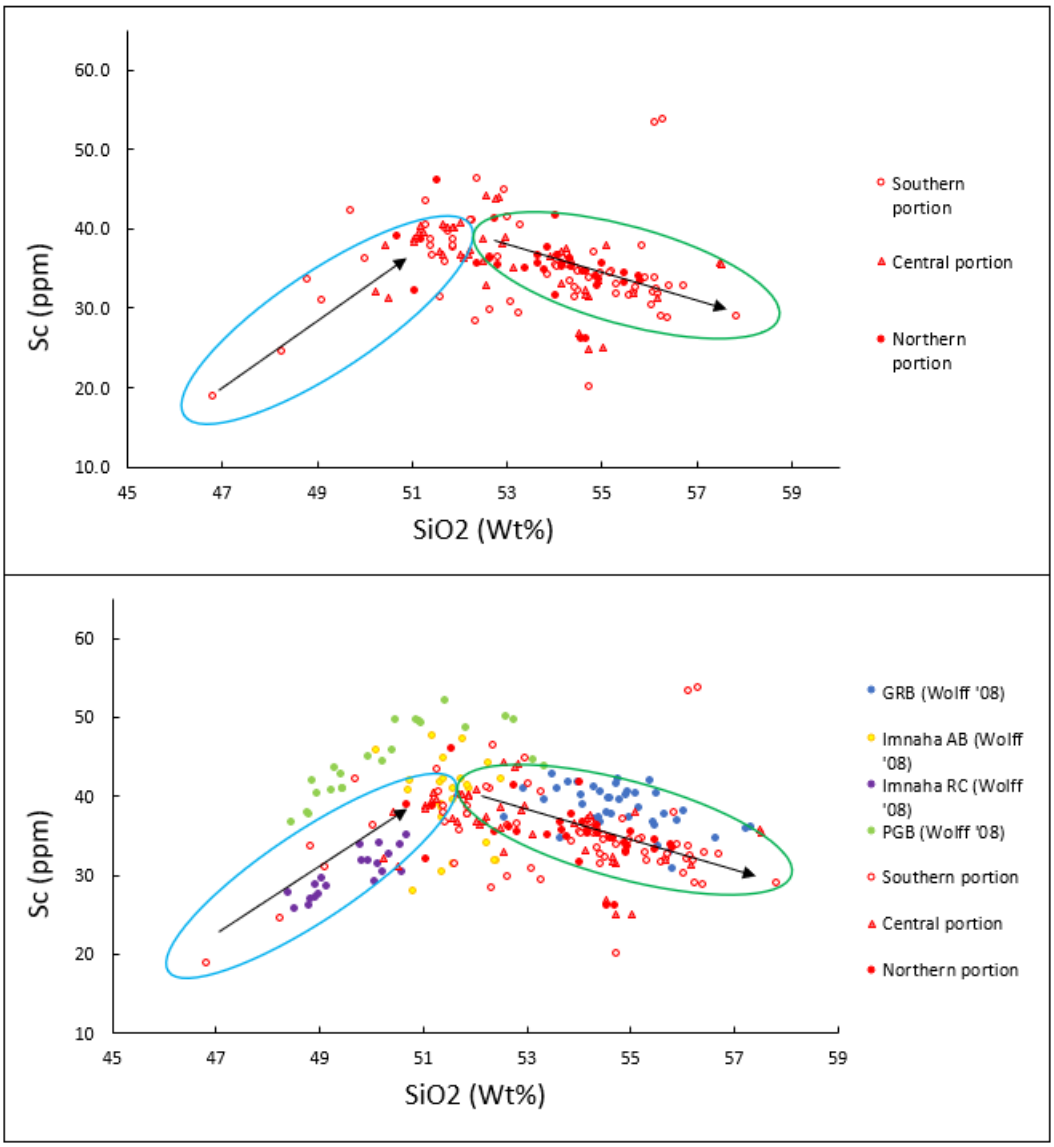

Figure 36. Low and high SiO_2 trends shown in a Sc vs. SiO_2 plot. Scandium is a great diagnostic element as it indicates pyroxene fraction. The blue envelope indicates what we've identified as the low Silica trend from 47% to 52% SiO_2 while the trend seen in the green envelope from 51% to 57% SiO_2 indicates the high Silica trend. Imnaha, GRB, and PGB geochemistry is from Wolff et al. (2008) and the data in red are from this study.

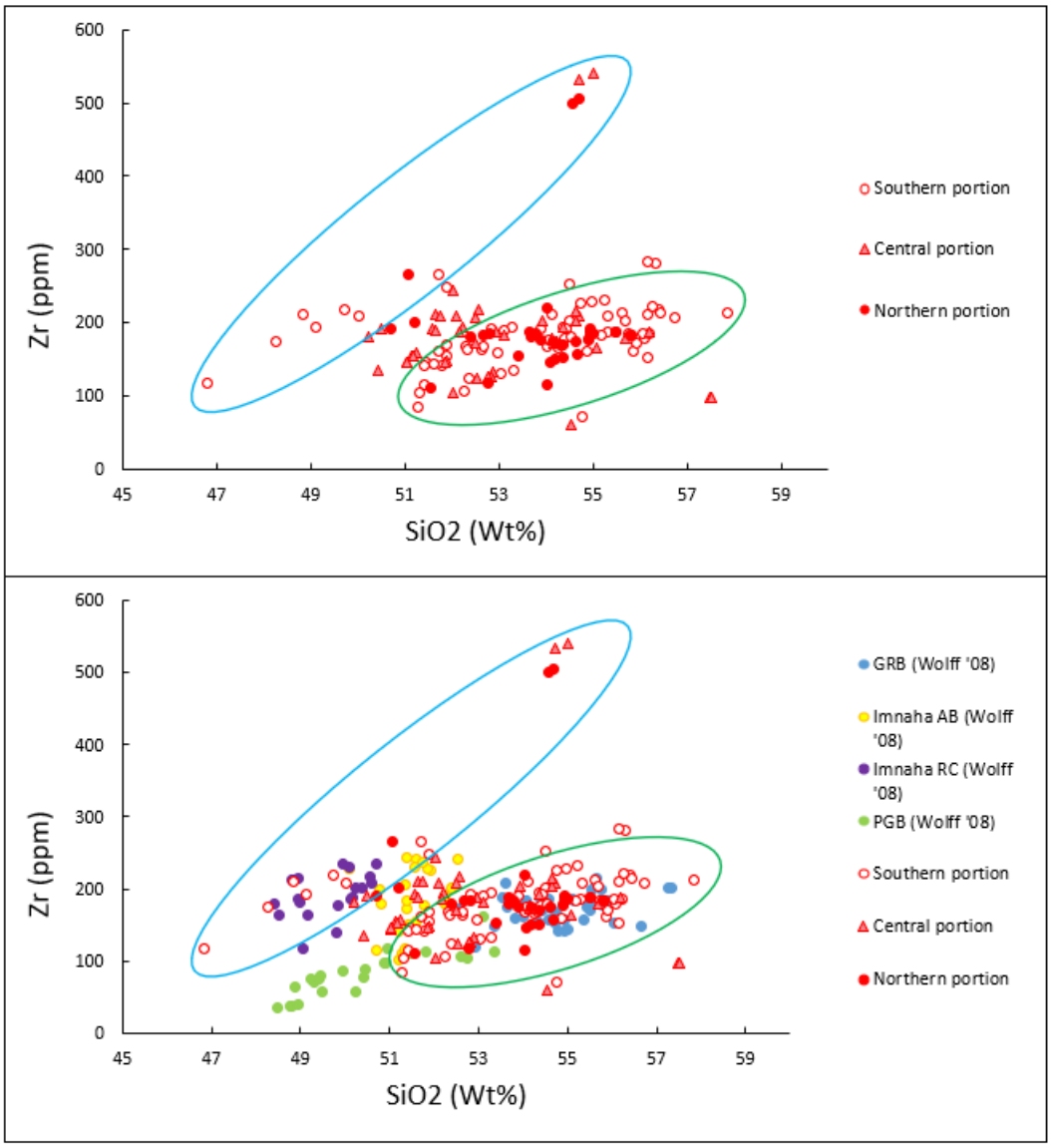

Figure 37. Low and high SiO_2 trends shown in a Zr vs. SiO_2 plot. Zirconium is a diagnostic trace element to differentiate amongst CRBG groups (Reidel et al., 2013). The blue envelope indicates what we've identified as the low Silica trend from 47% to 52% SiO_2 while the trend seen in the green envelope from 51% to 57% SiO_2 indicates the high Silica trend. Imnaha, GRB, and PGB geochemistry is from Wolff et al. (2008) and the data in red are from this study.

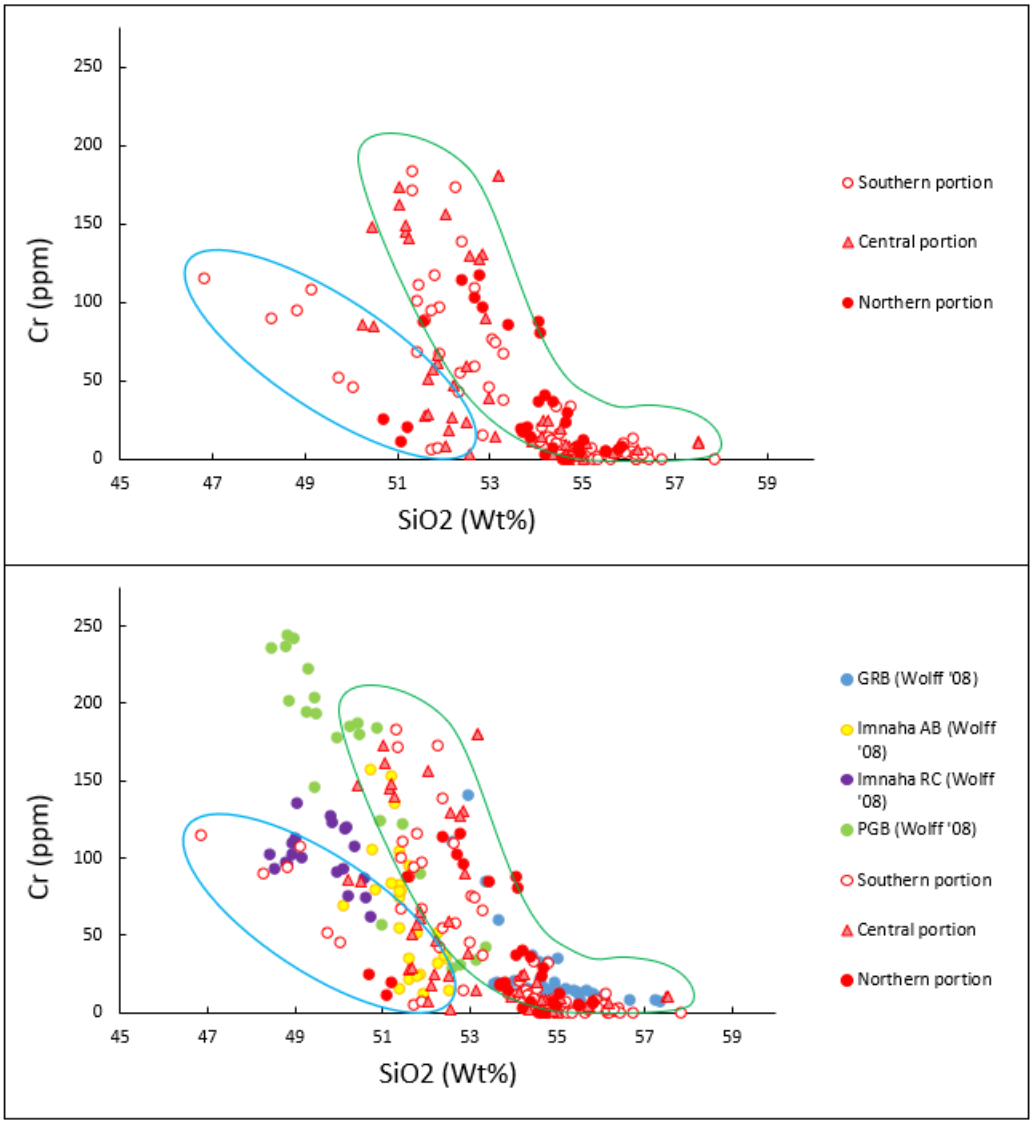

Figure 38. Low and high SiO_2 trends shown in a Cr vs. SiO_2 plot. Chromium is a diagnostic trace element to differentiate amongst CRBG groups (Reidel et al., 2013). The blue envelope indicates what we've identified as the low Silica trend from 47% to 52% SiO_2 while the trend seen in the green envelope from 51% to 57% SiO_2 indicates the high Silica trend. Imnaha, GRB, and PGB geochemistry is from Wolff et al. (2008) and the data in red are from this study.

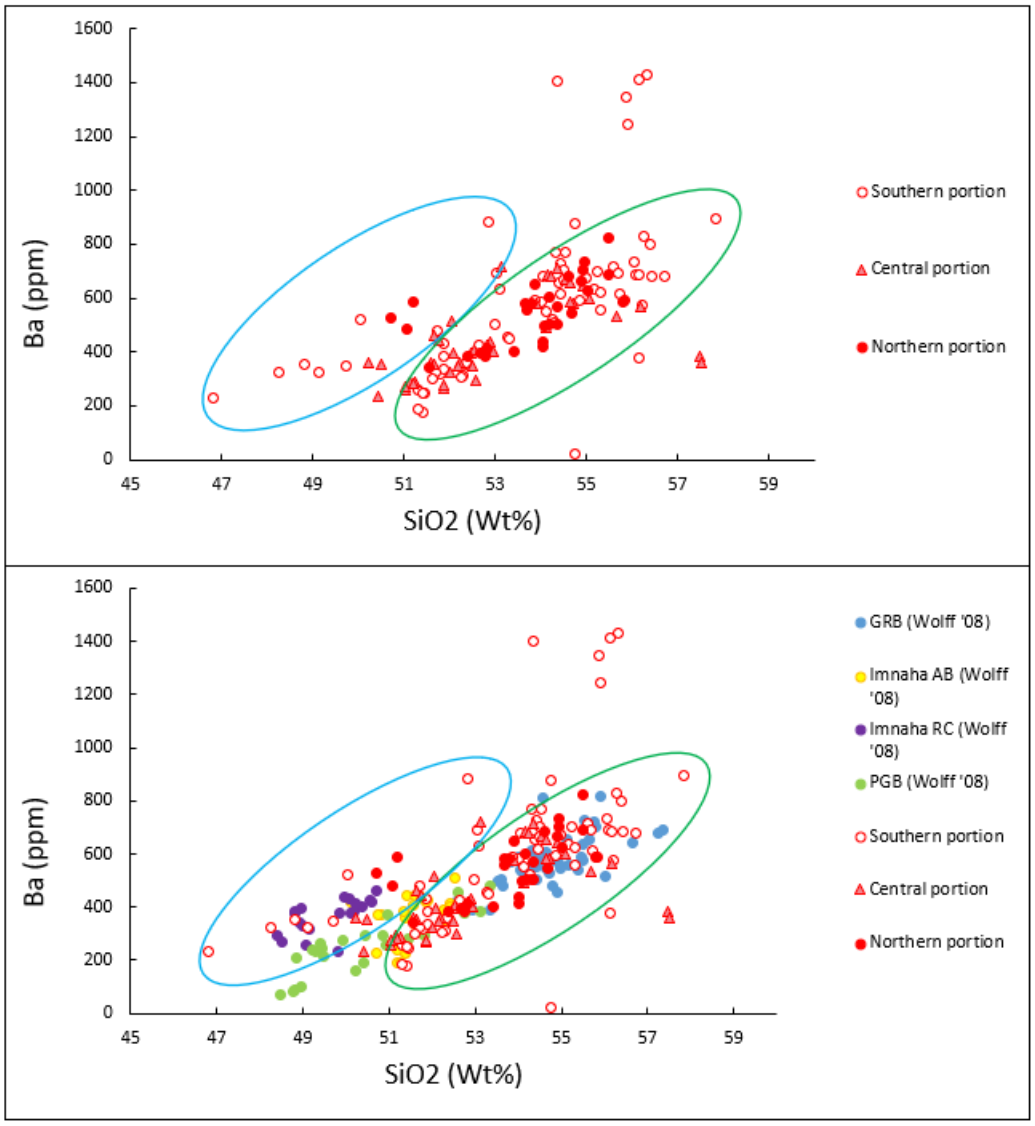

Figure 39. Low and high SiO_2 trends shown in a Ba vs. SiO_2 plot. Barium is a diagnostic trace element to differentiate amongst CRBG groups (Reidel et al., 2013). The blue envelope indicates what we've identified as the low Silica trend from 47% to 52% SiO_2 while the trend seen in the green envelope from 51% to 57% SiO_2 indicates the high Silica trend. Imnaha, GRB, and PGB geochemistry is from Wolff et al. (2008) and the data in red are from this study.

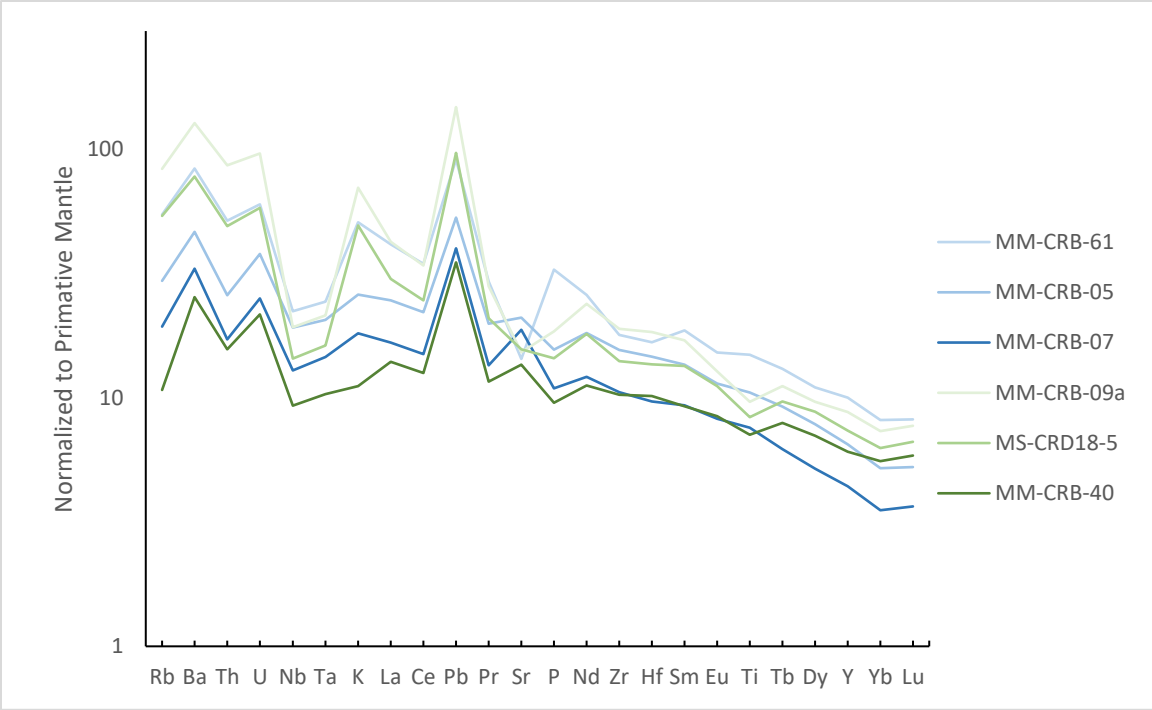

Figure 40. Select samples representative of the range of the low and high silica trends are shown in a mantle-normalized incompatible element diagram (Mantle normalization data taken from Sun and McDonough (1989). The low silica trend is shown in blue with the darkest blue being the highest MgO wt.% and the lightest blue being the lowest MgO wt.%. The high silica trend is shown in green with the darkest green being the highest MgO wt.% and the lightest green being the lowest MgO wt.%.

Select samples from the low and high silica trends and their MgO concentrations in relation to their incompatible trace element concentrations are shown in Figure 40. For both the high and low silica trends, the MgO correlates with the relative abundance of incompatible elements, i.e. the samples with the highest MgO indicate the lowest incompatible elements and while samples with the lowest MgO indicate the greatest enrichment in the incompatible elements. The high silica trend has a broader range of incompatible elements relative to the low silica trend and samples of the high silica-trend have a flatter pattern from Sr to Lu than samples of the low-silica trend. Also notable is that the samples with low MgO have a pronounced Nb-Ta trough.

Geochemical Trends across the strike of the Chief Joseph dike swarm

Along with observing petrographic and geochemical trends within the CJDS, this study is focused on documenting the presence of geochemical changes along the strike of the CJDS which is generally ESE-NNW. SiO_2 concentration increases slightly going north along strike to the ID-OR-WA border.

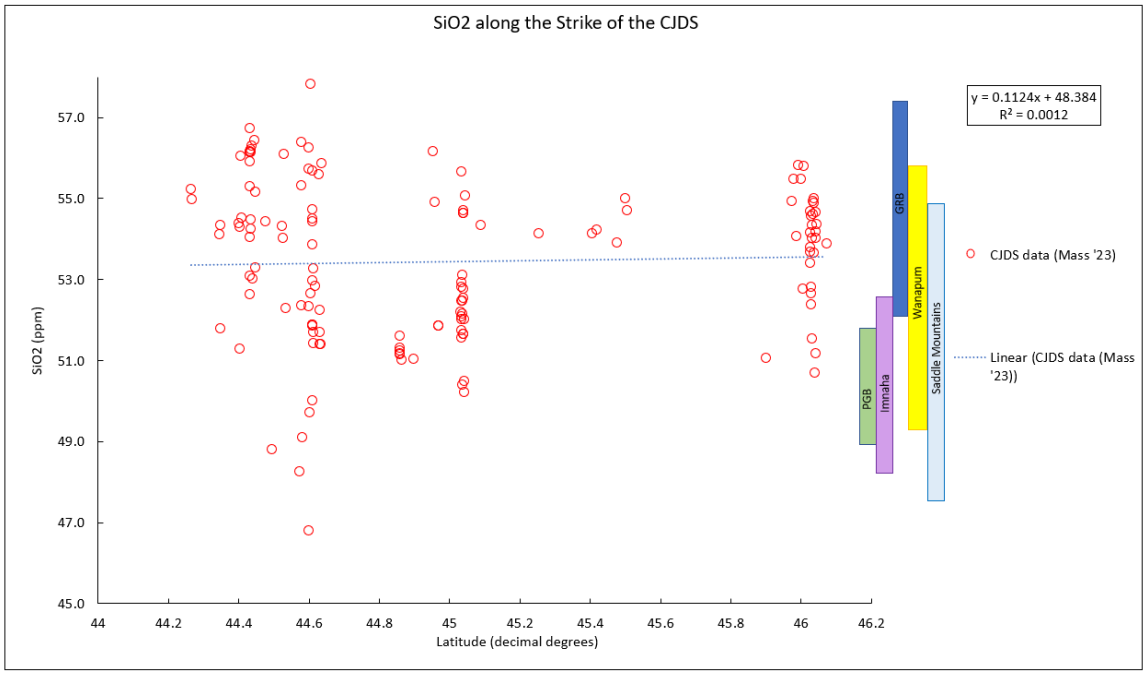

Figure 41. SiO_2 content along strike of the CJDS. Data in red is the CJDS geochemical data from this study. Imnaha and GRB data are from Wolff et al. (2008) and the PGB data are from Cahoon et al.(2020). Wanapum and Saddle Mountain data are from Reidel et al. (2013).

Al_2O_3 concentration decreases going north along strike to the ID-OR-WA border. The GRB has the lowest concentration of Al_2O_3, while the Steens basalts have the highest concentration.

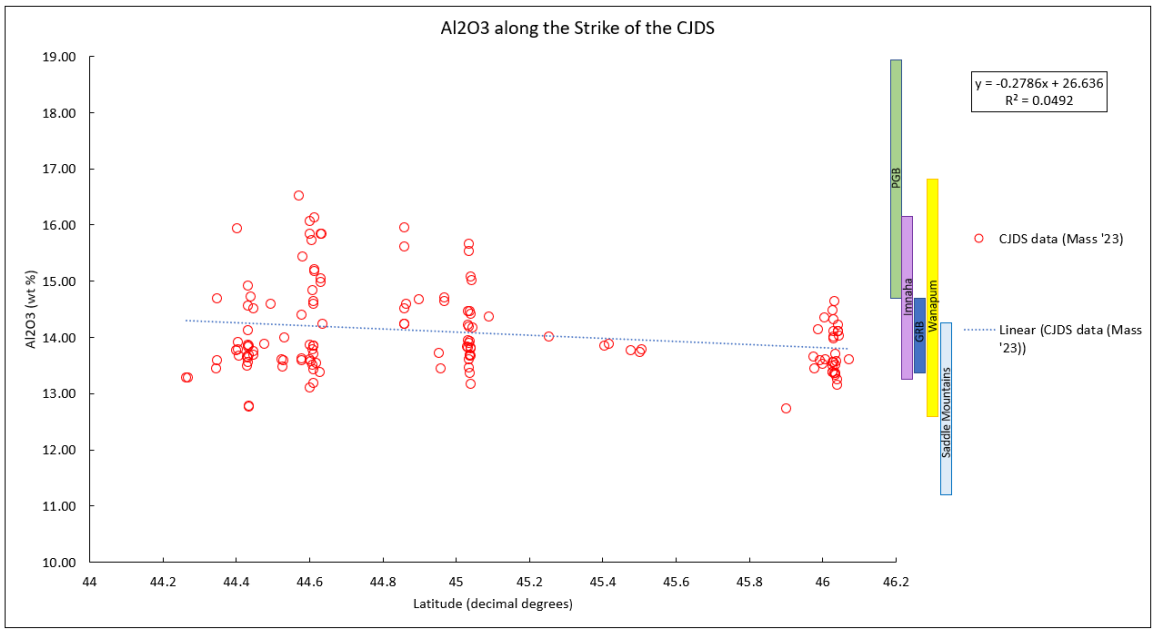

Figure 42. Al_2O_3 content along strike of the CJDS. Data in red is the CJDS geochemical data from this study. Imnaha and GRB data are from Wolff et al (2008) and the PGB data are from Cahoon et al,(2020). Wanapum and Saddle Mountain data are from Reidel et al., (2013).

TiO_2 is one of the diagnostic major elements for the CRBG—particularly for the GRB. The concentration increases going north along strike to the ID-OR-WA border. Samples in the northern area have the largest spread in TiO_2.

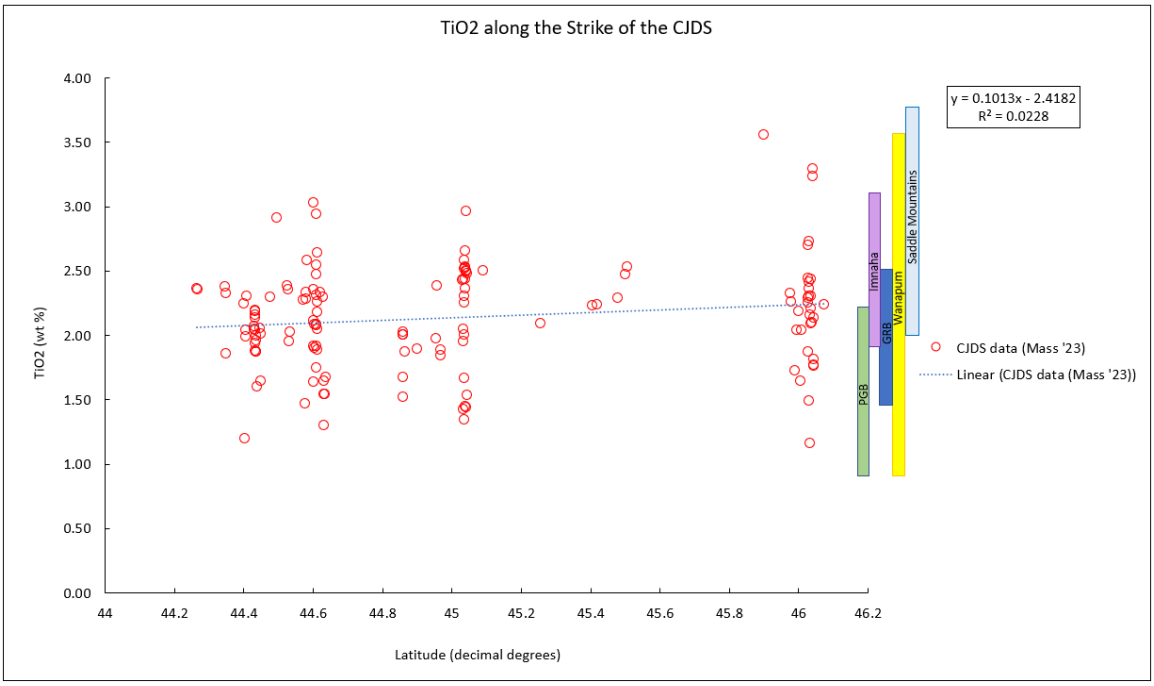

Figure 43. Ti_2O_3 content along strike of the CJDS. Data in red is the CJDS geochemical data from this study. Imnaha and GRB data are from (Wolff et al., 2008) and the PGB data are from (Cahoon et al., 2020). Wanapum and Saddle Mountain data are from (Reidel et al., 2013).

P_2O_5 is one of the diagnostic major elements of the GRB. The concentration increases going north along strike to the ID-OR-WA border. However, there are a few outliers that have very high P_2O_5.

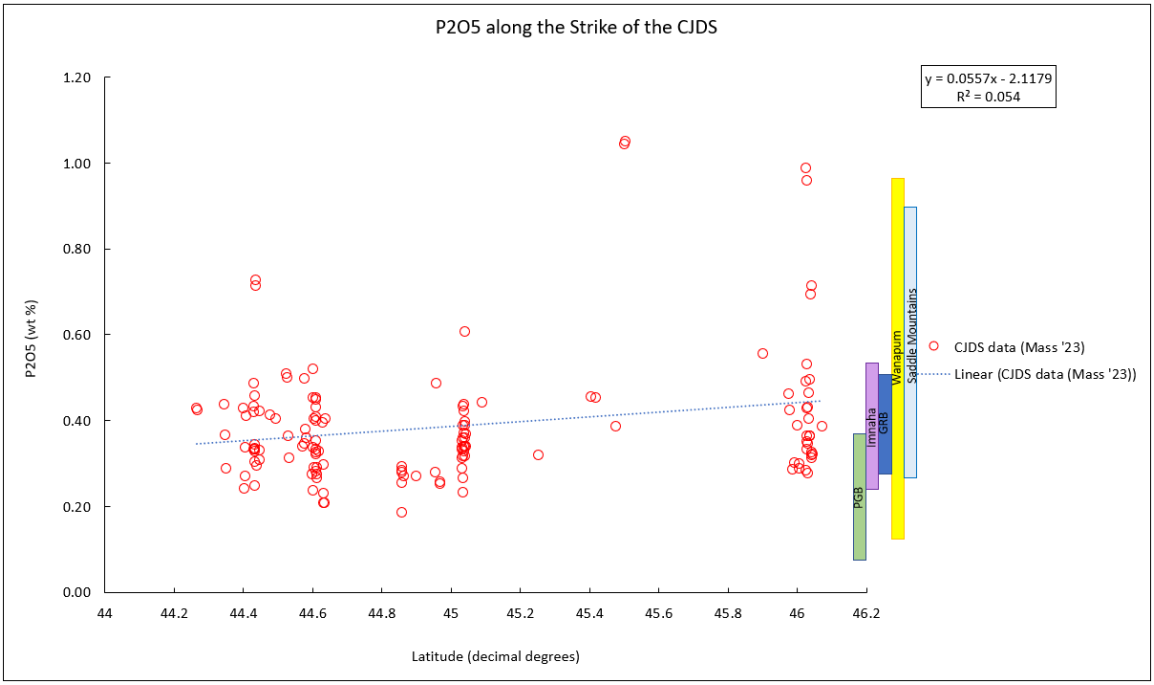

Figure 44. P_2O_5 content along strike of the CJDS. Data in red is the CJDS geochemical data from this study. Imnaha and GRB data are from Wolff et al. (2008) and the PGB data are from Cahoon et al. (2020). Wanapum and Saddle Mountain data are from Reidel et al. (2013).

Tantalum concentration increases going north along strike to the ID-OR-WA border. The GRB is the most tightly packed group followed by the PGB and the Steens Basalt. Samples from this study as well as the Imnaha have the largest spread in tantalum concentration.

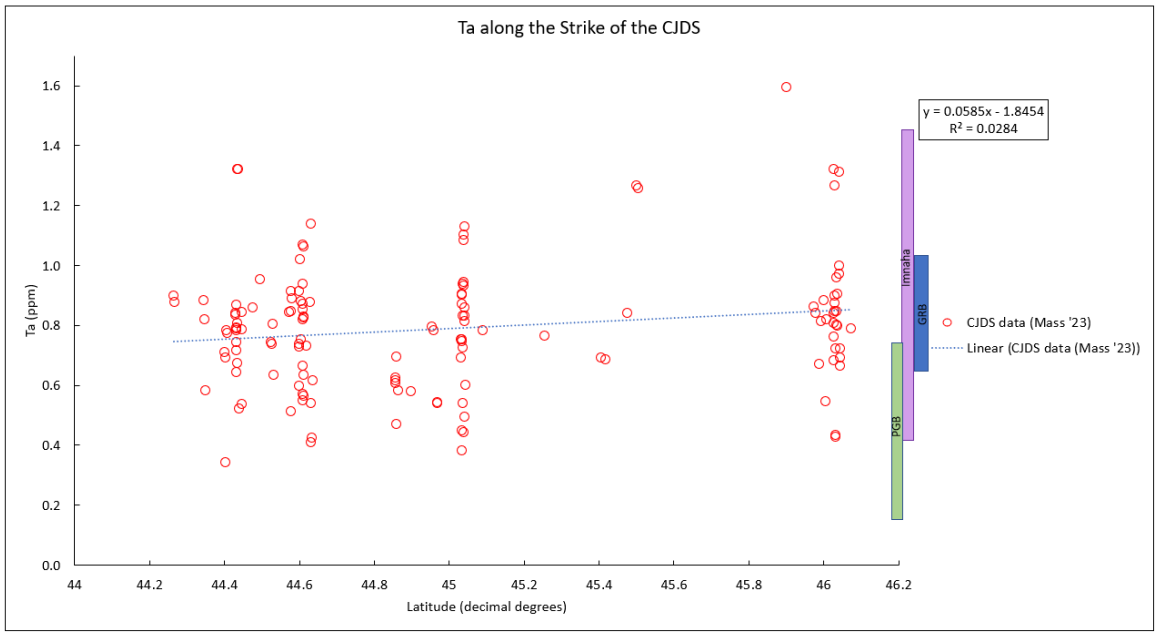

Figure 45. Ta content along strike of the CJDS. Data in red is the CJDS geochemical data from this study. Imnaha and GRB data are from Wolff et al. (2008) and the PGB data is from Cahoon et al. (2020).

Lanthanum concentration increases north along strike to the ID-OR-WA border. Samples from this study have the largest spread and have some outliers that are a significantly higher concentration than the main geochemical groups.

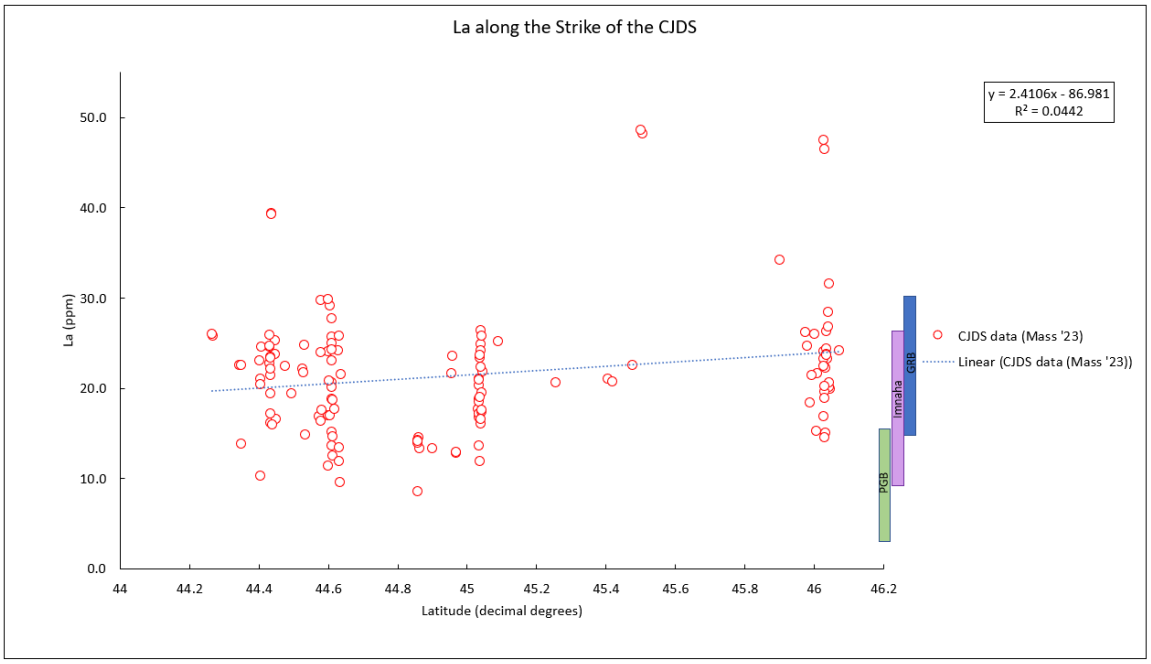

Figure 46. La content along strike of the CJDS. Data in red is the CJDS geochemical data from this study. Imnaha and GRB data are from Wolff et al. (2008) and the PGB data is from Cahoon et al. (2020).

Strontium concentration marginally decreases going north along strike to the ID-OR-WA border. A single outlier from the Imnaha samples has significantly higher Sr concentration than the main group averages.

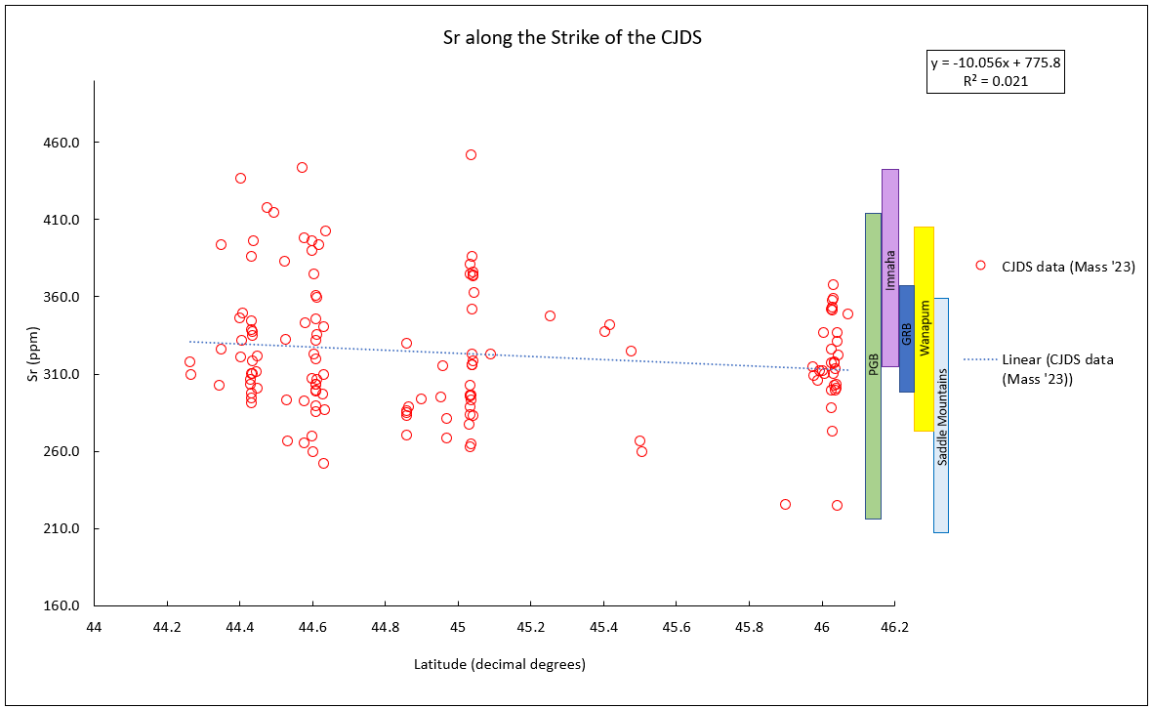

Figure 47. Sr content along strike of the CJDS. Data in red is the CJDS geochemical data from this study. Imnaha and GRB data are from Wolff et al. (2008) and the PGB data are from Cahoon et al. (2020). Wanapum and Saddle Mountain data are from Reidel et al. (2013).

Barium concentration increases north along strike to the ID-OR-WA border. There is a group of outliers in the Steens Basalt as well as samples from this study. The Imnaha has the smallest range in Barium of all groups.

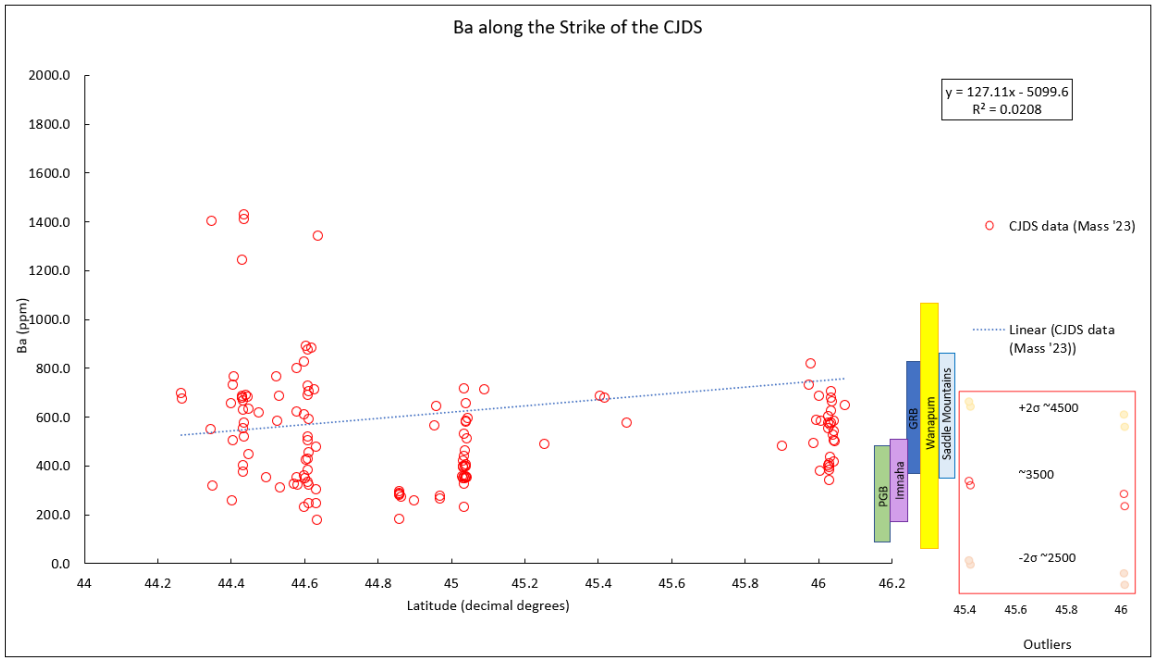

Figure 48. Ba content along strike of the CJDS. Data in red is the CJDS geochemical data from this study. Imnaha and GRB data are from Wolff et al. (2008) and the PGB data is from Cahoon et al. (2020). Wanapum and Saddle Mountain data are from Reidel et al. (2013).

Ba/Nb increases very slightly going north along strike to the OR-WA border. Samples from this study have the largest spread and have some outliers that are a significantly higher concentration than the main geochemical groups (these are the Umatilla member of the Saddle Mountain Formation).

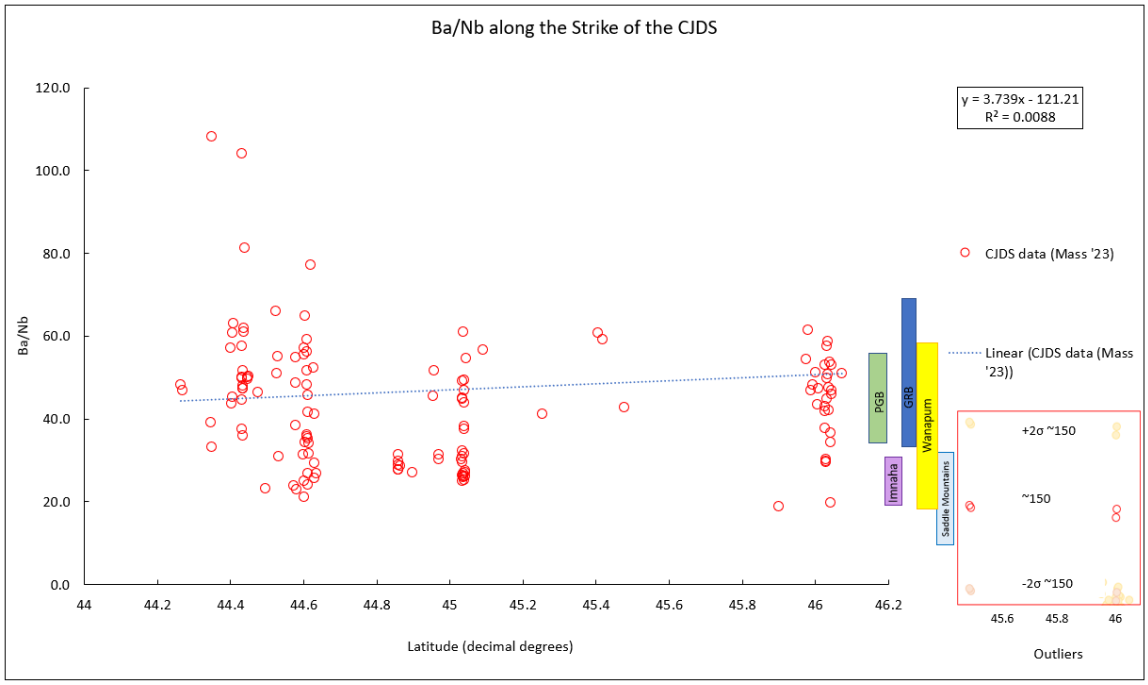

Figure 49. Ba/Nb content along strike of the CJDS. Data in red is the CJDS geochemical data from this study. Imnaha and GRB data are from Wolff et al. (2008) and the Steens data are from Moore (2019) and the PGB data are from Cahoon et al. (2020). Wanapum and Saddle Mountain data are from Reidel et al. (2013).

Zr/Nb ratios exhibit a very slight decrease going north along strike to the ID-OR-WA border. Samples from this study have some outliers that are at a significantly higher concentration than the main geochemical groups.

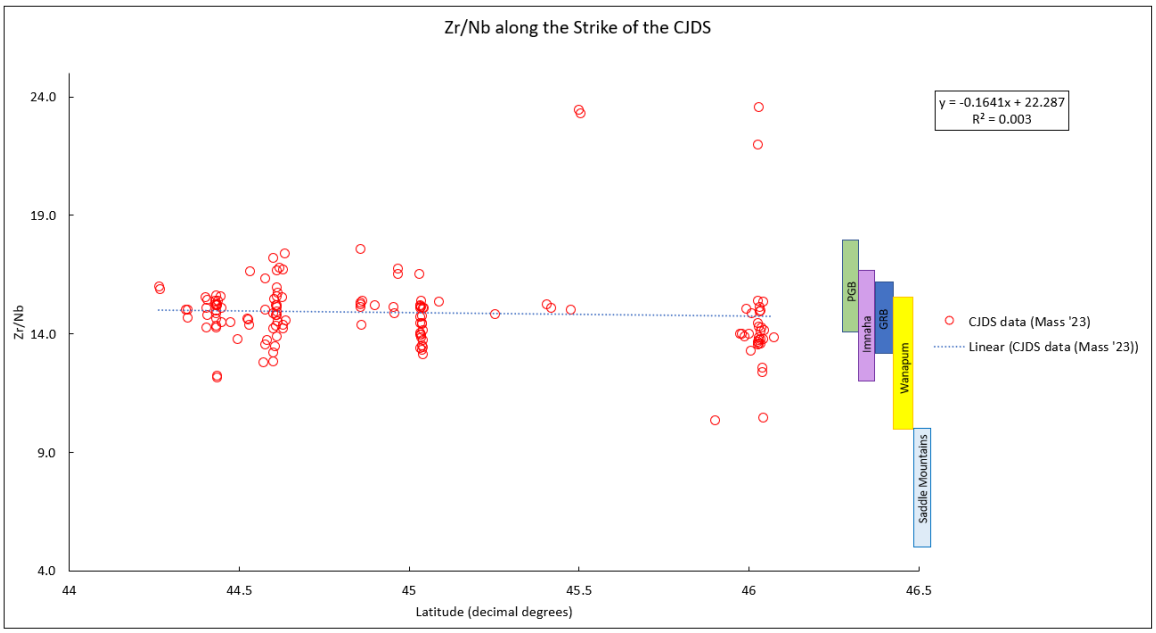

Figure 50. Zr/Nb content along strike of the CJDS. Data in red is the CJDS geochemical data from this study. Imnaha and GRB data are from Wolff et al. (2008) and the PGB data are from Cahoon et al. (2020). Wanapum and Saddle Mountain data are from Reidel et al. (2013).

Zr/Y ratios increase going north along strike, however samples in the south have a larger spread than in the north.

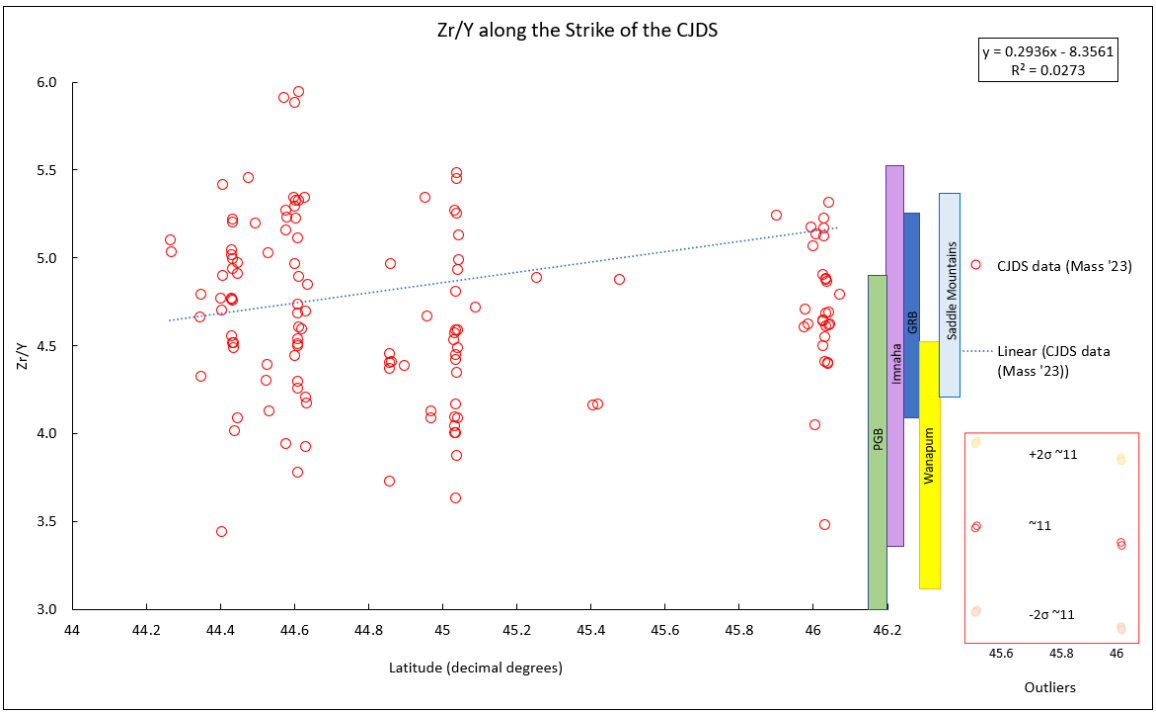

Figure 51. Zr/Y content along strike of the CJDS. Data in red is the CJDS geochemical data from this study. Imnaha and GRB data are from Wolff et al. (2008) and the PGB data are from Cahoon et al. (2020). Wanapum and Saddle Mountain data are from Reidel et al. (2013).

Sr/Sc ratios very slightly decrease going north along strike to the OR-WA border. There are some outliers that are a bit higher concentration than the main geochemical groups.

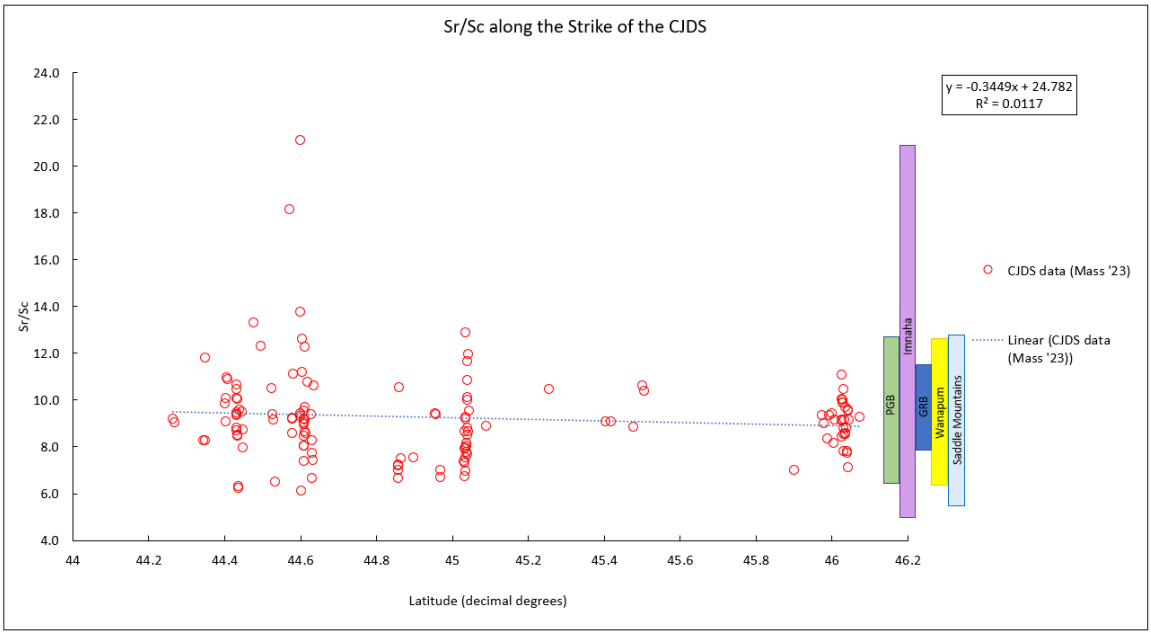

Figure 52. Sr/Sc content along strike of the CJDS. Data in red is the CJDS geochemical data from this study. Imnaha and GRB data are from Wolff et al. (2008) and the Steens data are from Moore (2019) and the PGB data are from Cahoon et al. (2020) Wanapum and Saddle Mountain data are from Reidel et al. (2013).

Petrographic trends

Thin sections were made of every sampled dike from the northern and southern portions of the Chief Joseph dike swarm; these are included in Appendix D. Samples were organized according to magnesium content, which is an indicator of magmatic evolution, to evaluate how petrographic characteristics change with changing MgO of the bulk rock. The thin sections were grouped into one percent MgO groups starting at the lowest MgO content in this study of ~2% and ending at the highest MgO content of 11.3%.

MgO 2-2.9%

There are four samples in this geochemical group, and all have similar petrography. They are fine-grained and contain a predominantly plagioclase rich groundmass and are aphyric. One sample (MM-CRB-64) contains a single and small (~ 227 µm) plagioclase phenocrysts (Figure 53).

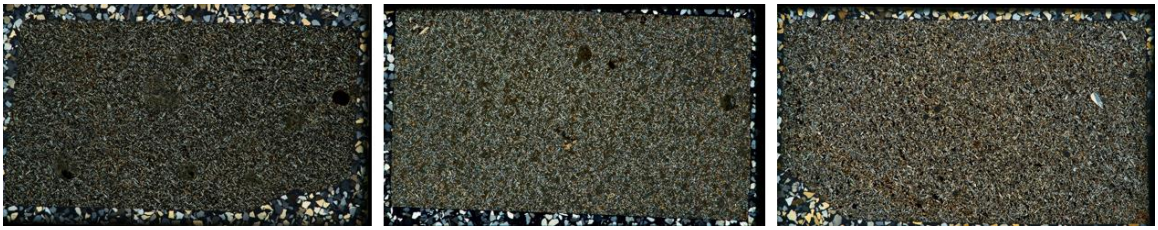

Figure 53. Petrographic characteristics of samples that contain 2-2.9% MgO. From left to right: MM-CRB-104, MM-CRB-09, MM-CRB-64 - not pictured in this geochemical group is sample MM-CRB-103.

MgO 3-3.9%

This geochemical group contains 29 total samples. Samples are still mostly fine-grained and aphyric (Figure 54). However, a few samples are also coarser-grained and sparsely phyric. Six samples (not shown) do not fit these characteristics, i.e. they have ~ MgO 3 wt%, but coarse-grained or plagioclase phenocrysts with a very fine-grained groundmass. The predominant mineral present is plagioclase, with microphenocrysts of plagioclase present in samples MM-CRB-55, MM-CRB-87, MM-CRB-83 while sample MM-CRB-11 with 4.9% MgO contains glomerocrysts of plagioclase.

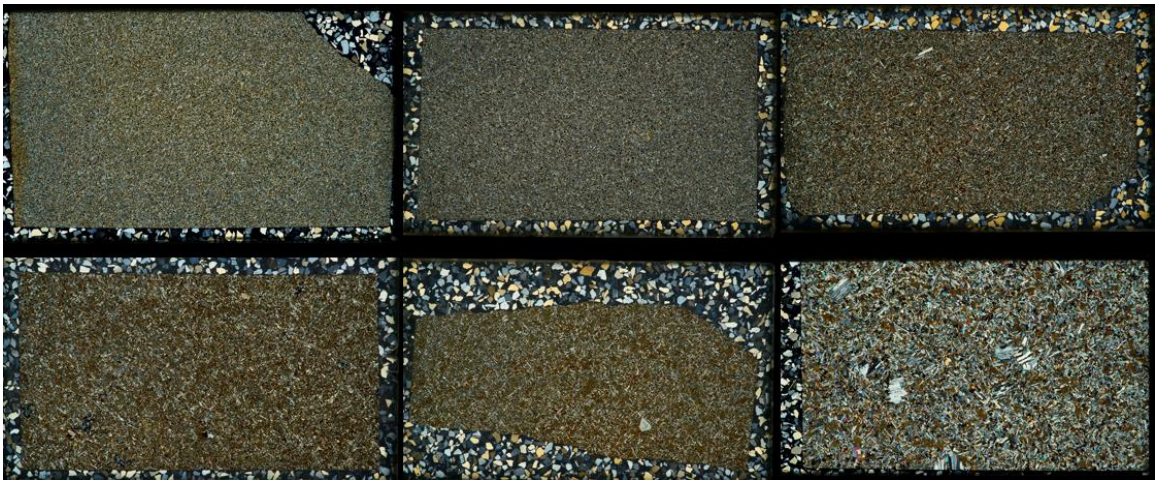

Figure 54. Petrographic features seen in samples that contain 3-3.9% MgO. From left to right on top: MM-CRB-18a, MM-CRB-88, MM-CRB-55. From left to right on bottom: MM-CRB-87, MM-CRB-83, MM-CRB-11. There are 29 samples in this geochemical group and 6 do not fit these characteristics. The six samples that do not fit these characteristics do not follow the increase in grain size with increasing MgO wt%.

MgO 4-4.9%

The geochemical group spanning from 4% through 5.9% MgO grades from fine-grained porphyritic samples with plagioclase phenocrysts or glomerocrysts to coarse-grained with plagioclase phenocrysts reaching ~ 632 µm (Figure 55).

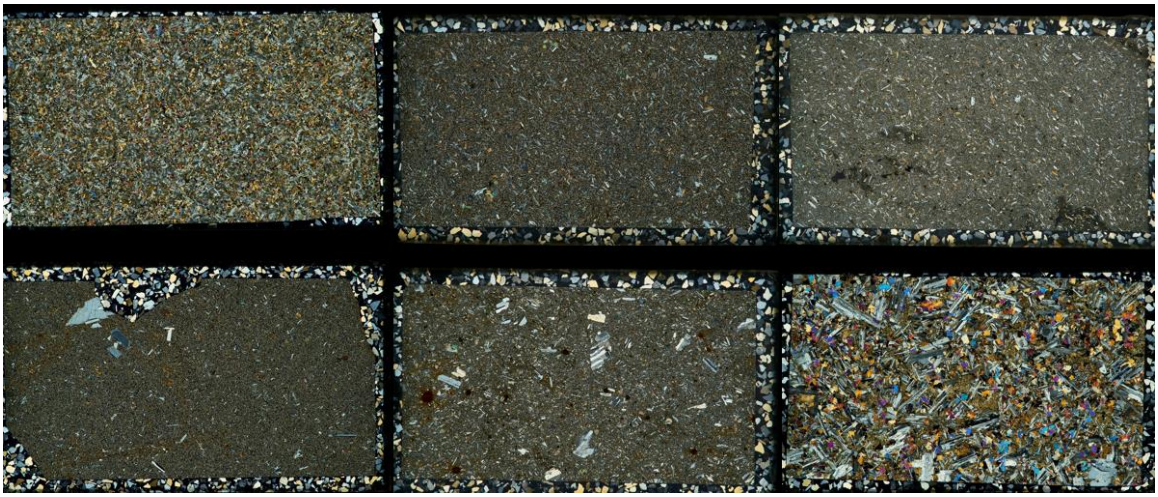

Figure 55. Petrographic trends seen in samples that contain 4-4.9% MgO. From left to right on top: MS-14-10, MS-CRB-105, MM-CRB-107. From left to right on bottom: MM-CRB-61, MM-CRB-96b, MM-CRB-28. There are 23 samples in this geochemical group and 2 do not fit this trend.

MgO 5-5.9%

Samples in this geochemical group contain two subgroups. The first group includes 23 samples and is seen in the upper row in Figure 59. Samples range from coarse-grained aphyric to plagioclase-phyric basalt with plagioclase-glomerocrysts followed by coarse-grained plagioclase-phyric basalt with plagioclase-glomerocrysts as the MgO concentration increases. The petrography of the second group, made up of 11 samples, is illustrated by the bottom row of Figure 56. These are fine-grained and aphyric with a predominantly plagioclase groundmass.

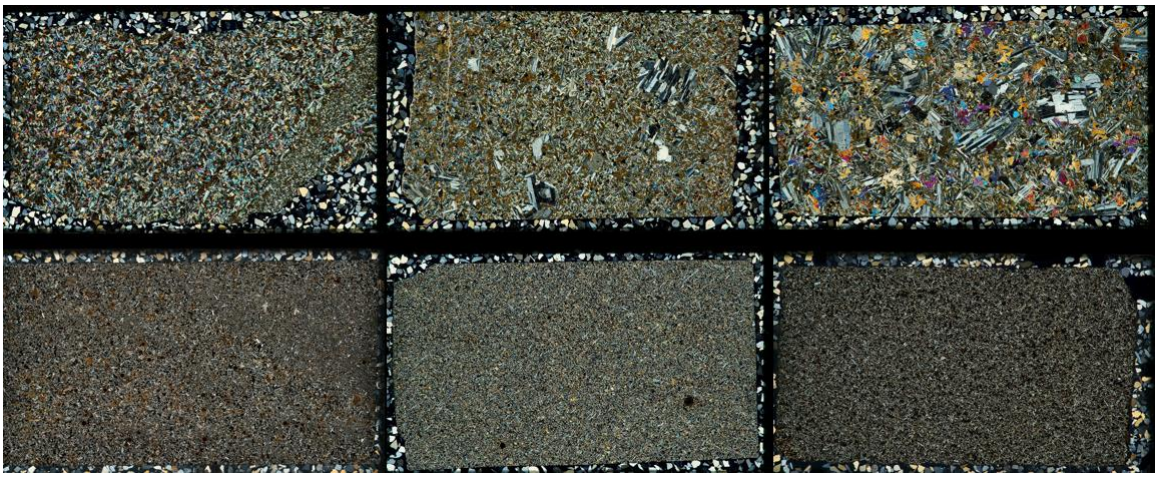

Figure 56. Petrographic trends seen in samples that contain 5-5.9% MgO. From left to right on top: MM-CRB-08, MM-CRB-29, MM-CRB-06. From left to right on bottom: MM-CRB-47b, MM-CRB-23, MM-CRB-85. There are 23 samples in this geochemical group and 11 are fine-grained and do not fit this trend.

MgO 6-6.9%

This geochemical group contains four samples. Those shown in the upper row of Figure 57 contain predominantly pyroxene and plagioclase as well as iddingsite. Samples on the lower row in Figure 57 contain the same mineralogy with the addition of plagioclase phenocrysts and glomerocrysts.

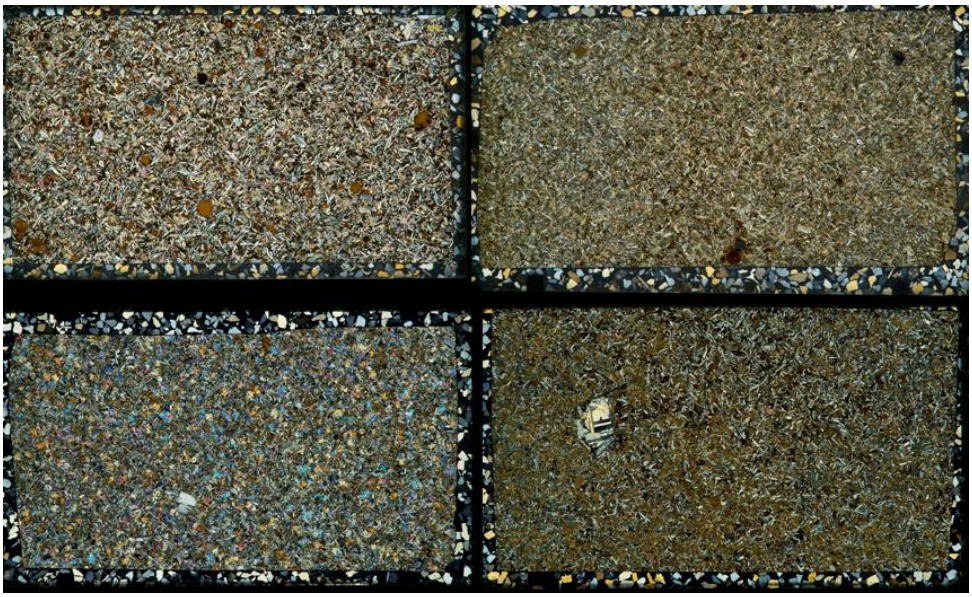

Figure 57. Petrographic trends seen in samples that contain 6-6.9% MgO. From left to right on top: MM-CRB-64, MM-CRB-63. From left to right on bottom: MM-CRB-38, MM-CRB-21. There are 4 samples in this geochemical group and 2 do not fit this trend.

MgO 7-7.9%

Only one dike sample has such MgO contents. MM-CRB-05 has 7.37% MgO and has coarser groundmass and is plag-ol-cpx-phyric, also containing plagioclase glomerocrysts.

Figure 58. Petrography of MM-CRB-05 that contains 7-7.9% MgO. There are not enough samples to establish common characteristics in this geochemical group however, the petrography differs from the previous group seen in Figure 57.

MgO 11-11.9%

There is only one sample in this study that has a Mg number over 60 and has an MgO of 11.3%, this is sample MM-CRB-07. This sample is coarse-grained and has a coarse-grained poikilitic groundmass that contains a few ol+plag+cpx phenocrysts. This sample is the most primitive sample from this study.

Figure 59. The most primitive sample from this study is seen here with 11.3% MgO.

$^{40}Ar/^{39}Ar$ Age Dates

Samples were selected for age dating based on sample freshness, whether dikes were drilled or future drill targets, and to cover magmatic evolution within samples of the high and low silica trend. When selecting samples for age dating, the following goals were considered. 1) to determine ages across samples defining the low and high SiO2 trends; 2) dikes belonging to the geochemical type for this area that is reminiscent of the Picture Gorge Basalt that erupted from the Monument dike swarm in central Oregon; 3) dikes identified as having compositions of Wapshilla Ridge basalt of the GRB; and 4) dike samples with compositions spanning the whole range of the CJDS, which could be used to look for age progressive trends. The samples selected from the low silica trend from least evolved to most evolved: MM-CRB-07, MM-CRB-06, and MM-CRB-61. The samples selected for the high silica trend are also from least evolved to most evolved and include MM-CRB-40, MM-CRB-31, MS-CRD18-5, MM-CRB-27, and MM-CRB-09a (Figure 60). I also selected samples that correlated with the Wapshilla Ridge unit—the flow member of the CRBG with the single largest volume—as they span the length of the CJDS to see

if there any age progressive trends. Based on the data, we observe that dikes in the south are older on average than dikes in the north (Figure 61).

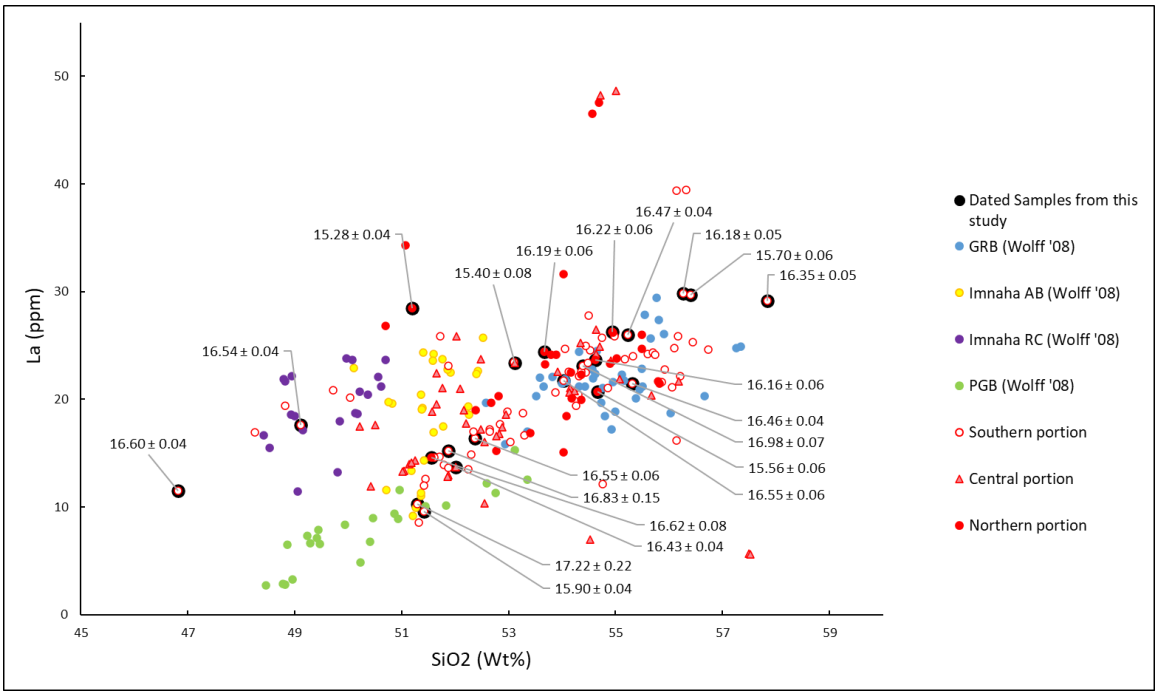

Figure 60. Age dates spanning both the low and high silica trends shown in this La vs. SiO2 plot. Imnaha, GRB, and PGB geochemistry is from Wolff et al. (2008) and the southern, central, and northern data in red is from this study.

Sample MM-CRB-07 is the oldest of the low silica trend and lacks a compositional lava flow counterpart as it is considerably more primitive at relatively high incompatible trace element concentrations. MM-CRB-06 and MM-CRB-61 are around the same age and are geochemically the most like the Imnaha Rock Creek and the Roza Basalt of Dodge respectively. The low end of both the low and high Si trends are predominantly samples from the south, these are also the oldest samples from this study. The oldest date of this study is sample MM-CRB-21 in the southern portion of the CJDS. The oldest date prior to this study for the Imnaha is 16.85 ± 0.21, yet the weighted plateau of the same sample yielded 16.67±0.15 Ma (Jarboe et al., 2010). The age of sample MM-CRB-21 extends the eruptive period of the CJDS to begin at 17.22 Ma.

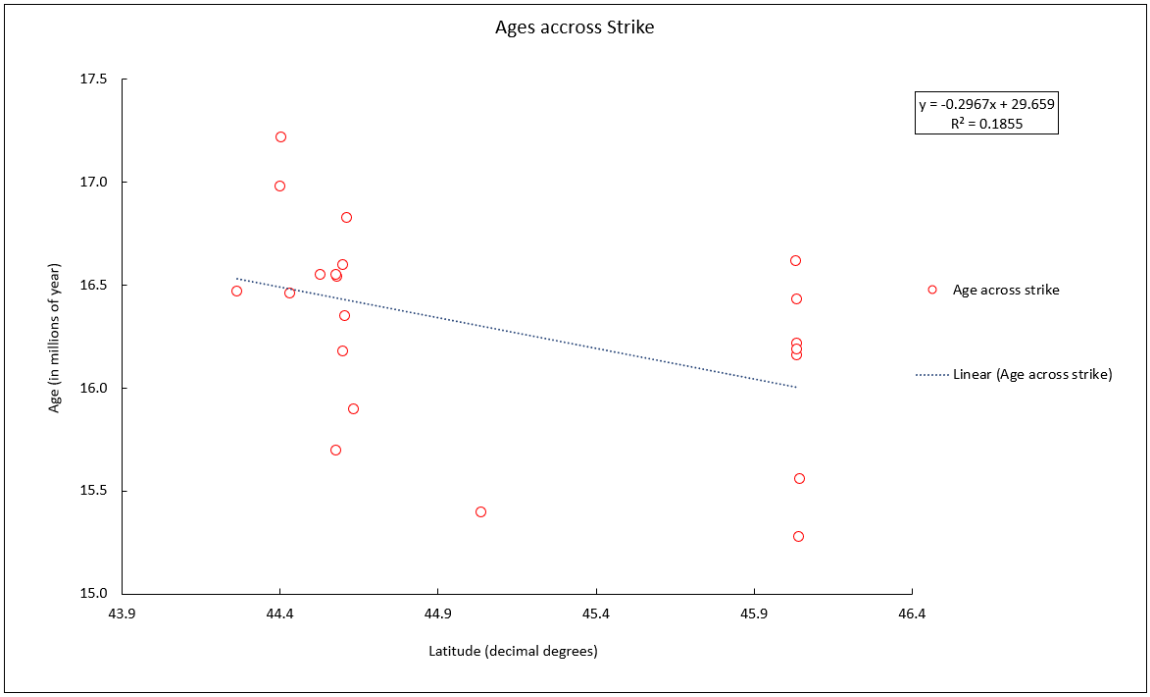

Figure 61. Ages across the strike of the CJDS in millions of years.

Table 1. Results from incremental age dating at the Oregon State University geochronology laboratory.

Table 1. Incremental Heating Age Determinations

				Plateau					Isochron				
Sample	ǂComposition	‡Rock type	§Material dated	Age (Ma)	± 2σ	Plateau steps	^{39}Ar	Plateau MSWD	Age (Ma)	± 2σ	^{40}Ar/^{39}Ar Intercept	± 2σ	Isochron MSWD
MS-CRD18-5	TH	BA	GM	15.56	0.06	5	27%	6.21	15.26	0.48	323.38	39.73	5.33
MM-CRB-61	TH	HKB	GM	15.28	0.04	9	69%	2.08	15.27	0.09	298.78	3.88	2.66
MM-CRB-27	TH	HKA	GM	15.7	0.06	13	48%	1.35	1,572	0.15	298.34	1.29	1.92
MM-CRB-09a	TH	HKA	GM	16.35	0.05	18	21%	1.62	16.39	0.08	296.35	3.04	1.58
MM-CRB-07	TH	B	Plag	16.6	0.04	16	77%	0.52	16.59	0.05	300.25	11.09	0.52
MM-CRB-06	TH	B	Plag	16.54	0.04	28	92%	0.77	16.53	0.04	308.34	9.14	0.63
MM-CRB-31	TH	B	Plag	16.83	0.15	9	27%	1.56	16.59	0.21	314.01	10.75	0.51
MM-CRB-40	TH	LKB	Plag	15.9	0.04	23	79%	0.61	15.92	0.05	294.22	6.3	0.78
MM-CRB-21	TH	LKB	Plag	17.22	0.22	31	99%	1.45	17.36	0.53	290.42	2.57	4.33
MM-CRB-59	TH	LKB	Plag	16.62	0.08	12	69%	1.31	16.65	0.12	295.35	7.53	1.17
MM-CRB-26	TH	B	Plag	16.55	0.06	26	96%	1.01	16.58	0.07	295.37	3.32	0.95
MM-CRB22-132	TH	B	Plag	16.43	0.04	26	96%	1.04	16.42	0.04	299.65	2.14	1.01
20-LK-TEI	TH	BA	Cpx	15.79	1.06	7	66%	2.15	15.53	2.32	297.52	4.23	2.44
MM-CRB-15	TH	BA	Plag	16.46	0.04	19	57%	1.62	16.48	0.04	293.86	2.97	1.2
MM-CRB-02	TH	BA	Plag	16.55	0.06	32	100%	1.25	16.54	0.1	294.01	1.32	1.49
MM-CRB22-120	TH	BA	GM	15.4	0.08	7	48%	3.85	15.48	0.38	297.44	5.04	5.61
MM-CRB-78	TH	BA	Plag	16.98	0.07	32	100%	0.57	17.02	0.07	295.95	2.25	0.53
MM-CRB-67	TH	BA	GM	16.19	0.06	8	42%	12.9	16.13	0.27	304.34	29.63	15.91
MM-CRB-77	TH	BA	GM	16.47	0.04	17	53%	1.92	16.45	0.06	293.11	1.38	3.18
MM-CRB-65	TH	HKA	GM	16.22	0.06	11	41%	4.15	16.01	0.32	304.35	8.46	4.06
MM-CRB-62	TH	HKA	GM	16.16	0.06	4	30%	11.92	16.18	0.88	296.09	93.7	18.89
MM-CRB-109	TH	HKA	Plag	16.18	0.05	23	74%	1.08	16.18	0.07	293.5	0.96	1.42
*MM-CRB-61	TH	HKB	Plag	16.55	0.13	25	99%	1.06	16.42	0.16	302.52	3.56	0.87
*MM-CRB-40	TH	LKB	Cpx	29.55	2.72	3	38%	1.09	33.25	8.12	297.14	2.85	1.26
*MM0CRB-07	TH	B	Cpx	15.68	1.03	16	98%	1.08	13.33	4.13	298.35	3.36	3.18
*MM-CRB-06	TH	B	Cpx	16.06	0.48	12	88%	1.11	17.17	1.02	295.78	2.19	1.27

Note: All samples in this study used the Fish Canyon Tuff (FCT-NM) standard R98 (4E36-14) = 28.201 Ma. Preferred ages referred to in this thesis are the plateau ages and the sample with the lowest MSWD of repeat samples . MSWD is the mean square of weighed deviates.

*Repeat

ǂTH—tholeiitic

‡B—basalt; HKB—high K basalt; LKB—low K basalt; BA—basaltic andesite; A—andesite; HKA—high K andesite.

§GM—groundmass; Plag—plagioclase; Cpx—clinopyroxene

Discussion

Although there is quite a bit of geochemical information available regarding the lava flows that erupted from the Chief Joseph dike swarm there is very little published geochemical data from the dikes themselves. The new geochemical data set from this study ties magmas to locations of intrusive activity across the Chief Joseph dike swarm. This allows us to tie magmatic geochemical signatures more directly to magma transport north-south across the dike swarm. This has implications for magma storage locations prior to eruption. In this discussion of magma storage and movement, I will first correlate the composition of the sampled dikes with subaerial lava flows and then combine this information with obtained age data of select dikes to make inferences on timing and on availability of magma in the subsurface through time.

Dike Classification

One of the goals of this study is to correlate magmas as recorded by dikes with CRBG formations, members, and, if possible, flows and to identify those that do not fit into the current classification. Correlation with CRBG units was initially performed by Ashley Steiner at the GeoAnalytical Lab at Washington State University where she used her Supervised Machine Learning (SML) program. The SML program did well correlating most of the CRBG formations such as GRB and Imnaha American Bar (AB) members with a confidence of > 95%. However, a handful of samples run in the SML had a confidence < 95%. This lower confidence is due to a lack of similar samples in the learning database. Because of this issue, I plotted all my samples on bivariate plots to identify the formation and mantle normalized incompatible element diagrams (Spider diagrams) to identify the members and flows when possible.

Correlation with CRBG formations

To correlate samples with formations and members I used correlative bivariate plots highlighted by Reidel, Tolan, and Barton in GSA's Special publication 497 (Reidel et al., 2013).

Correlation with the Imnaha and PGB Formations

I plotted all the samples that the SML program identified as Imnaha and Eckler Mountain, as it is PGB-like on a bivariate MgO vs. TiO2 plot, to separate samples that are typically Imnaha and those that are PGB-like (Figure 62; modified from Reidel et al., 2013).

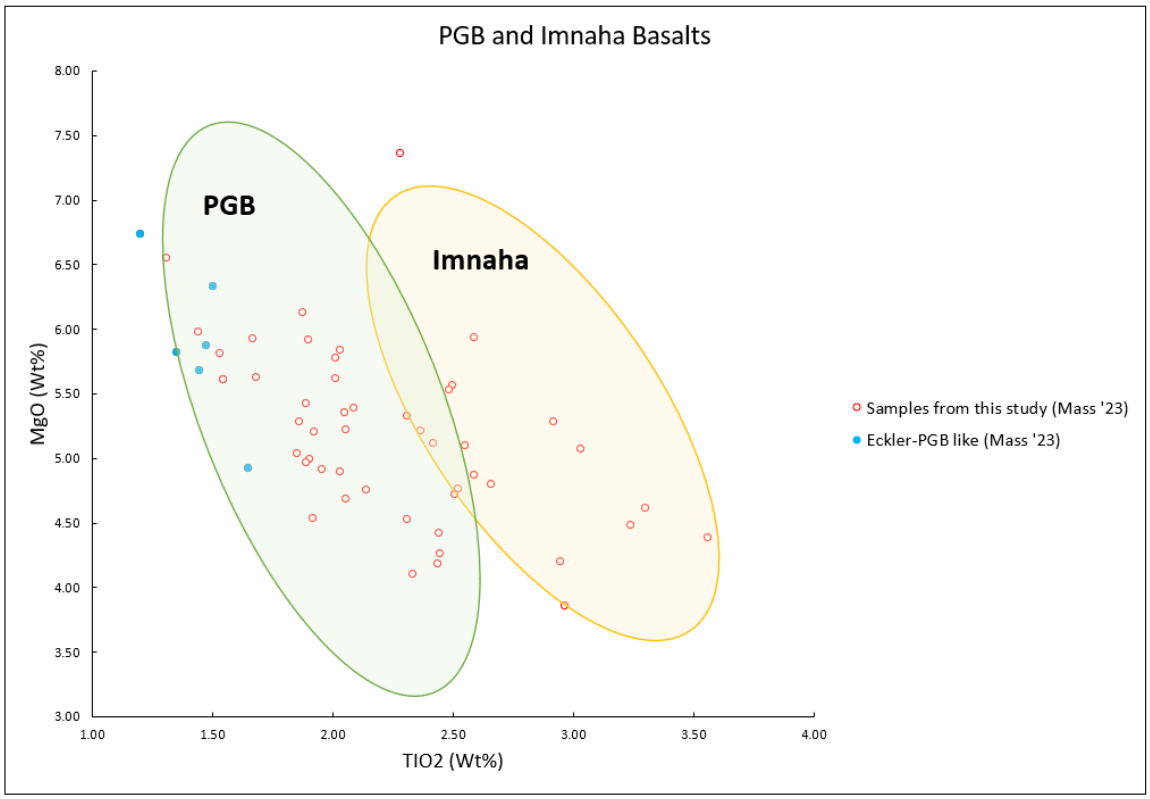

Figure 62. Samples from this study grouped into Imnaha and PGB-like designations defined by Reidel et al., (2013). The samples plotted are ones identified by the machine learning program as Imnaha.

Correlations with the GRB and Wanapum Formations

After classifying samples with Imnaha and PGB-like characteristics, data from the remaining dike samples were plotted on a MgO vs P_2O_5 bivariate plot established in the literature and referenced by Reidel et al. (2013).

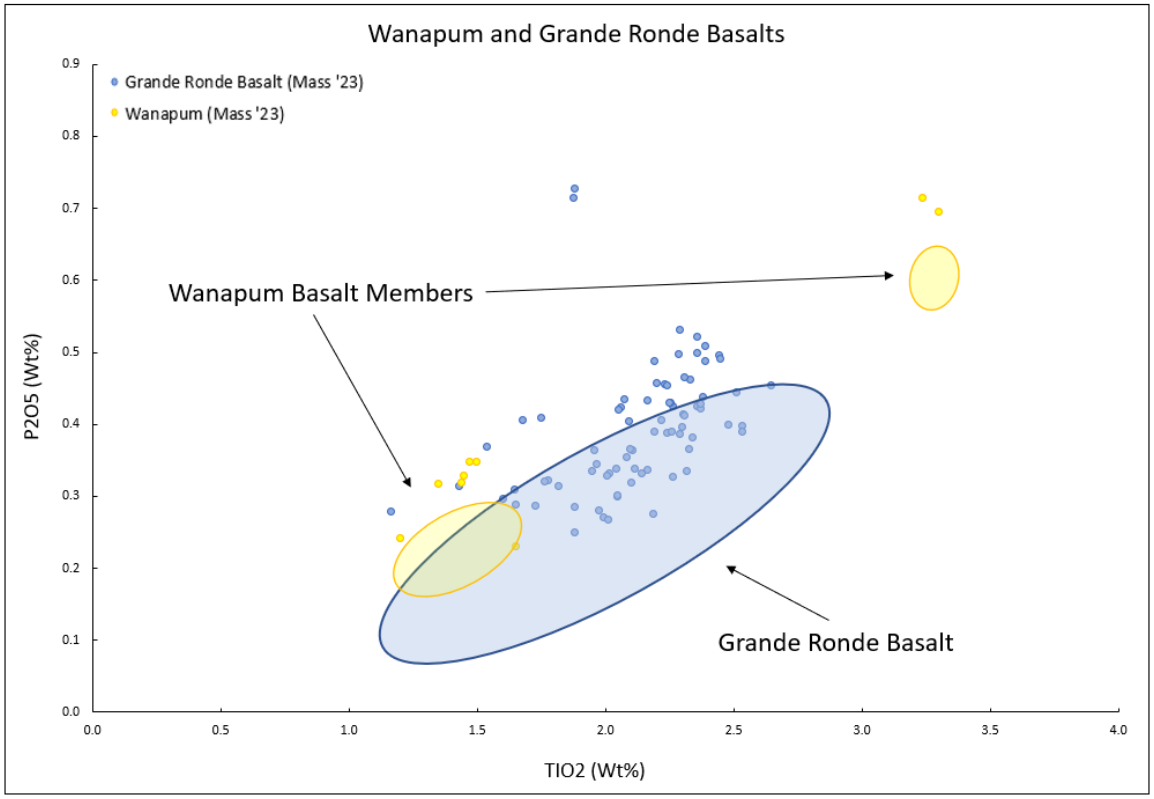

Figure 63. Samples from this study grouped into Wanapum and GRB designations defined by Reidel et al., (2013). The samples plotted are ones identified by the machine learning program as GRB and Wanapum.

Correlation with Imnaha members

Although the Imnaha and PGB formation differentiation plot works for an initial classification, it is not good enough to establish a more detailed classification (Figure 62). For that, I compared each sample that was classified as Imnaha or PGB-like to known members of the AB 1&2, AB 3+, Rock Creek, Fall Creek, and Log Creek. An example of this is illustrated in Figure 65-74. The final member classification was established when incompatible trace element patterns were matched as close as possible to patterns of flows of specific member that were established by previous researchers (Figure 65-74; Wolff et al., 2008; Cahoon et al., 2020; Fredenberg, 2022). If a sample has a pattern that resembles two or more members, then the immobile elements Zr, Hf, Th, and Nb were particularly closely observed. Additionally, the slopes between elements Ba and Th, Th and U, and Yb and Lu were matched as these appear unique to each member. In some cases, the samples could be matched to a single flow or

several similar flows. However, many of my samples were unable to be matched to individual flows due to the lack of ICP-MS data available for most individual flows which makes correlating without the stratigraphical context difficult.

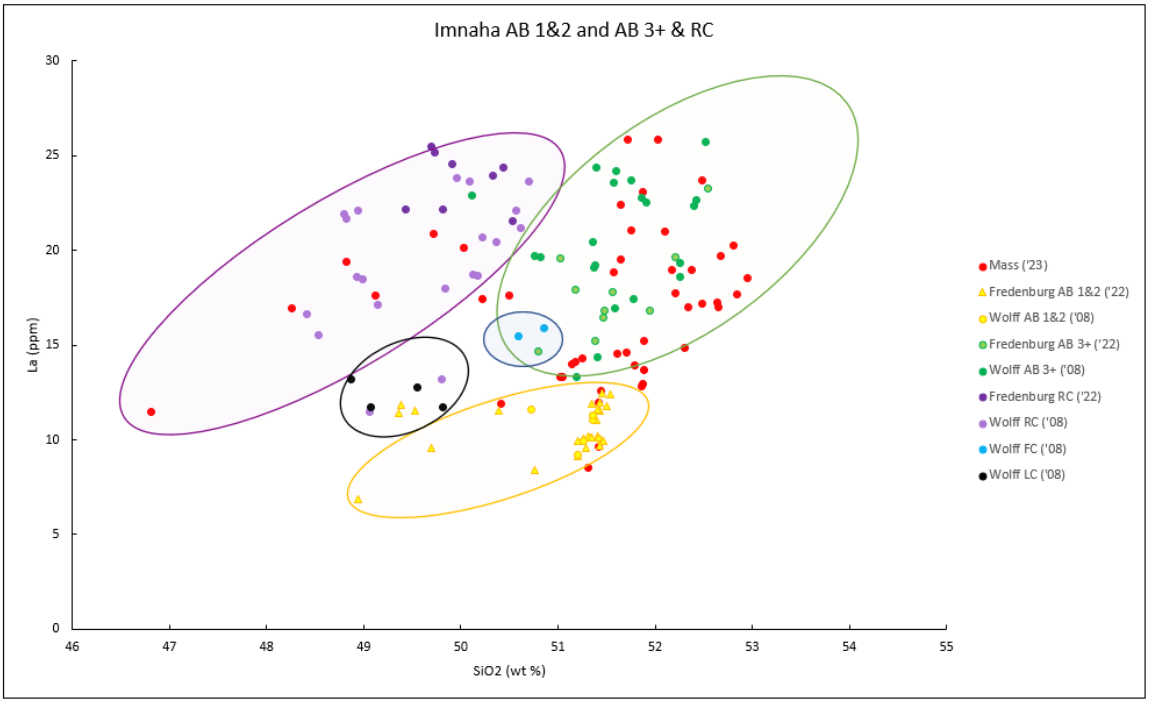

Figure 64. Samples from this study compared to samples with previous established flow unit association. The samples plotted from this study are ones identified by the machine learning program as Imnaha and Eckler Mountain. Comparison samples from Wolff et al., 2008; Cahoon et al., 2020; Fredenberg, 2022.

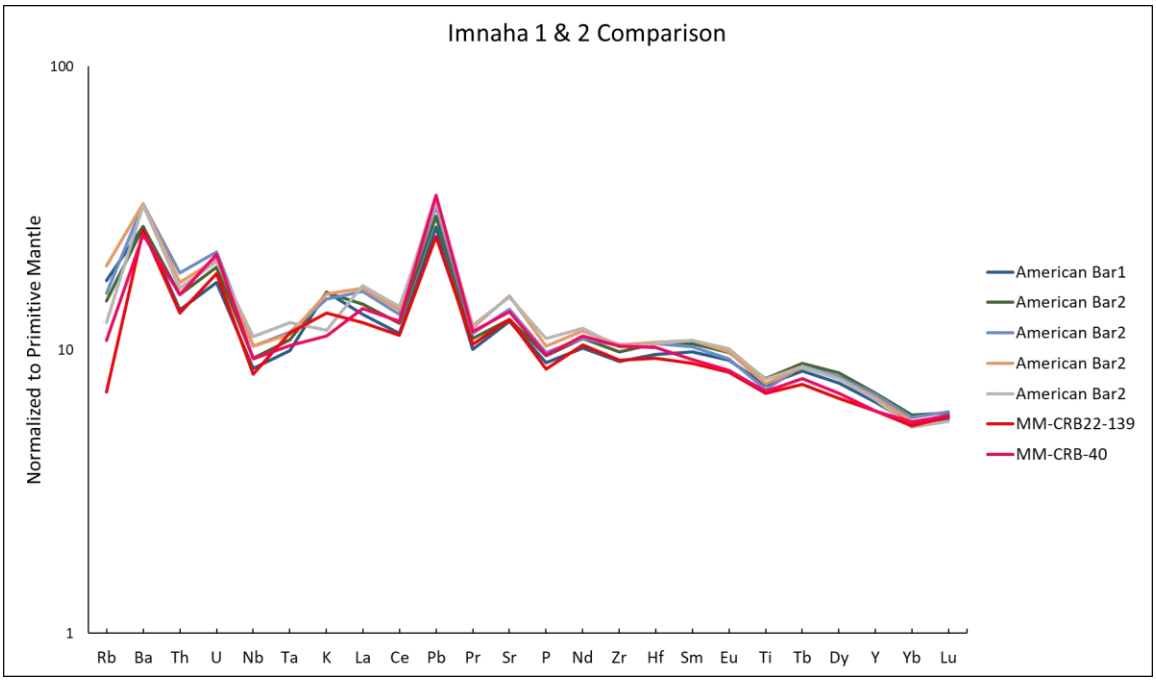

Figure 65. An example of matching samples from this study—in this case: MM-CRB22-139 and MM-CRB22-40—to samples established by previous works. Comparison samples from (Wolff et al., 2008).

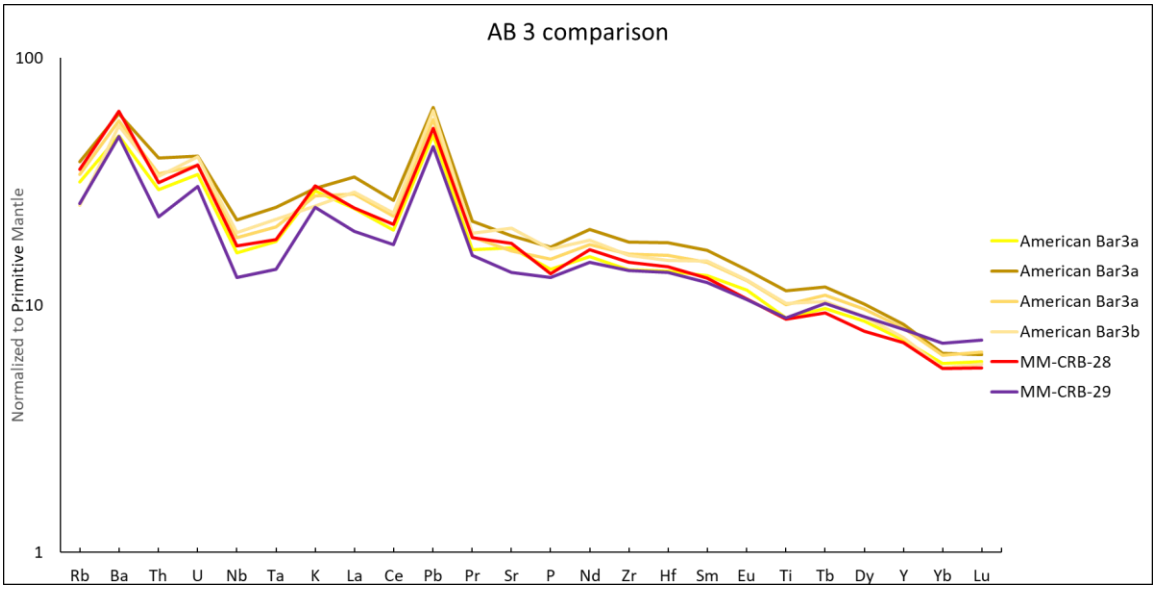

Figure 66. An example of matching samples from this study—in this case: MM-CRB-28 and MM-CRB22-29—to samples established by previous works. Comparison samples from (Wolff et al., 2008).

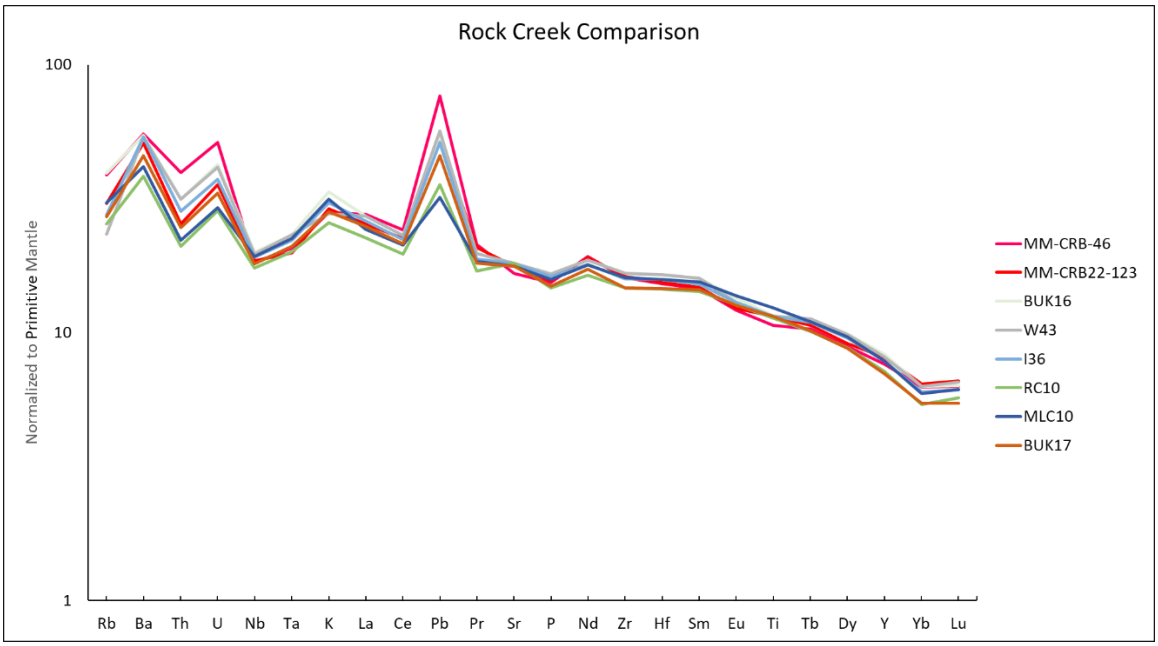

Figure 67. An example of matching samples from this study—in this case: MM-CRB-46 and MM-CRB22-123—to samples established by previous workers. Comparison samples from (Wolff et al., 2008).

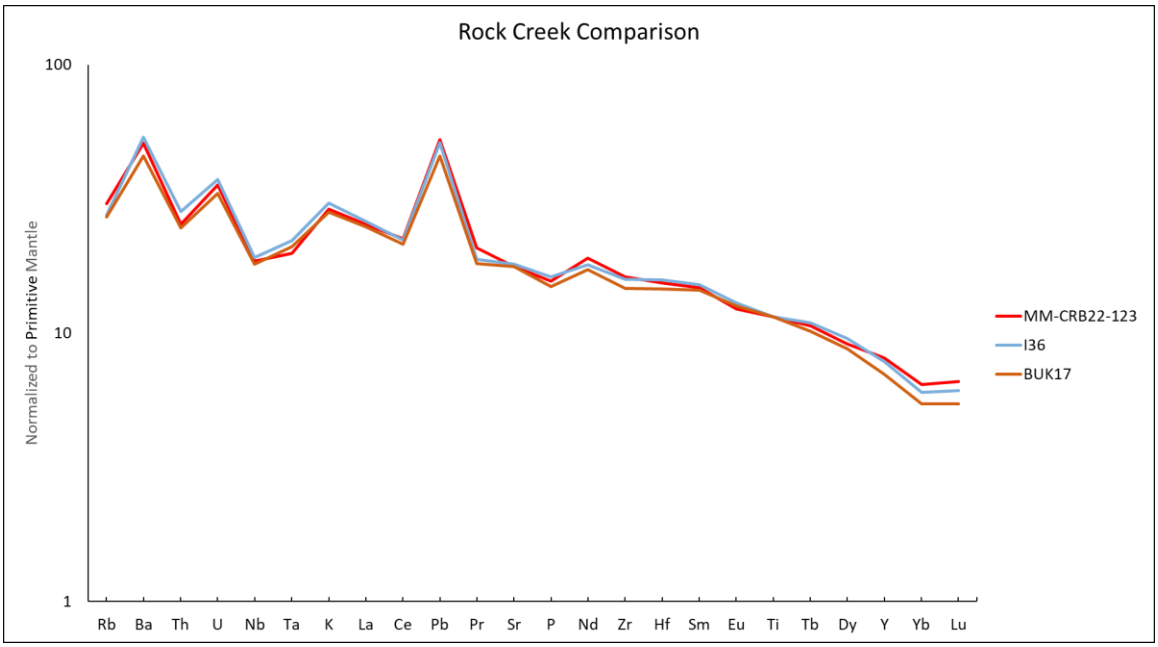

Figure 68. An example of matching a sample to—in this case—two possible flows. Comparison samples from (Wolff et al., 2008).

Correlation with Grande Ronde Basalt members

Samples grouped with the GRB formation in Figure 63 were plotted in bivariate plots established by Reidel and Tolan (2013) to determine the member.

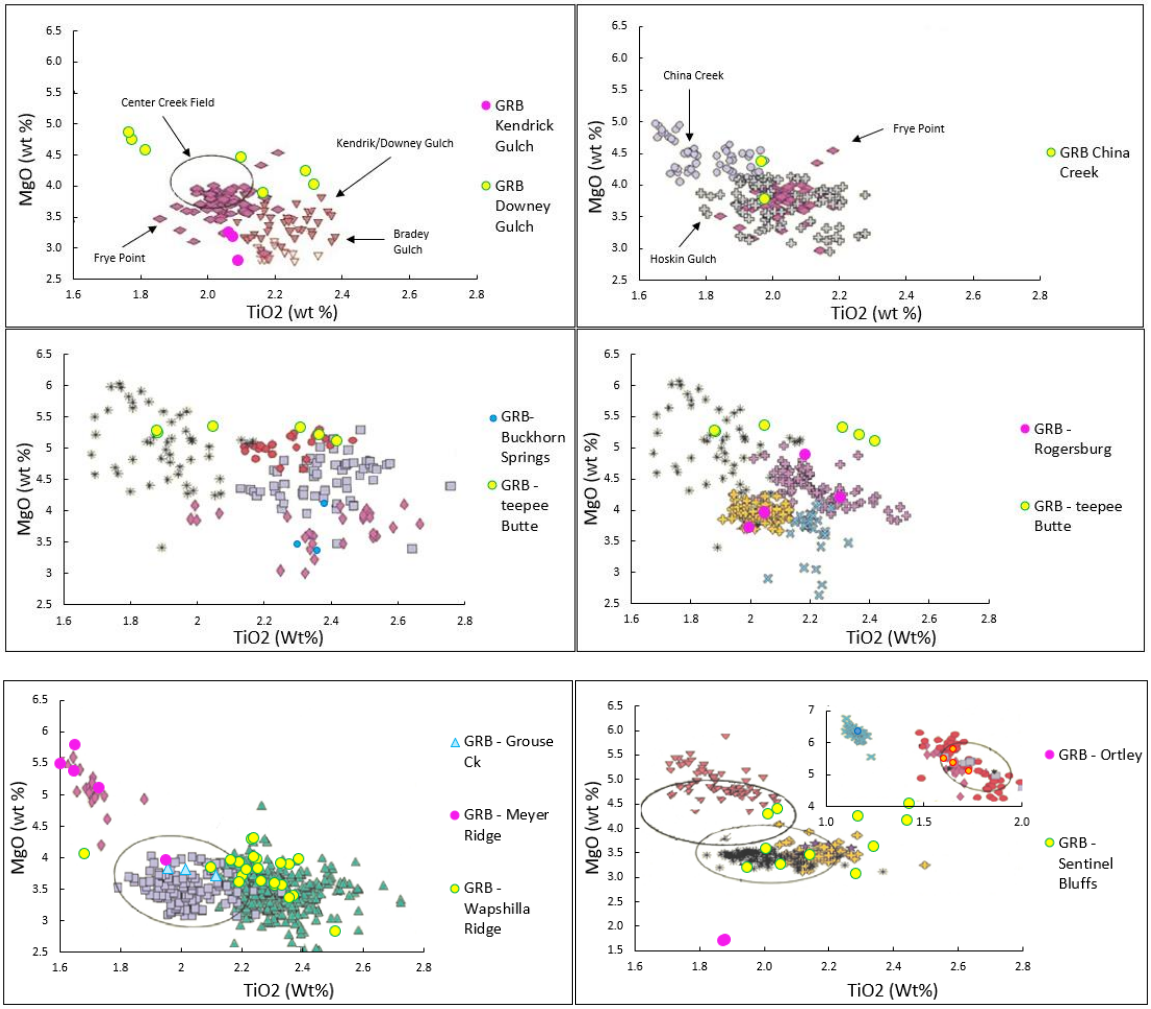

Figure 69. Samples from this study are shown in hot pink, bright blue, and bright yellow with green borders—they are compared to samples associated with specific GRB members. The samples plotted from this study are the ones identified by the machine learning program as GRB. Modified image and comparison samples from Reidel et al. (2013).

Correlation with Wanapum members

Samples grouped with the Wanapum formation or any of those outside of the GRB group seen in Figure 63 were plotted in bivariate plots referenced by Reidel and Tolan (2013) to determine the member. My samples plot within the trend of the average sample chemistry of both the Roza and the Eckler Mtn. members, however they are more enriched in incompatible elements relative to the established groups. This could be due to a small sample data set that defined the original groupings in the literature. Another option could be that the sampled dikes are Roza and Eckler Mountain-like but are not actually those units.

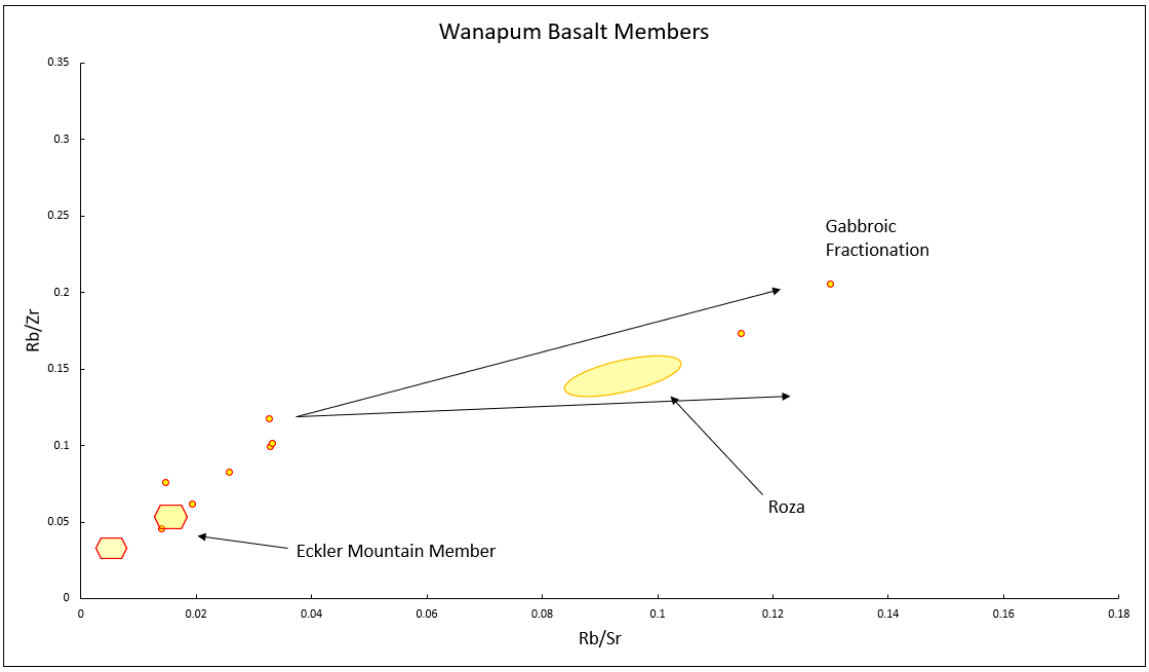

Figure 70. Samples from this study compared to samples established by previous workers for Wanapum members as they were defined in Martin et al. (2013). The samples plotted from this study are ones identified by the machine learning program as Eckler Mtn. and Roza.

Ages of Dikes

The ages obtained range from an Eckler-PGB like sample at 17.22 Ma to 15.40 Ma of a sample with Wapshilla Ridge composition (Table 1). The oldest dates obtained in this study are on the more primitive end of both the low and high SiO_2 trends, and represent dikes in the southern area (Figure 60, Figure 61). This is consistent with and could partially be a function of exposed dike country rocks, pre-Cenozoic rocks in the south and central area vs. CRBG lavas in the northern area.

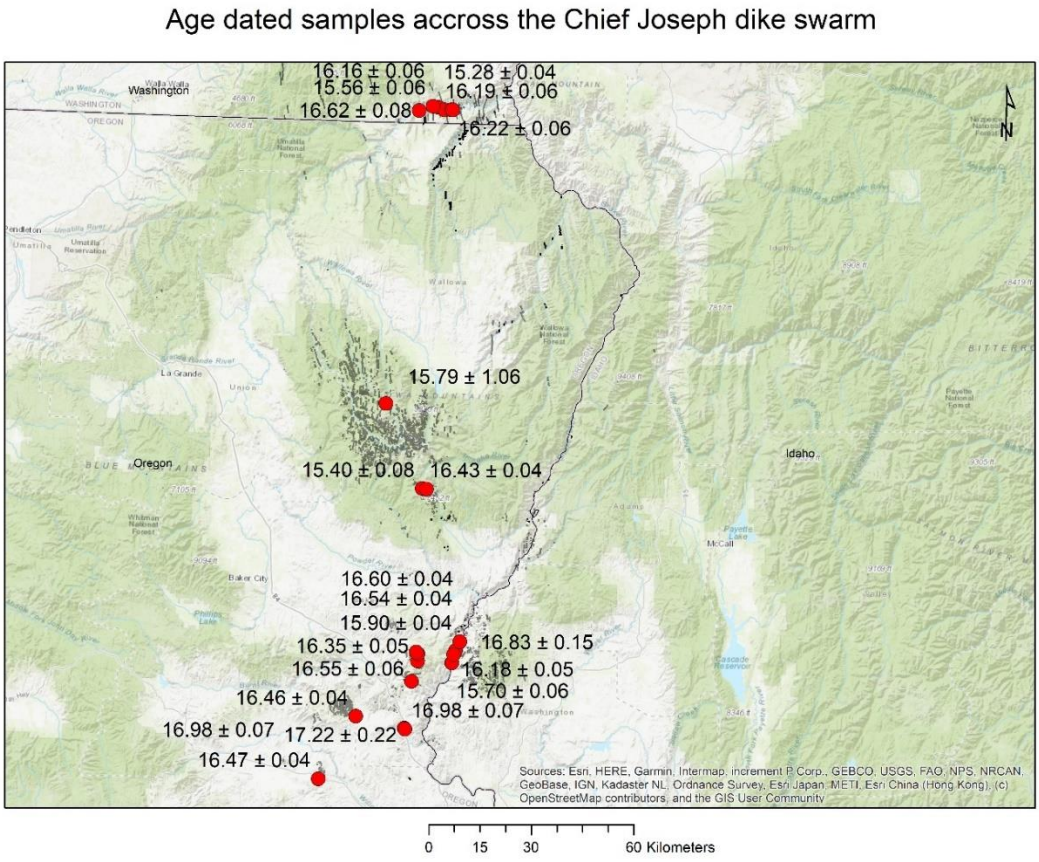

Figure 71. All dates across the CJDS from this study, showing age progressive trends of younger dikes to the north.

Ages of the low SiO2 trend

Samples that make up the low silica trend primarily consist of samples that are identified as Imnaha Rock Creek member. However, samples of this trend at higher concentrations of La and SiO_2 (about midway if low Si trend includes the Umatilla member that plot at the highest concentrations) are classified as the Roza member of the Wanapum Basalt. In the south portion of the CJDS, the two samples dated are Imnaha RC member with similar ages of 16.54 Ma and 16.60 Ma. The sample at the higher La and Si range comes from the north portion and this sample has been classified as a Roza dike; it has an age of 15.28 Ma. The oldest accepted date for the Imnaha is 16.85 ± 0.21 (Jarboe, 2010). On the other hand, the Imnaha Basalt was dated 16.57 Ma by Kasbohm and Schoene (2018). Neither the Jarboe sample nor the Kasbohm and Schoene sample is assigned to any Imnaha subunits. It appears the Kasbohm and

Schoene sample is within the Imnaha stratigraphy thus likely above the basal American Bar samples and our ages perfectly agree with this date. An interbed within basalts immediately above the Roza flow was dated at 15.9 Ma (Kasbohm and Schoene, 2018) which makes our date of the Roza member younger than this. The thin section for our Roza samples do have the blocky rectangular zoned plagioclase and aphyric groundmass that are characteristic of Roza (Martin, 1991). This dike was also found just west along the Grande Ronde River within the eruptive region of the Roza dikes.

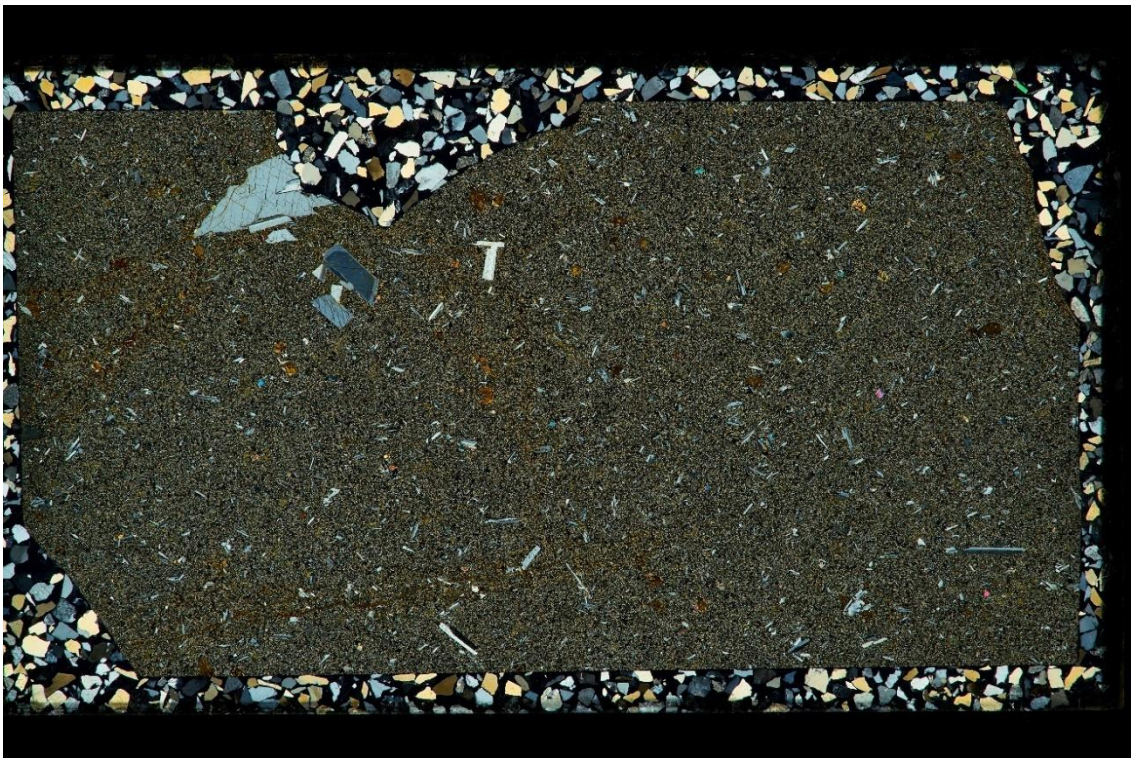

Figure 72. Image of Roza-like sample along the Grande Ronde River, pictured is MM-CRB-61.

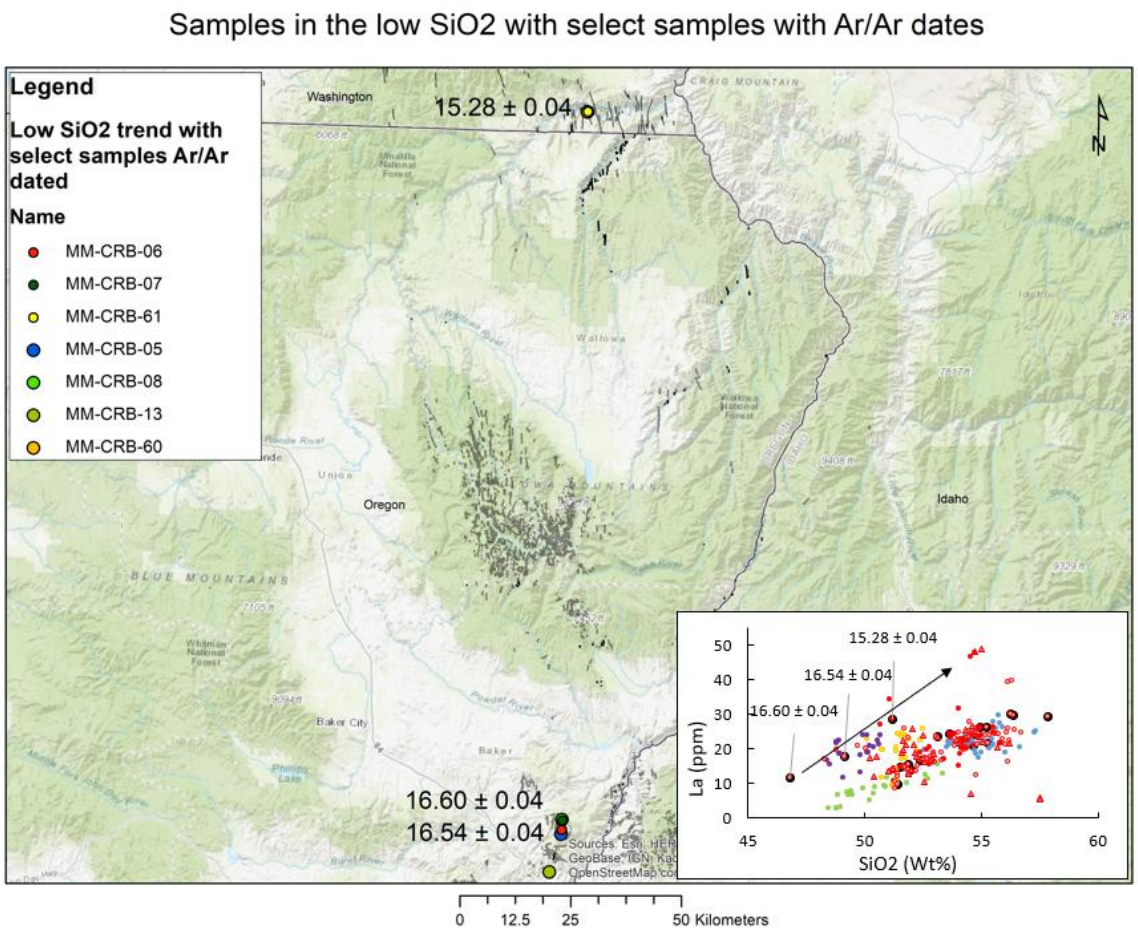

Figure 73. Ages of dikes within the low SiO_2 trend.

Ages of all Eckler Mountain-like dikes

Samples that have been grouped as Eckler Mtn. basalts from the machine learning program have a basalt of Dodge-like composition. Their ages range from 15.90 ± 0.04 Ma to 17.22 ± 0.22 Ma. Although these samples are compositionally almost identical to the basalt of Dodge, they are far away from their expected eruptive area located at the Idaho, Washington, and Oregon border. These dikes are found across the dike swarm all the way to the south. The age of the Eckler Mountain flows is between the age of the Vantage sediments dated at 16.06 Ma and the basalt members immediately overlying the Roza flow with an age of 15.9 Ma (Kasbohm and Schoene, 2018). There is only one age date for the Eckler Mtn. in the literature which is a basalt of Dodge sample The Vantage sediments underlies the Wanapum and overlie

the GRB which in turn marks the end of the GRB eruptive period (Figure 74). There is however an age date of 16.20 Ma for the Frenchmen Springs member that stratigraphically overlies the Eckler Mountain member (Barry et al., 2013). Studies have pointed out this age places Wanapum volcanism in conflict with the eruption of the Grande Ronde Basalts unless the volcanism was contemporaneous (Barry et al., 2013). Because of the presence of the Vantage sediments in the eruptive area of the Eckler Mtn. basalts, this has so far been unresolved as Eckler Mtn. vents have not been found elsewhere. The Eckler Mtn-like dikes from this study could resolve the debate and show that Wanapum magmatic activity was ongoing at the same time as the GRB. Another possibility could be that these samples are geochemically very similar to the Eckler Mtn. but are in fact a previously unidentified unit of the CRBG's. Even more intriguing, Eckler Mtn basalts resemble PGB.

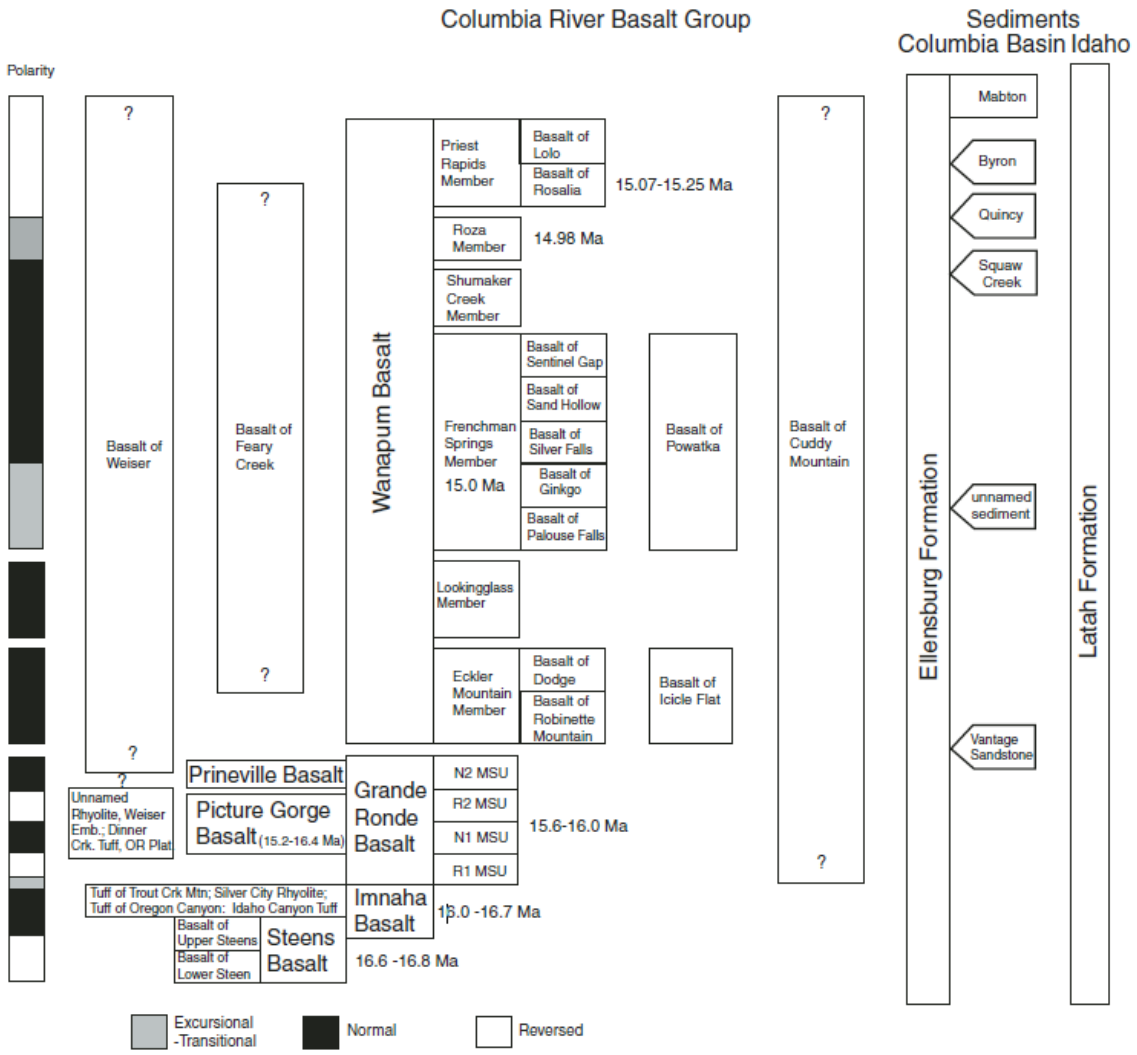

Figure 74. Stratigraphy of the CRBGs. Figure from Barry et al. (2013).

PGB-like samples have been noted in previous studies of NE Oregon (Hooper, 1974; Kleck, 1976; Swanson et al., 1979; Cahoon et al., 2020; Fredenberg, 2022) and these flows are stratigraphically early Imnaha American Bar. I have informally grouped the samples from this study as Eckler Mtn.-like (Samples included in this group are listed in Figure 75). I have compared the incompatible trace element patterns of the dikes in question to PGB, American Bar, Rock Creek and Eckler Mtn basalts. Based on this assessment, I have grouped them as most similar to the Eckler Mountain – basalt of Dodge as seen in Figure 75.

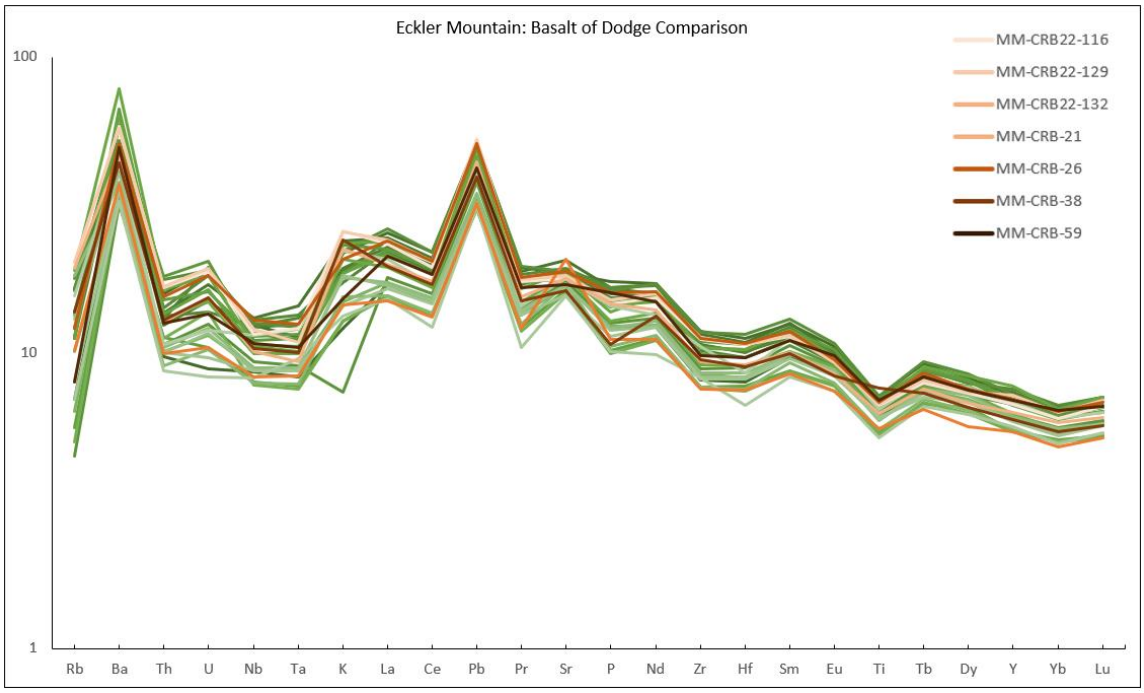

Figure 75. Samples from this study in shades of red compared to samples of Eckler Mountain basalt of Dodge (unpublished Eckler Mountain data from Rachelle Hart at WSU).

The implications for the ages obtained for these PGB-Eckler-like samples is that they cannot be Eckler basalts but are geochemically very similar. Activity began in the southern portion of the CJDS at 17.22 ± 0.22 Ma with these Eckler-PGB like magmas. Ages of dated samples generally get younger along strike going to the northern portion of the dikes swarm (Figure 61).

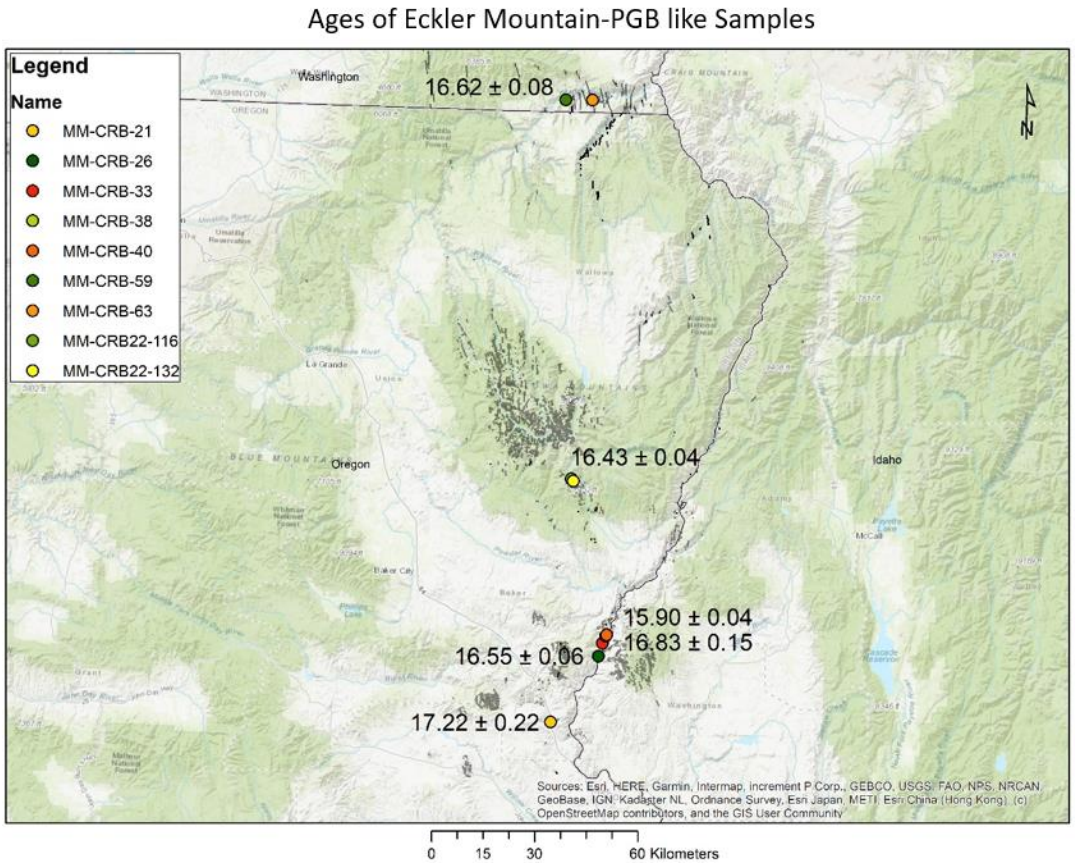

Figure 76. Samples from this study that are Eckler-PGB like.

Ages of all GRB dikes

Samples of the GRB formation that were selected for dating were primarily dikes identified as Wapshilla Ridge member, as it is so voluminous and is found across the whole Chief Joseph dike swarm. A few other members were also selected as they were represented in the north and the south: Downey Gulch, Kendrick Grade, and Sentinel Bluffs McCoy Canyon. All the A few other members were also selected as they were represented in the north and the south: Downey Gulch, Kendrick Grade, and Sentinel Bluffs McCoy Canyon. All the Wapshilla Ridge samples have very similar incompatible trace element patterns). Because the Downey Gulch and Kendrick grade member erupted back-to-back and are geochemically similar, one was picked in the north and the south to date (Figure 78).

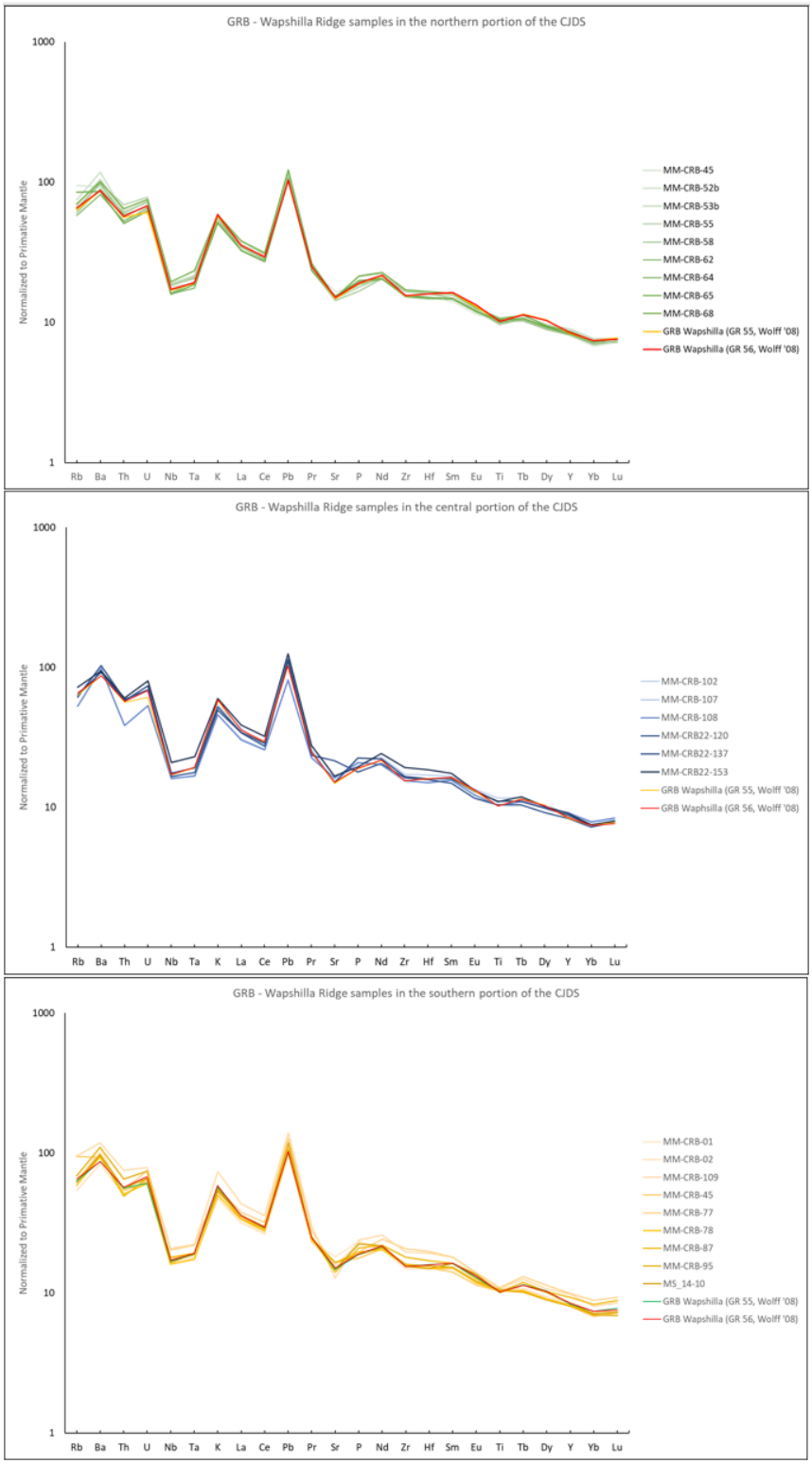

Figure 77. Geochemical incompatible trace element diagram of all Wapshilla Ridge samples across the strike of the CJDS from this study.

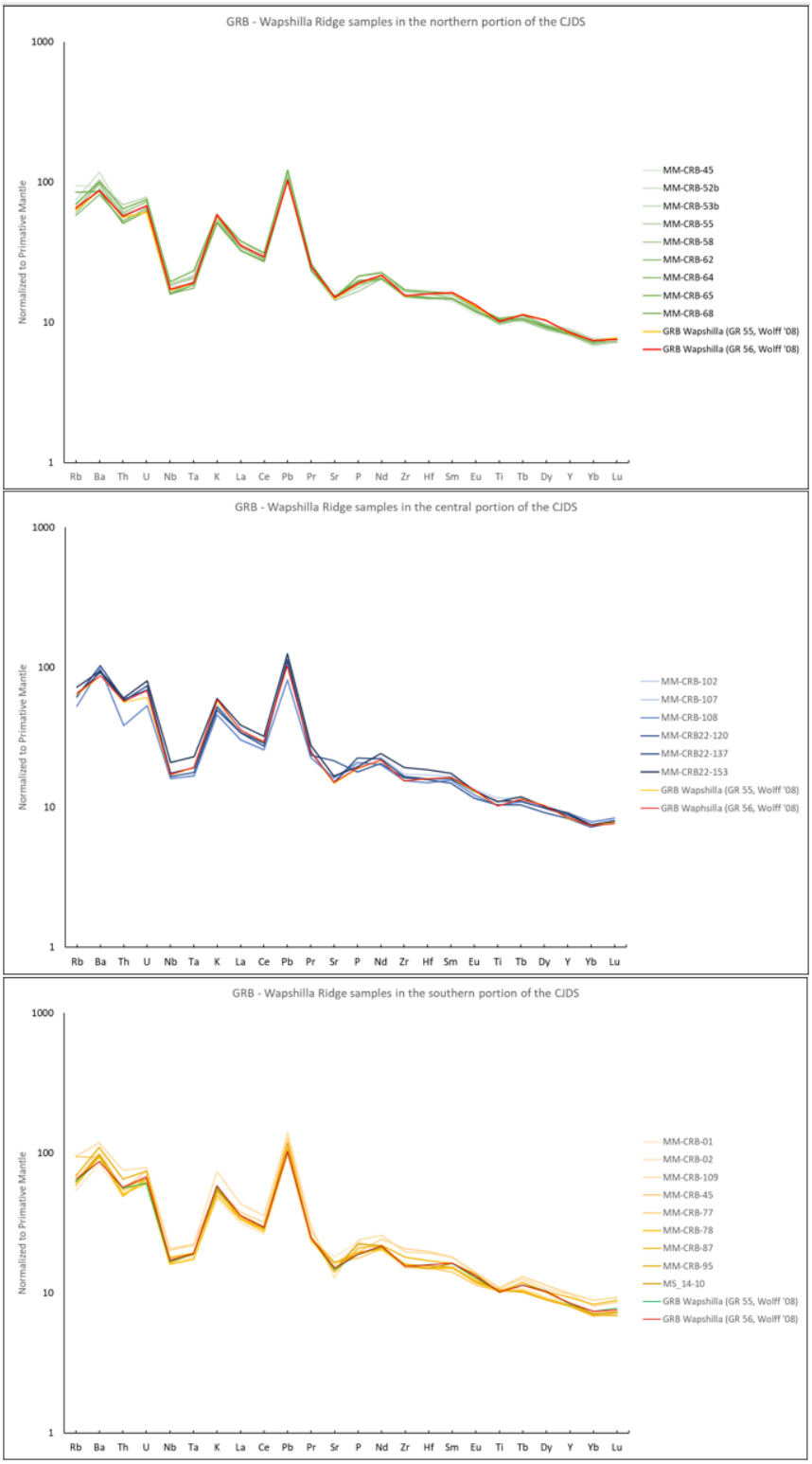

Figure 77. Geochemical incompatible trace element diagram of all Wapshilla Ridge samples across the strike of the CJDS from this study.

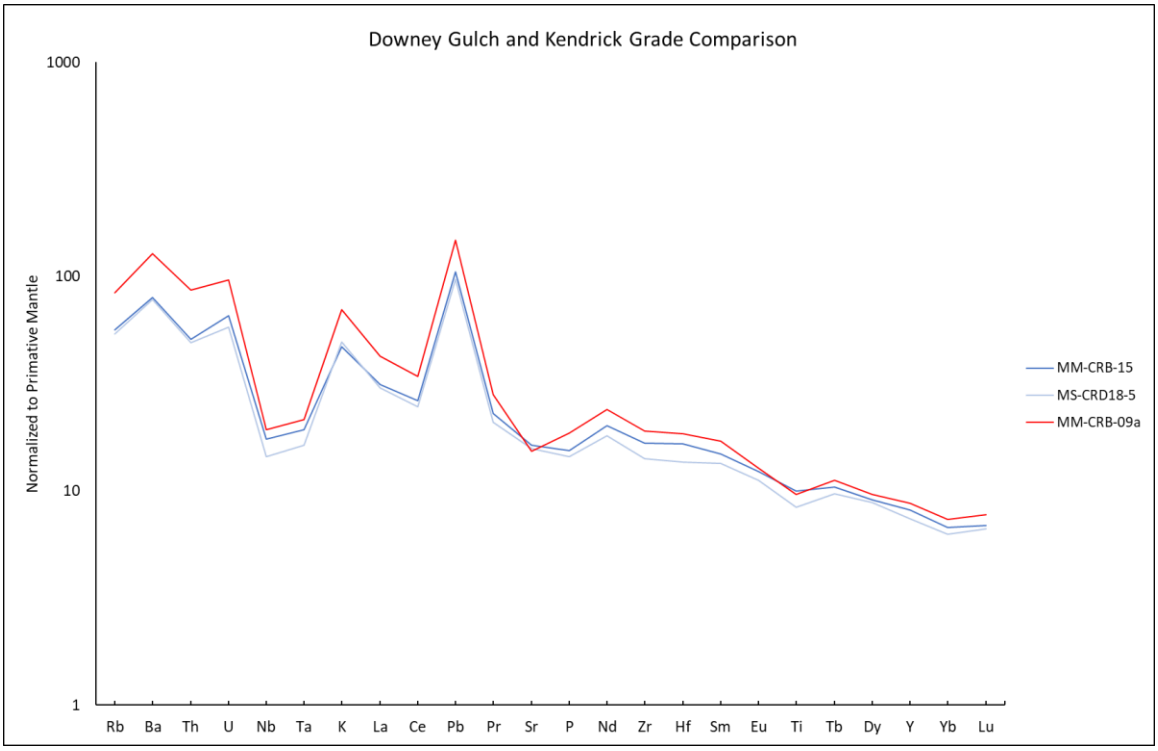

Figure 78. Geochemical incompatible trace element diagram of two Downey Gulch samples (MM-CRB-15 and MS-CRD18-5) and one Kendrick grade sample (MM-CRB-09a) from this study.

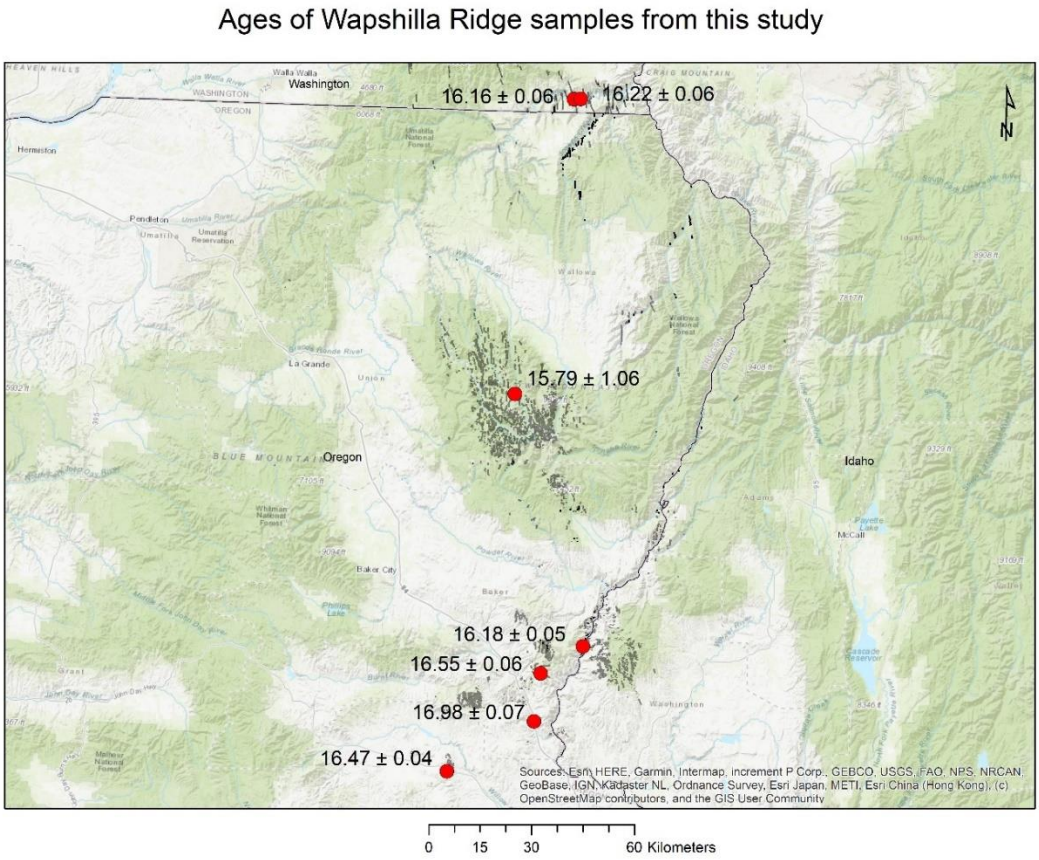

Figure 79. Ages of the GRB Wapshilla Ridge member from this study.

The age of Wapshilla Ridge dikes across the CJDS gets younger as you go north, with only a single exception: a dike in the Wallowa Mountains – however the error for this sample is ± 1.06 Ma and should be excluded from consideration (Figure 82).

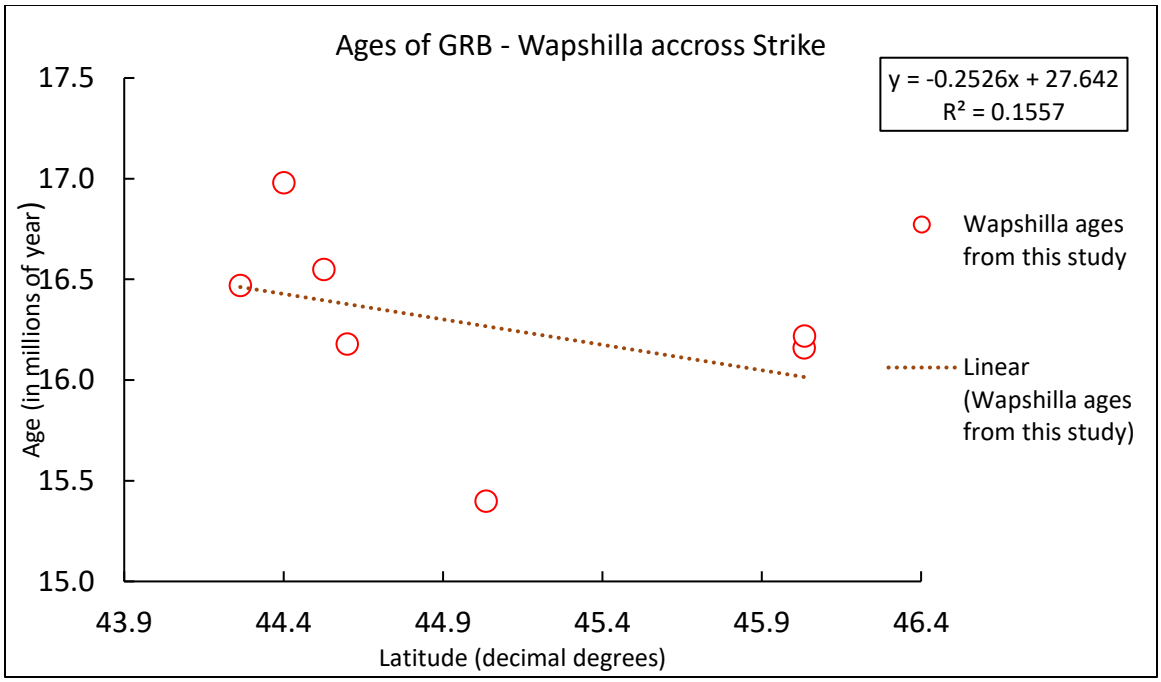

Figure 80. Ages of GRB Wapshilla Ridge dikes across the CJDS.

Intrusive duration vs. subaerial stratigraphy

Age discrepancies of dikes relative to surface flow members.

Age dating yielded some ages outside of the expected range based on the member identity as classified by the machine learning algorithm. One of these is the Roza dike in the northern portion of the dike swarm with an age of 15.28 Ma. This age is 600,000 years younger than the current age of the Roza member 15.895 ± 0.019/0.026 Ma (Kasbohm and Schoene, 2018). Several possibilities exist to explain this: 1) the new age date reported here could be wrong; 2) the previous accepted age could be wrong; 3) the deviation could be explained by intrusive activity not expressed at the surface; or 4) the unit assignment is wrong. There are also dikes that are older than the proposed activity for the earliest eruptive member of the CJDS—the Imnaha with age ranges from 16.85 – 16.57 Ma (Jarboe, 2010; Kasbohm and Schoene, 2018). However there is an older unpublished K/Ar date of 17.67±0.32 Ma that is quoted in the following papers, but not generally accepted (Reidel and Hooper, 1989; Baksi, 2004). The two older dikes from this study in the south produced ages of 16.98 ± 0.07 Ma and

17.22 ± 0.22 Ma correlated with Wapshilla Ridge member and Eckler Mtn basalt, respectively. For the sample with the 17.22 Ma date, the plateau is consistent and flat. This experiment was conducted with a full run of heat steps; the margin of error is a bit larger due to excess argon at the very end of the experiment. Despite this margin of error, this age has a good spread of data which can be seen in both in the plateau and the inverse isochron (Figure 81) it should be considered an excellent result. This age of this sample does correlate with the age range of the PGB and will extend the eruptive range of the CJDS.

Lastly, generated ages of dikes with Wapshilla Ridge compositions ranges from 16.16 ± 0.06 Ma to 16.98 ± 0.07 Ma which is well outside of the eruptive period of Wapshilla Ridge lavas thought to center on 16.288 ± 0.039 (Kasbohm and Schoene, 2018). Younger ages of Wapshilla Ridge compositional types are represented by Birch Creek lavas and Hunter Creek Basalt of the Malheur Gorge erupted at ~16.1 Ma (e.g. Webb et al., 2018). This rather corroborates the dispersion of age of volcanic vs intrusive activity.

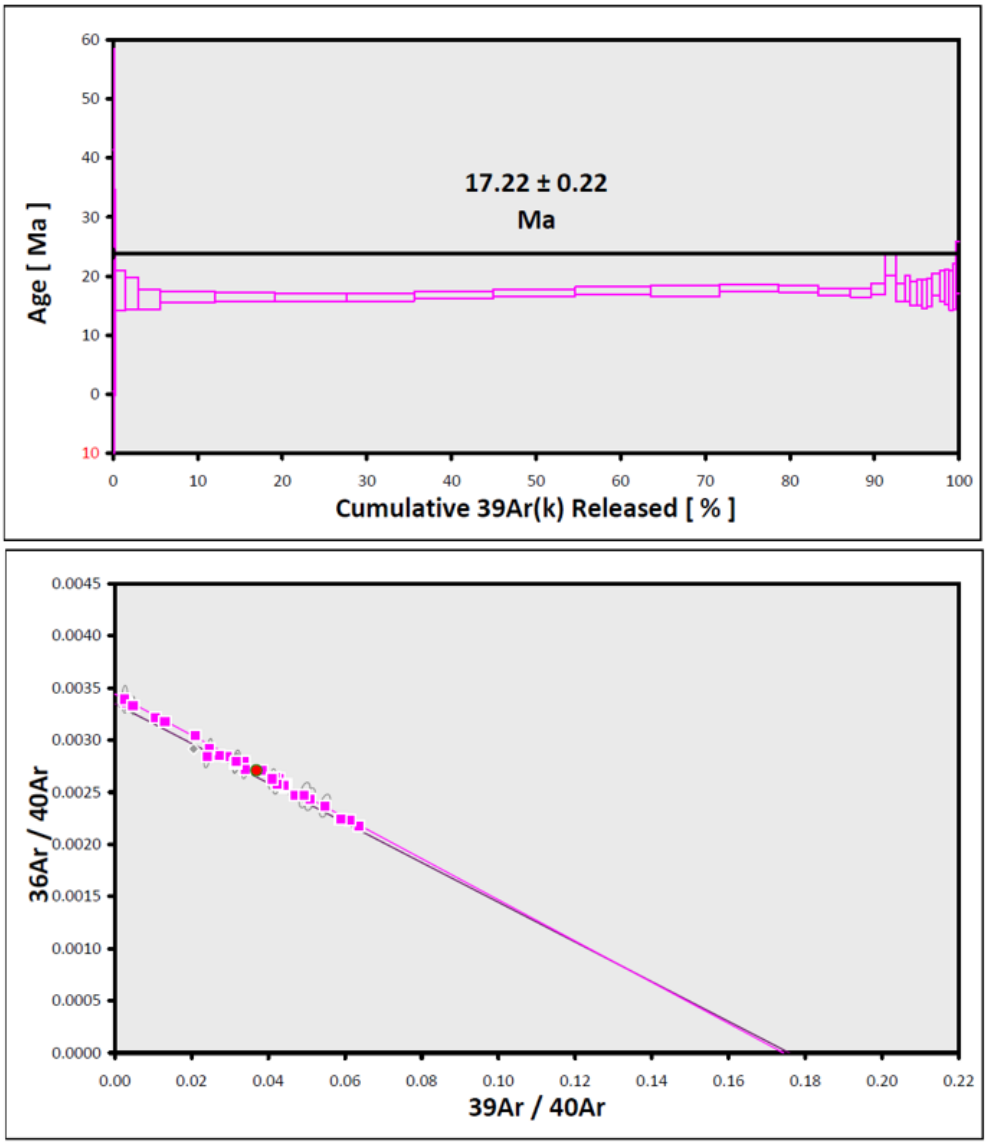

Figure 81. Age plateau of sample MM-CRB-21 in the south, above figure is the plateau age and below shows the data spread over the inverse isochron.

Similar magma types present at depth over considerable time.

As mentioned previously, there are a few ages both from this study and in the literature that suggest that similar magma types have been persistently tapped over some significant time interval during the overall activity period of the Chief Joseph dike swarm. One of these is the magma compositionally represented by Birch Creek lavas/Hunter Creek Basalt erupting in

Malheur Gorge and the Wapshilla Ridge lava member. Both belong to the GRB but have different ages, yet they have indistinguishable compositions (Figure 82)

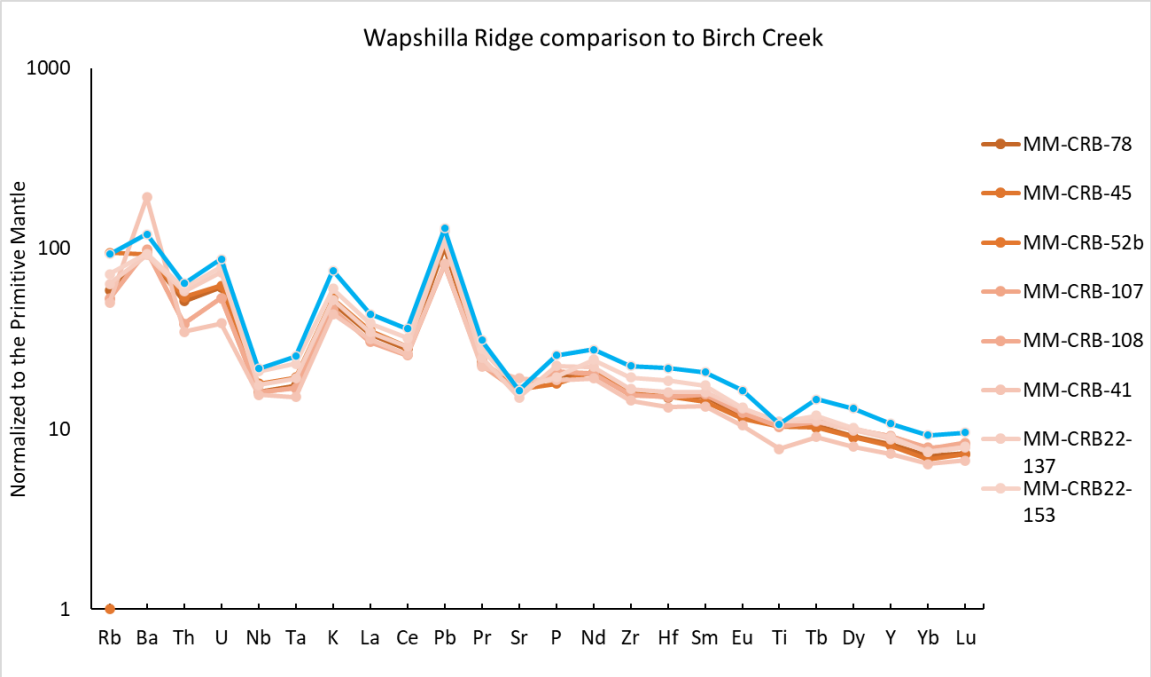

Figure 82. A comparison between Wapshilla Ridge and Birch Creek members of the GRB. Birch Creek data from Webb et al. (2019).

The age of the Hunter Creek Basalt is closely constrained to 16.1 Ma and the underlying Birch Creek lavas are thought to be close in age to Hunter Creek Basalt (Webb et al., 2018). On the other hand, middle to upper lavas of the Wapshilla Ridge member erupted between 16.29 to 16.25 Ma (Kasbohm and Schoene, 2018). Including the ages reported here indicates Wapshilla Ridge-Hunter Creek Basalt-like magmas existed even earlier. Another example of a magma type that was available for some time is the PGB-Eckler Mountain Basalt compositions. From this study, we know that this magma composition is recorded across the Chief Joseph dike swarm with the oldest age at 17.22 ± .22 Ma. This is much older than the local Eckler Mtn. Basalt of Dodge type at the OR, ID, WA border dated at 15.76 ± 0.17 Ma (Barry et al., 2013). This suggests that that there are similar magma types stored or resupplied at depth in stable magma chambers that have been stored for some time to create homogeneous magmas over time.

Similar magmas of the GRB and Birch creek members suggest longer storage in the crust proceeding a voluminous eruption. The primitive character of Eckler Mtn. and similar magmas suggests a recharging magma chamber with shorter residence times. The circular pattern of MgO and SiO_2 reflect recharge, residence time, contamination, and eruption of magmas (Reidel and Tolan, 2013).

Age Distributions for low and high SiO_2 trends.

The low SiO_2 trend has an eruptive interval of 16.55 Ma to 15.28 Ma based on the reported dike ages. The high SiO_2 trend however has a longer activity of 17.22 Ma to 15.4 Ma. Assuming these two trends broadly express evolutionary trends starting with more primitive magmas changing into evolved magmas, the age span for both suggests that the magma reservoir system that was tapped to produce the low SiO_2 trend was active for a shorter time relative to the high SiO_2 trend. This also agrees with what we see in the geochemical types represented in both trends. The low silica trend has more diverse magmas with less individual flows relative to the high silica trend. The high SiO_2 trend represents a longer-lived magma chamber system with similar magma composition reappearing over time producing more homogeneous magmas like the GRB. On the other hand, the lower SiO_2 trend represents a shorter-lived magma chamber system that produced heterogeneous magmas that were shorter lived.

Implications of magma reservoirs and magma plumbing regarding ages

The new ages from this study suggest that there were multiple magma types active in the Chief Joseph dike swarm with an apparent gradual northward progression through time which could be solely due to the exposure level of dikes as many of the dikes in the north are covered by younger CRBG flows. If not, then one could infer that dike formation migrated northward. If this is the case, the next question would be whether this is driven by lateral

magma transport in the crust or due to migration of the magma generation location in the mantle (e.g. migration of the plume head). The data from this study show that the dikes in the south are older and have greater geochemical diversity, supporting the idea that magma was stored in the southern portion of the CJDS. The lack of CRBG related silicic volcanism in the central and northern portions of the dike swarm suggests that there was a lack of storage for the magmas erupted in these areas. Another important finding of this study is that the Chief Joseph dike swarm began its activity at the same time that the Picture Gorge Basalts began erupting from the Monument dike swarm, as eruptions began there at 17.23 ± 0.04 Ma (Cahoon et al., 2020). This suggests that there were several magma chamber systems erupting contemporaneous over considerable distance. Further studies will be required to determine more details regarding magma storage and magma movement between and within these dike swarms.

Conclusions

This study investigated the Chief Joseph Dike swarm from the Oregon – Washington state border in the north to its southern termination near an axis between the towns of Brown and Huntington, eastern Oregon. Samples of 147 dikes were analyzed for their major and trace elemental composition and petrographic analysis were performed on thin sections of all sampled dikes. The combined compositional data spread (without prejudging eruptive unit correlation) varies widely but indicates two geochemical trends with numerous samples falling in between. These trends are observed when select major and trace element data are plotted against silica, thus identified here as low and high silica trends. After the correlation of dike composition with known eruptive units, it becomes apparent that the low Si trend corresponds to samples of the Imnaha Rock Creek, Roza, and the Saddle Mountain Umatilla members from this study. One previously lacking anchor point is found in a high Mg (11.3 wt.% MgO) dike that

newly defines a primitive starting point of the low Si trend. The high Si trend includes lavas of the Imnaha American Bar, the GRB, and Wanapum Eckler Mountain-PGB-like basalt. Samples of the southern dikes include the most primitive samples from this study but also capture the diversity of the CJDS while northern dikes are more evolved and homogenous.

New ages for dikes within the Chief Joseph dike swarm establish ages of intrusive dike magmas within the swarm. While many of the ages of the sampled dikes correlate very well with ages of eruptive units, there is both divergence and wider spread than what is reported for eruptive lavas. Some ages are older than those reported with eruptive correlative lavas, potentially suggesting the age of magmas at depth is broader than the eruptive age of these units. A new date for the Roza member is 15.28 Ma which is 600,000 years younger than the eruptive age in the literature. New ages of dikes correlative with lavas of the Grande Ronde Basalt include the Wapshilla Ridge member with a new intrusive age range of 16.98 Ma to 15.40 Ma with only the ages around 16.2 Ma correlating with the eruptive age of the Wapshilla member. New ages for the Imnaha Basalt range from 16.83 to 15.90 Ma. An Eckler-PGB like lave type has been identified in the north, central, and south areas with an age range of 17.22 Ma to 16.45 Ma. New ages of the Imnaha Rock Creek member of 16.54 Ma and 16 60 Ma are consistent with the literature. We conclude that the Chief Joseph dike swarm was active at 17.22 Ma beginning with an Eckler-PGB like basalt at the same time as the Monument dike swarm began its activity. It has been suggested by Peter Hooper and others (1995) to upgrade Eckler Mountain to a formation, the newly identified Eckler-PGB like group is nearly indistinguishable from the Eckler Mtn. basalt of Dodge and adds support for upgrading the Eckler Mountain to a Formation. The ages and geochemistry from this study supports the idea that there are age progressive trends of younger samples to the north. Samples are more diverse and more primitive in the south relative to the north. This study also supports the

magma storage model put forth by Wolff et al. (2008) and Webb et al. (2019) where the main magma storage location is located in the Vale region of central eastern Oregon (Figure 3). This is supported by the geochemical diversity found in the southern portion which lies in the Vale region, there is a wider and older age range of dikes established in this area, and lastly the lack of silicic volcanism in the central or northern portion of the CJDS suggest little to no storage time of magmas sourcing the dikes there. This suggests that magma traveled from the southern portion of the CJDS in the Vale region to other eruptive locations throughout the swarm.

References

Baksi, A.K., 2004, Ages of the Steens and Columbia River flood basalts and their relationship to extension related calc-alkalic volcanism in eastern Oregon: Discussion: GSA Bulletin, v. 116, p. 247–248, doi:10.1130/B25310.1.

Barry, T., Kelley, S., Reidel, S., Camp, V., S, S., NA, J., RA, D., and Renne, P., 2013, Eruption Chronology of the Columbia River Basalt Group: Special Paper of the Geological Society of America, v. Special Paper 497, p. 45–66, doi:10.1130/2013.2497(2).

Brooks, H.C., 2006, Geologic Map of the Mormon Basin Quadrangle, Baker and Malheur Counties, Oregon: Open-File Report O-06-25.

Cahoon, E.B., Streck, M.J., Koppers, A.A.P., and Miggins, D.P., 2020, Reshuffling the Columbia River Basalt chronology—Picture Gorge Basalt, the earliest- and longest-erupting formation: Geology, doi:10.1130/G47122.1.

Camp, V.E., 1995, Mid-Miocene propagation of the Yellowstone mantle plume head beneath the Columbia River basalt source region: , p. 4.

Camp, V.E., 2013, Origin of Columbia River Basalt: Passive rise of shallow mantle, or active upwelling of a deep-mantle plume?, *in* Reidel, S.P., Camp, V.E., Ross, M.E., Wolff, J.A., Martin, B.S., Tolan, T.L., and Wells, R.E. eds., The Columbia River Flood Basalt Province, Geological Society of America, v. 497, p. 0, doi:10.1130/2013.2497(07).

Camp, V.E., and Hanan, B.B., 2008, A plume-triggered delamination origin for the Columbia River Basalt Group: Geosphere, v. 4, p. 480–495, doi:10.1130/GES00175.1.

Camp, V.E., Ross, M.E., Duncan, R.A., Jarboe, N.A., Coe, R.S., Hanan, B.B., and Johnson, J.A., 2013, The Steens Basalt: Earliest lavas of the Columbia River Basalt Group, *in* Geological Society of America Special Papers, Geological Society of America, v. 497, p. 87–116, doi:10.1130/2013.2497(04).

Duncan, R.A., and Keller, R.A., 2004, Radiometric ages for basement rocks from the Emperor Seamounts, ODP Leg 197: Geochemistry, Geophysics, Geosystems, v. 5, doi:10.1029/2004GC000704.

Ernst, R.E., Liikane, D.A., Jowitt, S.M., Buchan, K.L., and Blanchard, J.A., 2019, A new plumbing system framework for mantle plume-related continental Large Igneous Provinces and their mafic-ultramafic intrusions: Journal of Volcanology and Geothermal Research, v. 384, p. 75–84, doi:10.1016/j.jvolgeores.2019.07.007.

Fredenberg, L., 2022, Investigation of Basal Imnaha Basalt Flows and their Relationship to the Picture Gorge Basalt of the Columbia River Basalt Group [Master of Science in Geology]: Portland State University, doi:10.15760/etd.8056.

Hales, T.C., Abt, D.L., Humphreys, E.D., and Roering, J.J., 2005, A lithospheric instability origin for Columbia River flood basalts and Wallowa Mountains uplift in northeast Oregon: Nature, v. 438, p. 842–845, doi:10.1038/nature04313.

HOOPER, P.R., 1974, Petrology and Chemistry of the Rock Creek Flow, Columbia River Basalt, Idaho: GSA Bulletin, v. 85, p. 15–26, doi:10.1130/0016-7606(1974)85<15:PACOTR>2.0.CO;2.

Hooper, P.R., Binger, G.B., and Bradshaw, K., 2002, Ages of the Steens and Columbia River flood basalts and their relationship to extension-related calc-alkalic volcanism in eastern Oregon: Geological Society of America Bulletin, v. 114, p. 43–50, doi:10.1130/0016-7606(2002)114<0043:AOTSAC>2.0.CO;2.

Hooper, P.R., Gillespie, B.A., and Ross, M.E., 1995, The Eckler Mountain basalts and associated flows, Columbia River Basalt Group: Canadian Journal of Earth Sciences, v. 32, p. 410–423, doi:10.1139/e95-035.

Jarboe, N.A., 2010, THE STEENS BASALT OF THE OREGON PLATEAU: A GEOMAGNETIC POLARITY REVERSAL AND THE AGE OF THE COLUMBIA RIVER BASALT GROUP:

Kasbohm, J., and Schoene, B., 2018, Rapid eruption of the Columbia River flood basalt and correlation with the mid-Miocene climate optimum: Science Advances, v. 4, p. eaat8223, doi:10.1126/sciadv.aat8223.

KLECK, W.D., 1976, CHEMISTRY, PETROGRAPHY, AND STRATIGRAPHY OF THE COLUMBIA RIVER GROUP IN THE IMNAHA RIVER VALLEY REGION, EASTERN OREGON AND WESTERN IDAHO: ProQuest Dissertations Publishing.

Koppers, A., Staudigel, H., and Duncan, R., 2003, High-resolution $^{40}Ar/^{39}Ar$ dating of the oldest oceanic basement basalts in the western Pacific basin: Geochem. Geophys. Geosyst., v. 4, doi:10.1029/2003GC000574.

Kuiper, K.F., Deino, A., Hilgen, F., Krijgsman, W., Renne, P., and Wijbrans, J.R., 2008, Synchronizing Rock Clocks of Earth History: Science (New York, N.Y.), v. 320, p. 500–4, doi:10.1126/science.1154339.

Landon, R.D., and Long, P.E., 1989, Detailed stratigraphy of the N2 Grande Ronde Basalt, Columbia River Basalt Group, in the central Columbia Plateau, *in* Geological Society of America Special Papers, Geological Society of America, v. 239, p. 55–66, doi:10.1130/SPE239-p55.

Maitre, R.W., 1989, A classification of igneous rocks and glossary of terms: Recommendations of the International Union of Geological Sciences Subcommission on the Systematics of Igneous Rocks, doi:10.1017/CBO9780511535581.005.

Marshall, D.P., 1996, Ternplot: An excel spreadsheet for ternary diagrams: Computers & Geosciences, v. 22, p. 697–699, doi:10.1016/0098-3004(96)00012-X.

Martin, B.S., 1991, Geochemical variations within the Roza Member, Wanapum Basalt, Columbia River Basalt Group: Implications for the magmatic processes affecting continental flood basalts: Doctoral Dissertations Available from Proquest, p. 1–531.

Martin, B.S., Tolan, T.L., and Reidel, S.P., 2013, Revisions to the stratigraphy and distribution of the Frenchman Springs Member, Wanapum Basalt, *in* Reidel, S.P., Camp, V.E., Ross, M.E., Wolff, J.A., Martin, B.S., Tolan, T.L., and Wells, R.E. eds., The Columbia River Flood Basalt Province, Geological Society of America, v. 497, p. 0, doi:10.1130/2013.2497(06).

Moore, N.E. Petrogenesis of the Steens Basalt : Variation in Source Contributions and Effects of Crustal Passage During the Onset of Columbia River Flood Basalt Volcanism:

Morriss, M.C., Karlstrom, L., Nasholds, M.W.M., and Wolff, J.A., 2020a, The Chief Joseph dike swarm of the Columbia River flood basalts, and the legacy data set of William H. Taubeneck: Geosphere, v. 16, p. 1082–1106, doi:10.1130/GES02173.1.

Morriss, M.C., Karlstrom, L., Nasholds, M.W.M., and Wolff, J.A., 2020b, The Chief Joseph dike swarm of the Columbia River flood basalts, and the legacy data set of William H. Taubeneck: Geosphere, v. 16, p. 1082–1106, doi:10.1130/GES02173.1.

Reidel, S., Camp, V., Tolan, T.L., and BS, M., 2013, The Columbia River Flood-Basalt Province: stratigraphy, areal extent, volume, and physical volcanology: Special Paper of the Geological Society of America, v. Special Paper 497, p. 1–43, doi:10.1130/2013.2497(1).

Reidel, S.P., and Hooper, P.R. (Eds.), 1989, Volcanism and tectonism in the Columbia River flood-basalt province: Boulder, Colo, Geological Society of America, Special paper / Geological Society of America 239, 386 p.

Reidel, S.P., and Tolan, T.L., 2013, The Grande Ronde Basalt, Columbia River Basalt Group, *in* Reidel, S.P., Camp, V.E., Ross, M.E., Wolff, J.A., Martin, B.S., Tolan, T.L., and Wells, R.E. eds., The Columbia River Flood Basalt Province, Geological Society of America, v. 497, p. 0, doi:10.1130/2013.2497(05).

Reidel, S.P., Tolan, T.L., Hooper, P.R., Beeson, M.H., Fecht, K.R., Bentley, R.D., and Anderson, J.L., 1989, The Grande Ronde Basalt, Columbia River Basalt Group; Stratigraphic descriptions and correlations in Washington, Oregon, and Idaho, *in* Reidel, S.P. and Hooper, P.R. eds., Volcanism and Tectonism in the Columbia River Flood-Basalt Province, Geological Society of America, v. 239, p. 0, doi:10.1130/SPE239-p21.

Ross, C.P., 1938, The Geology of Part of the Wallowa Mountains: DOGAMI Bulletin Number 3, https://www.oregongeology.org/pubs/B/B-003.pdf.

Schmandt, B., and Humphreys, E., 2011, Seismically imaged relict slab from the 55 Ma Siletzia accretion to the northwest United States: Geology, v. 39, p. 175–178, doi:10.1130/G31558.1.

Steiger, R.H., and Jäger, E., 1977, Subcommission on geochronology: Convention on the use of decay constants in geo- and cosmochronology: Earth and Planetary Science Letters, v. 36, p. 359–362, doi:10.1016/0012-821X(77)90060-7.

Stiener, A., and Wolff, J., 2020, Supervised Machine Learning for Columbia River Basalt Group Classification | Showcase | Washington State University,

https://showcase.wsu.edu/2020/04/09/supervised-machine-learning-for-columbia-river-basalt-group-classification/ (accessed May 2023).

Streck, M.J., Ferns, M.L., and McIntosh, W., 2015, Large, persistent rhyolitic magma reservoirs above Columbia River Basalt storage sites: The Dinner Creek Tuff Eruptive Center, eastern Oregon: Geosphere, v. 11, p. 226–235, doi:10.1130/GES01086.1.

Streck, M.J., Swenton, V.M., McIntosh, W., Ferns, M.L., and Heizler, M., 2023, Columbia River Rhyolites: Age-Distribution Patterns and Their Implications for Arrival, Location, and Dispersion of Continental Flood Basalt Magmas in the Crust: Geosciences, v. 13, p. 46, doi:10.3390/geosciences13020046.

Streck, M.J., Wolff, J.A., and Koppers, A., 2019, Testing competing models for the origin and magma transport dynamics of the Columbia River LIP.

Sun, W., and McDonough, W., 1989, Chemical and isotopic systematics of oceanic basalts: Implications for mantle composition and processes, *in* Geological Society, London, Special Publications, v. 42, doi:10.1144/GSL.SP.1989.042.01.19.

Swanson, D.A., and Bentley, R.D., 1979, Revisions in stratigraphic nomenclature of the Columbia River Basalt Group:, doi:10.3133/b1457G.

United States. Department of Energy, 1982, Basalt waste isolation project, Hanford site characterization report.: Volumes held: B1 (3 v) p., https://catalog.hathitrust.org/Record/100982734 (accessed November 2020).

Vallier, T.L., 1794, A preliminary report on the geology of part of the Snake River Canyon, Oregon and Idaho: DOGAMI GMS-6, https://www.oregongeology.org/pubs/gms/p-GMS.htm.

Webb, B.M., Streck, M.J., McIntosh, W.C., and Ferns, M.L., 2019, The Littlefield Rhyolite and associated mafic lavas: Bimodal volcanism of the Columbia River magmatic province, with constraints on age and storage sites of Grande Ronde Basalt magmas: Geosphere, v. 15, p. 60–84, doi:10.1130/GES01695.1.

Wells, R., Bukry, D., Friedman, R., Pyle, D., Duncan, R., Haeussler, P., and Wooden, J., 2014, Geologic history of Siletzia, a large igneous province in the Oregon and Washington Coast Range: Correlation to the geomagnetic polarity time scale and implications for a long-lived Yellowstone hotspot: Geosphere, v. 10, p. 692–719, doi:10.1130/GES01018.1.

Wolff, J.A., and Ramos, F.C., 2013, Source materials for the main phase of the Columbia River Basalt Group: Geochemical evidence and implications for magma storage and transport, *in* Reidel, S.P., Camp, V.E., Ross, M.E., Wolff, J.A., Martin, B.S., Tolan, T.L., and Wells, R.E. eds., The Columbia River Flood Basalt Province, Geological Society of America, v. 497, p. 0, doi:10.1130/2013.2497(11).

Wolff, J.A., Ramos, F.C., Hart, G.L., Patterson, J., and Brandon, A.D., 2008, Columbia River flood basalts from a centralized crustal magmatic system, doi:10.1038/ngeo124.

Appendix A: Sample Whole Rock (XRF & ICP-MS) and Location Data

Sample location and geochemical data (XRF and ICP-MS analyses) attached as supplementary file.

File name: Appendix_A_XRF_ICPMS Geochemical and Sample Location Data (Mass 2023)

Type: .pdf

File Size: 781 KB

Special Hardware: none

Appendix B: XRF & ICPMS procedures (WSU)

Washington State University XRF and ICP-MS lab procedures are attached as a supplementary file.

File name: Appendix_B_Methods for XRF and ICP-MS WSU

Type: .pdf

File Size: 196 KB

Special Hardware: none

Appendix C: $^{40}Ar/^{39}Ar$ Age Spectra (Plateaus and Inverse Isochrons)

$^{40}Ar/^{39}Ar$ Age Spectra attached as a supplementary file.

File name: Appendix_C_ArAr Age Spectra (Mass 2023)

Type: .pdf

File Size: 13,825 KB

Special Hardware: none

Appendix D: Age Dating Procedures (OSU)

Oregon State University Argon lab procedures are attached as a supplementary file.

File name: Appendix_D_Methods for mineral separation and acid leaching OSU

Type: .pdf

File Size: 1,248 KB

Special Hardware: none

Appendix E: Thin Section Photos

Thin section photos are attached as a supplementary file.

File name: Appendix _E_CRBG dike thin section photos (Mass 2023)

Type: .pdf

File Size: 52,585 KB

Special Hardware: none